A Resampling Theory for Non-bandlimited Signals and Its Applications

Beilei Huang

A thesis presented for the partial fulfillment of the requirements
for the degree of
Doctor of Philosophy
in
Engineering

at
Massey University, Wellington
New Zealand

2008

Abstract

Currently, digital signal processing systems typically assume that the signals are bandlimited. This is due to our knowledge based on the uniform sampling theorem for bandlimited signals which was established over 50 years ago by the works of Whittaker, Kotel'nikov and Shannon. However, in practice the digital signals are mostly of finite length. This kind of signals are not strictly bandlimited. Furthermore, advances in electronics have led to the use of very wide bandwidth signals and systems, such as Ultra-Wide Band (UWB) communication systems with signal bandwidths of several giga-hertz. This kind of signals can effectively be viewed as having infinite bandwidth. Thus there is a need to extend existing theory and techniques for signals of finite bandwidths to that for non-bandlimited signals.

Two recent approaches to a more general sampling theory for non-bandlimited signals have been published. One is for signals with finite rate of innovation. The other introduced the concept of consistent sampling. It views sampling and reconstruction as projections of signals onto subspaces spanned by the sampling (acquisition) and reconstruction (synthesis) functions. Consistent sampling is achieved if the same discrete signal is obtained when the reconstructed continuous signal is sampled. However, it has been shown that when this generalized theory is applied to the de-interlacing of video signals, incorrect results are obtained. This is because de-interlacing is essentially a resampling problem rather than a sampling problem because both the input and output are discrete. While the theory for the resampling for bandlimited signals is well established, the problem of resampling without bandlimited constraints is largely unexplored.

The aim of this thesis is to develop a resampling theory for non-bandlimited discrete signals and explore some of its potential applications. The first major contribution is the the theory and techniques for designing an optimal resampling system for signals in the general Hilbert Space when noise is not present. The system is optimal in the sense that the input of the system can always be obtained from the output. The theory is based on the concept of consistent resampling which means that the same continuous signal will be obtained when either the original or the resampled discrete signal is presented to the reconstruction filter.

While comparing the input and output of a sampling/reconstruction system is relatively simple since both are continuous signals, comparing the discrete input and output of a resampling system is not. The second major contribution of this thesis is the proposal of a metric that allows us to evaluate the performance of a resampling system. The performance is analyzed in the Fourier domain as well. This performance metric also provides a way by which different resampling algorithms can be compared effectively. It therefore facilitates the process of choosing proper resampling schemes for a particular purpose.

Unfortunately consistent resampling cannot always be achieved if noise is present in the signal or the system. Based on the performance metric proposed, the third major contribution of this thesis is the development of procedures for designing resampling systems in the presence of noise which is optimal in the mean squared error (MSE) sense. Both discrete and continuous noise are considered. The problem is formulated as a semi-definite program which can be solved efficiently by existing techniques.

The usefulness and correctness of the consistent resampling theory is demonstrated by its application to the video de-interlacing problem, image processing, the demodulation of ultra-wideband communication signals and mobile channel detection. The results show that the proposed resampling system has many advantages over existing approaches, including lower computational and time complexities, more accurate prediction of system performances, as well as robustness against noise.

Acknowledgments

First of all, I would like to express my sincere thanks to my supervisor, Dr Edmund Lai, for his continuous support and invaluable guidance throughout my postgraduate studies. He has led me into the fantastic world of digital signal processing. The many fruitful discussions with him are the inspiration for this dissertation. I also thank Dr A. P. Vinod for his co-supervision and great help while I was transferring to Massey University.

I owe my gratitude to staff at the Institute of Information Science & Technology. They provided me with an excellent environment and support for my work. I thank Ms Minyi Orams for her helpful coordination. I also thank Mr Michael O'Brien and Mr Adams Stephen for providing me all the equipment and software that I needed for my research.

I was with School of Computer Engineering (SCE), Nanyang Technological University (NTU), Singapore in the early stages of my studies. Dr Guan Yong Liang, Dr Peter Chong, and Dr Ng Boon Chong had been helpful in providing me with an understanding of wireless communication systems. My special thanks to Dr Henry Lew, Dr Sirajudeen Gulam Razul for their great tips in pure mathematics. I also thank NTU for their financial support during my studies there.

I thank all my colleagues and friends at the SCE, NTU. They helped me to escape from lectures and made sure I was on time for all assignments. My thanks to Ms Xiao Shu, for her effort in maintaining the research group server and suggestions in formatting this dissertation. I thank my friend Ms Li Wei, Ms Li Te, Mr Zhang Yan and many others whom I have pleasure of sharing time with. You all made my life cheerful and easy to handle.

Lastly, my deepest appreciation goes to my parents for their unconditional love, support, understanding throughout my whole life. I dedicate this thesis to them.

Contents

List of Figures

List of Tables

Chapter 1

Introduction

1.1 Background and Motivation

Most signals encountered in areas such as telecommunications, medical imaging, radar and sonar, speech and music are analog (or continuous) in time or space. While there are some advantages in processing these signals using analog electronics, they are now increasingly being processed digitally to take advantage of efficient low cost digital processors and advanced digital signal processing algorithms. In order to do so, analog signals will need to be converted to digital (discrete) form. This involves *sampling* and *quantization*. After processing the digital signal, some applications require that the resulting signal be converted back into analog form. This involves *interpolation* and *smoothing*. Figure 1.1 shows the general structure of a digital signal processing (DSP) system that includes all these processes.

The digital signal that is obtained by sampling a continuous signal must preserve all the characteristics of the latter. Whittaker, Kotel'nikov and Shannon independently studied the conditions under which this can be done [2]. For signals that are strictly bandlimited, it turns out that the sampling rate required to preserve the characteristics of the continuous signal is greater or equal to twice its bandwidth. This result is summarized by a theorem which we shall refer to as *Shannon's uniform sampling theorem*. It states that if a signal is uniformly sampled at a rate no less than twice its bandwidth, then the

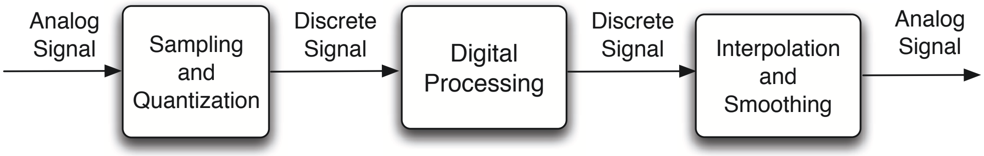

Figure 1.1: A general digital signal processing system.

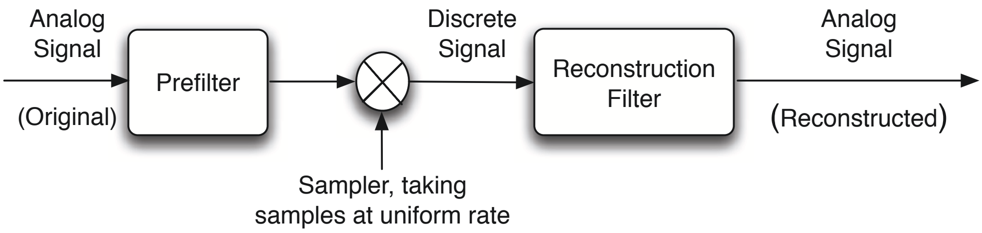

Figure 1.2: Sampling and reconstruction.

analog signal can be perfectly reconstructed from its samples. Thus the lower bound on the sampling rate for a strictly bandlimited signal with a bandwidth of W Hz is $2W$ Hz. However, if a signal is not strictly bandlimited, then there will be aliasing in its frequency spectrum and we will not be able to reproduce the analog signal perfectly. Conceptually, the performance of the sampling process is evaluated by how closely the reconstructed signal resembles the original signal. Figure 1.2 illustrates this process.

This sampling theorem is of central importance in digital signal processing. Even though processing may be performed entirely in the digital domain with no explicit conversion to or from the analog, the sampling rate of the digital signal often needs to be increased or decreased according to the requirements of a particular processing stage. To change the sampling rate of a digital signal, a two-step process is involved [3]. First, the original digital signal is converted, conceptually, to analog form. Then this analog

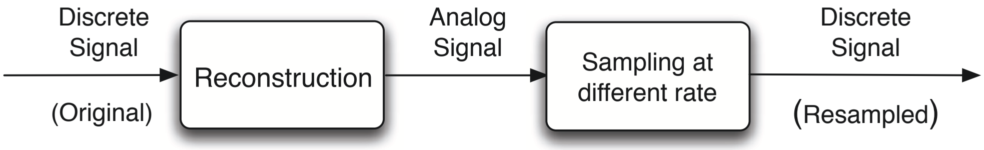

Figure 1.3: Block diagram of a sample rate conversion system.

signal is resampled at a different sampling rate or at different sampling locations. The allowable resampling rates are governed by Shannon's uniform sampling theorem. The block diagram of a sample rate conversion (SRC) system is shown in Figure 1.3. In this thesis, an SRC system is referred to it as a *resampling system* which includes cases where the sampling rate is unchanged but the sampling locations are.

In practice, most signals are not strictly bandlimited. Typically an anti-aliasing filter, which is an analog low-pass filter, is used to ensure that the signal to be sampled is sufficiently bandlimited. However, there are situations where the frontend acquisition filtering is non-ideal [4].

Furthermore, recently there have been proposals to use signals and systems with very wide bandwidths. An example is Ultra-Wide Band (UWB) communication systems. UWB radio is a wireless technology for transmitting digital data at high rates over a very wide frequency spectrum using very low power. The Federal Communications Commission (FCC) of the United States has mandated that UWB radio transmission can legally operate in the frequency range from 3.1 GHz to 10.6 GHz at a transmit power of 1 dBm/MHz [5, 6]. This kind of signal can effectively be viewed as having infinite bandwidth. Owing to the wide bandwidth used, the issues involved in transceiver design for wide band systems are different from those for other narrow band systems. The challenge of implementing a fully digital UWB receiver is particularly daunting. According to Shannon's sampling theorem, the minimum sampling rate for UWB signals would be 21.2 GHz. This sampling rate is way beyond the current analog-to-digital conversion technologies. Therefore, there is a need to extend existing theories and techniques for signals with finite bandwidths to that for signals with non-bandlimited responses.

Two approaches to a generalized sampling theory for non-bandlimited signals have recently been proposed. The first one considers signals with a finite rate of innovation [7]. It is based on the fact that even though many signals are non-bandlimited, such as a triangular or rectangular signal, nonetheless they only require a finite number of parameters per unit time to characterize. In other words, the degree of freedom per unit time or the rate of innovation is finite. If these parameters are available, then perfect reconstruction from the samples is possible. It has been demonstrated through examples that if this type of signal is uniformly sampled at a rate not less than the rate of innovation, then perfect reconstruction is possible. For a stream of Pulse-Position Modulated (PPM) impulses (Diracs), which is similar to those used for UWB impulse radio, it is possible to obtain good estimates of the position of these pulses using a sampling frequency in the range of hundreds of mega-hertz instead of over 20 GHz as mentioned earlier. We shall refer to this approach as *innovation sampling*.

Mathematically, sampling can be viewed as a projection of the signal onto a subspace spanned by the reconstruction function [4, 8]. If the sampling and reconstruction functions are the classic $Dirac - sinc$ function pair, then it is exactly Shannon's sampling theorem. However, this view of sampling and reconstruction admits functions other than these two functions. If the sampled signal does not belong to the subspace spanned by the reconstruction function, then it is not possible to perfectly reconstruct the original analog signal. This is the case for non-bandlimited signals. The concept of *consistent sampling* was introduced in [4] for these situations. A signal is consistently sampled if the reconstructed analog signal, when re-inserted into the sampling process, produces the same discrete sampled sequence. For arbitrary sampling and reconstruction functions which are not duals of each other like the $Dirac - sinc$ pair, consistent sampling can be achieved by optimally projecting the sampled signal onto the reconstruction subspace the sampled signal by a digital corrected filter. We shall refer to this approach to the sampling of non-bandlimited signals as *generalized sampling* or *consistent sampling*.

These theories should in principle be applicable also to resampling of non-bandlimited signals since resampling also involves interpolation and sampling, albeit in the reverse order of sampling and reconstruction. However, in [9], an incorrect result is reported when the stability theory of generalized sampling is applied to de-interlacing of video signals. It turns out although the theory is correct, it is not directly applicable to this application which is essentially a resampling problem. The problem is further illustrated in Section 2.7. This is because in sampling and reconstruction, both the input and output are continuous as shown in Figure 1.2. But a resampling system has discrete input and output as shown in Figure 1.3. Since many DSP applications involve resampling, this problem motivated us to research into a generalized resampling theory for non-bandlimited discrete signals.

1.2 Scope and Objectives

The main objective of this research is to develop a generalized resampling theory for discrete signals without bandlimiting constraints. Our approach resembles the consistent sampling theory. The concept of consistent resampling shall be defined and its properties and applicability to a generalized resampling theory shall be investigated. One of the main issues that need to be tackled is a meaningful performance measure of the resampling system. The performance of a sampling-reconstruction system can be easily measured by comparing the original and reconstructed continuous functions. However, since the both the input and output of a resampling system are discrete and the sampling periods are most likely different, we cannot compare them sample by sample. Both noiseless and noisy resampling shall be considered.

1.2.1 Assumptions

The continuous and discrete signals we consider in this work are assumed to be in the Hilbert space $\mathcal{H}$ and have finite energy. Mathematically, continuous signals are in the L^2 space while discrete signals lie in the space ℓ^2. These are not overly restrictive assumptions and includes almost all natural signals. For example, sound waves or seismic signals are of finite duration. Even for signals with infinite spread such as sonar or radar signal, typically only a finite period is analyzed at a time. Consequently, they can also be considered as finite energy signals as well.

Only uniform sampling will be considered. The techniques developed could be extended to non-uniform sampled sequences. The only application to non-uniform sampling will be the demodulation of UWB impulse radio signals presented in Section 3.4.1.

The functions for sampling, interpolation and resampling are assumed to be in the Hilbert space. We only consider those functions that can be implemented as a simple filter. There are other admissibility constraints that the functions should satisfy in order that the processes are stable. These constraints will be discussed in Section 2.2.

1.2.2 Objectives

In this thesis, a theory of consistent resampling shall be developed so that discrete signals can be resampled in an optimal way. It is important that this resampling theory will overcome the problem of applying sampling theory to a resampling system as pointed out in [9]. The architecture and implementation of a consistent resampling system shall be considered for noiseless signals and systems. Cases where either the input signal or the resampling system is noisy shall also be studied. A performance metric for measuring the input and output of a resampling quantitatively will need to be proposed and based on which optimality is measured.

Further, constraints on the resampling rate should also be studied. The minimum resampling rate above which the input sequence can be reconstructed in relation to the reconstruction and resampling filters used will need to be established. The rate of innovation of the signal provides us with a possible solution to this problem.

1.3 Significance

Currently, resampling systems are treated using the theory of sampling system. Referring to Figure 1.1, however, a resampling system is generally different from a sampling system. While a sampling system is concerned with how the analog signals can be represented by digital sequences, a resampling system deals with how a digital sequence can be represented by another one such that the information carried by the original sequence is changed as little as possible.

The work presented in this thesis consider the generalized resampling system whose input is not necessarily ideally sampled and whose output can be used directly to reconstruct signals even of non-bandlimited response. The consistent resampling theory presented here overcomes the limitation of applying the generalized sampling theory to resampling such as de-interlacing as pointed out in [9]. The consistent theory considers the unique resampling process on its own instead of approximating it by its embedded sampling process. The theory for noiseless as well as noisy signals are developed so that it can be applied to a variety of situations. While it is based on some of the concepts from the generalized or consistent sampling theory, a large part of our resampling theory is new. This is because in our case both the input and output are discrete signals while those of a sampling-reconstruction system are continuous.

The application of our consistent resampling theory can be found in many areas such as sample rate conversion, image resizing, rotation and denoising. Other applications include de-interlacing, UWB impulse radio signal detection, and channel estimation using pilot symbol assisted modulation. These examples are considered in subsequent chapters. The theory can also be applied to spatially scalable video codecs where the upsampling of a low resolution signal into a high resolution one as well as the reverse process of downsampling is required [10, 11]. Another potential application is in meteorological data processing. These data are usually collected at irregularly distributed locations. For ease of further processing, the data are often resampled to fit a regular grid [12, 13].

1.4 Original Contributions

The main original contributions of this thesis are summarized as follows.

- The development of a theory of consistent resampling for non-bandlimited discrete signals. It is optimal in the sense that the input signals can always be reconstructed from the output, i.e. the resampling is informationally lossless.

- The development of techniques for designing the correction filter for consistent resampling systems when noise is not present. The design allows the use of more general interpolation and resampling functions. The choice of these functions are decoupled, leading to greatly improved flexibility.

- Our theory leads to consistent results in de-interlacing which are previously not achievable through the generalized sampling theory as pointed out in [9].

- The development of techniques to demodulate UWB impulse radio signals that is based on consistent resampling. The Pulse Position Modulated (PPM) signals are treated as non-uniformly sampled discrete signals. They are resampled according to the consistent resampling theory such that the positions of the pulses can be recovered.

- The application of the consistent resampling theory to image resizing and rotation. It is observed that the details of the image are better preserved than other linear approaches for the same computational complexity. It demonstrates the advantage of not having the bandlimited restrictions in processing high frequency components in the images.

- The proposal of a metric which evaluates the performance of resampling system. The metric measures the distance between two discrete signals in the frame of resampling and indicates the resampling performance in a Mean Square Error (MSE) manner. It provides a way by which different resampling algorithms can be compared directly and effectively.

- The design of procedures for designing resampling systems when noise is present based on our performance metric. Both discrete and continuous noises are considered. The system is optimal in the MSE sense such that the maximum error is minimized. This problem is formulated as a convex optimization problem, which can be solved efficiently by using existing numerical techniques.

- The design of the resampling system when noise is present for the channel estimation problem for Pilot Symbol Assisted Modulation (PSAM) digital communication schemes. It results in a lower Bit Error Rate (BER) for given Signal to Noise Ratio (SNR) than the optimal Wiener Filter. It shows that the consistent resampling theory is robust against noise.

- A bound on the rate of innovation for signals in shift invariant spaces is established.

- The minimum resampling rate above which an input sequence can be perfectly reconstructed from its resampled output for a given pair of interpolation and resampling functions is established. This completes the remaining issue in the consistent resampling theory.

1.5 Thesis Organization

This rest of this thesis is organized as follows. In Chapter 2, the major results of the sampling techniques for non-bandlimited signals are reviewed. In particular, the generalized sampling theory proposed in [4] as well as the sampling theory for signals with finite rate of innovation [7] and their related works are examined in detail. The use of non-ideal samplers and their dual functions in the sampling system are discussed. The principle of consistency which leads to optimal sampling results is introduced. Since a large part of the research reported in this thesis relates to resampling, the conventional theory and implementation of resampling for bandlimited signals are also reviewed.

In Chapter 3, the theory of consistent resampling for non-bandlimited signals is developed. The design formula for the correction filter to achieve consistent resampling is derived. The problem that previously existed when the generalized sampling theory is applied to de-interlacing discussed in [9] is overcome by the use of our resampling theory. The effectiveness of this theory is illustrated through two applications. The first one is the demodulation of UWB impulse radio signals. The second one is image resizing and rotation.

A quantitative metric is proposed in Chapter 4 to analyze the performance of the resampling system. The analysis is carried out in the frequency domain. This metric enables us to compare different resampling algorithms efficiently and effectively.

In Chapter 5, the metric defined in Chapter 4 is deployed to design resampling systems when noise is present. The noise may be introduced to the discrete signal as measurement error or to the interpolated continuous signal such as white noise present in the communication channel. Optimal resampling is achieved when the maximum distance between the input and output sequence is minimized. The effectiveness of this approach is illustrated through the examples of image de-noising and Pilot Symbol Assisted Demodulation (PSAM).

In Chapter 6, we return to the sampling theory for signals with finite rates of innovation. A bound on the rate of innovation for signals in shift invariant spaces is established. Based on this, the minimum sampling rate for which such signals can be perfectly reconstructed from the output of a resampling system is established.

Finally, the conclusions are presented in Chapter 7 and a number of possible future research directions are discussed.

Chapter 2

Review of Sampling and Resampling Techniques

In this chapter, existing theories on uniform sampling and resampling for bandlimited and non-bandlimited signals are reviewed. Sampling refers to the conversion of a continuous signal into a discrete signal (or sequence). The discrete sequence should be a good representation of the continuous signal in that the continuous signal can be perfectly reconstructed from the discrete representation. Resampling refers to the process where a discrete signal is to be converted to another discrete signal. The two signals should possess the same characteristics. Resampling is often necessary in digital signal processing systems where the sampling rate or the sample locations have to be changed.

The focus of this chapter is on (1) the mathematical foundation of sampling and resampling and (2) techniques for high performance sampling and resampling systems. The main purpose is to introduce the relevant background and put the work in this thesis in its context.

2.1 Bandlimited Signals

2.1.1 Shannon's Sampling Theory

A continuous signal $f(x)$ is integrable if $\int_x f(x)dx < \infty$. Such a signal has a Fourier Transform defined by

$$F(\Omega) = \int f(x)e^{-j\Omega x}dx \tag{2.1}$$

Throughout this thesis we shall use Ω to represent the frequency variable of a continuous signal. If $F(\Omega) = 0$ for $|\Omega| > \Omega_0$, then $f(x)$ is bandlimited with a bandwidth of Ω_0.

Shannon's uniform sampling theory states that $f(x)$ can be reconstructed perfectly from its samples $\{f[nT]\}_{n\in\mathbb{N}}$ which are spaced T seconds apart provided that the sampling rate $f_s = 1/T$ satisfies $f_s \geq \Omega_0/\pi$ [14, 15]. We shall denote the discrete sequence by $\mathbf{f}_T$ with the subscript T indicating the sampling period The samples in the sequence is denoted by $f_T[n]$. The lower bound Ω_0/π of the sampling rate is called the *Nyquist Rate*.

The continuous signal can be reconstructed from $\mathbf{f}_T$ by convolving f_T, defined by

$$f_T = \sum_n f_T[n]\delta(x - nT) \qquad n \in \mathbb{Z} \tag{2.2}$$

for all integer n with a properly dilated *sinc* function where

$$sinc(x) = sin(\pi x)/\pi x \tag{2.3}$$

and

$$\int_{-\infty}^{\infty} \delta(x)f(x)dx = f(0) \tag{2.4}$$

is the Dirac delta function. This convolution gives us the continuous signal

$$\begin{aligned} \widetilde{f}(x) &= f_T * sinc\left(\frac{x}{T}\right) \\ &= \int \sum_n f_T[n]\delta(\tau - nT) sinc\frac{1}{T}(x-\tau)dx \\ &= \sum_n f_T[n] sinc\left(\frac{x}{T} - n\right) \end{aligned} \tag{2.5}$$

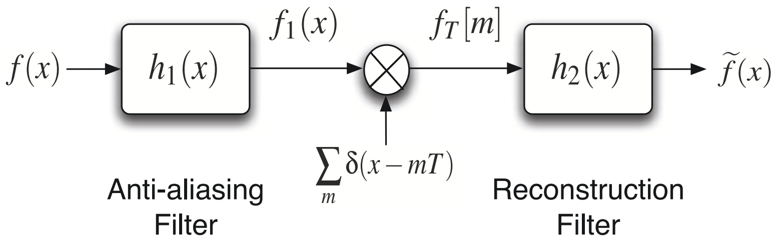

Figure 2.1: The sampling and reconstruction system.

where $*$ denotes the linear convolution operation. If the sampling rate is at least as high as the Nyquist rate, $\widetilde{f}(x) = f(x)$ and the reconstruction is said to be perfect.

If the sampling rate is lower than the Nyquist rate, aliasing occurs and perfect reconstruction is no longer possible. In practice, the continuous signal is usually low-pass filtered before sampling to avoid aliasing. A typical sampling system with an anti-aliasing prefilter is shown in Figure 2.1. The reconstruction filter is also a low-pass filter with a cutoff frequency not less than that of the anti-aliasing filter. The loss of the high frequency components due to pre-filtering is non-recoverable.

Shannon's sampling theorem has been extended in many different directions [16], including non-uniform sampling [17–24] and bandpass sampling [25, 26].

2.1.2 Resampling

A resampling system converts one discrete signal to another with as little change to the information carried by the signal as possible [12]. One of the main reasons for such conversions is to change the sampling rate of the signal. Another reason is to obtain values at locations where the input signal does not provide. Multirate signal processing [3] can be found in systems such as digital communication receivers, subband audio and image coders and decoders. Common signal processing operations that require resampling includes image resizing and image rotation. Some other applications can also be formulated as a resampling problem as we shall see in Chapters 3 to 5.

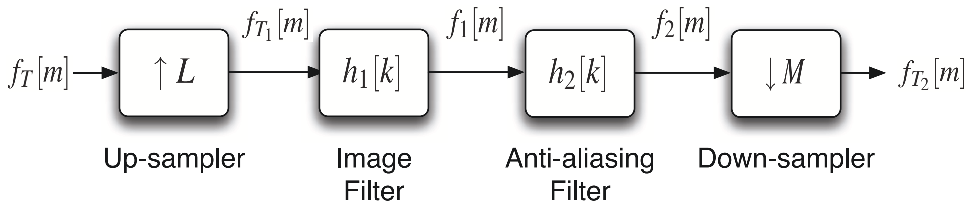

Figure 2.2: Block representation of the SRC system.

Conceptually, resampling is a two-step process. In the first step, the original discrete signal is converted into an analog signal. Then in the second step, this analog signal is sampled at a different rate and/or different locations to produce the output discrete signal. The complete process is illustrated in Figure 1.3.

In practice, resampling is performed entirely in the digital domain via digital filters. Figure 2.2 shows a sample rate conversion system that achieves a conversion ratio of $T/T_2 = L/M$, where T and T_2 are the sampling periods of the input and output signals respectively. L and M are integers and therefore L/M is a rational number. The first block is the up-sampler that changes the effective sampling period to T_1. The output of the up-sampler is given by

$$f_{T_1}[m] = \begin{cases} f_T[m/L], & m = nL,\ n \in \mathbb{Z} \\ 0 & otherwise \end{cases} \tag{2.6}$$

In the frequency domain, $F_{T_1}(\omega)$ is an L-fold compressed version of $F_T(\omega)$ where $F_{T_1}(\omega)$ and $F_T(\omega)$ are the Discrete Time Fourier Transforms (DTFT) of $f_{T_1}[m]$ and $f_T[m]$ respectively [3]. In this thesis, we use ω to denote the normalized digital frequency. The relationship with the analog frequency Ω is that $\omega = \Omega T$ for a sampling period of T. Figures 2.3.a shows the frequency spectra of the original continuous signal f (not shown in Figure 2.2). Figure 2.3.b and 2.3.c show the spectrum of f_T and $f_T[m]$ respectively. It can be noticed that f_T is the modulated signal of $f_T[m]$ and the discrete frequency ω is defined by the normalized continuous frequency Ω, $\omega = \Omega T$. Figure 2.3.d shows the spectra for $L = 3$.

The up-sampled signal $\mathbf{f}_{T_1}$ is then convolved with a digital filter with impulse response $\{h_1[k]\}_{k\in\mathbb{N}}$ called the image filter. This filter removes the duplicates of the spectrum so that only the spectrum in $[-\pi, \pi]$ remains. The resulting spectrum is shown in Figure 2.3.e.

The anti-aliasing filter ensures that $F_1(\omega)$ is bandlimited to $|\omega| < \frac{\pi}{M}$ to avoid aliasing in the down-sampled signal. Finally, the down-sampler reduces the sampling rate of $f_2[m]$ by a factor of M so that

$$f_{T_2}[m] = f_2[mM] \tag{2.7}$$

Figure 2.3.f shows the spectrum of $f_{T_2}[m]$.

While the performance of a sampling system can be quantitatively accessed by $\|\widetilde{f}(x) - f(x)\|_{L^2}$, a direct comparison between the input and output of a resampling system is generally not meaningful. This is because they are discrete sequence of numbers which are, in general, of different length. However, we may compare their Fourier spectra instead [27–29]. If the magnitude spectra of the input and output are the same, then the information in the input is preserved by the output.

A natural extension of the single channel resampling system is the multi-channel implementation. The spectrum of the input signal can be divided into equal or unequal sub-bands. This allows the subband signals to be processed at a rate lower than the Nyquist Rate of the original signal [30–34]. The multi-channel system has been further extended to allow non-uniformly sampled inputs and outputs. In [35], the conditions and average sampling rates for each channel is derived such that the resampling system is invertible.

However, due to the increased hardware cost to implement multichannel systems, researchers have been working toward a more general theory of sampling for signals with large bandwidths or effectively non-bandlimited signals.

2.2 Sampling Non-bandlimited Signals

Many signals encountered in practice are of finite duration and therefore are not bandlimited [36]. There are also signals that are designated to have very wide bandwidths,.

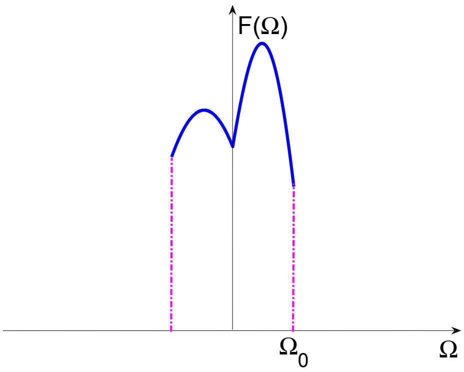

2.3.a: $F(\Omega)$

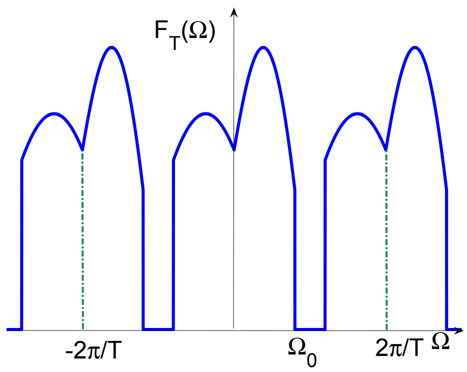

2.3.b: $F_T(\Omega)$

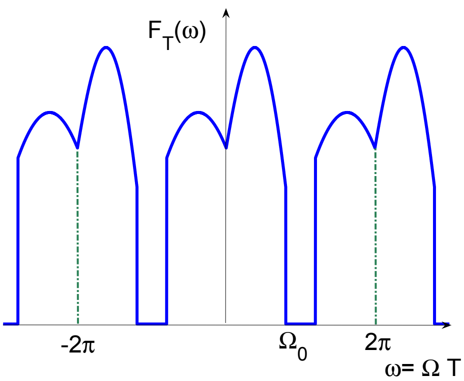

2.3.c: $F_T(\omega)$

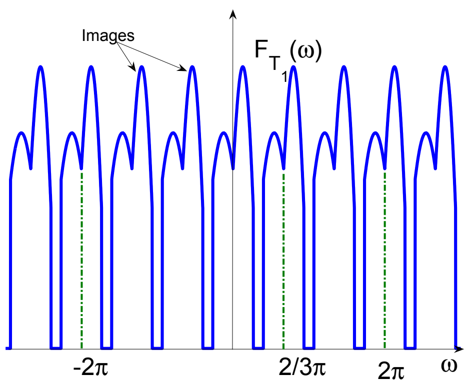

2.3.d: $F_{T1}(\omega)$

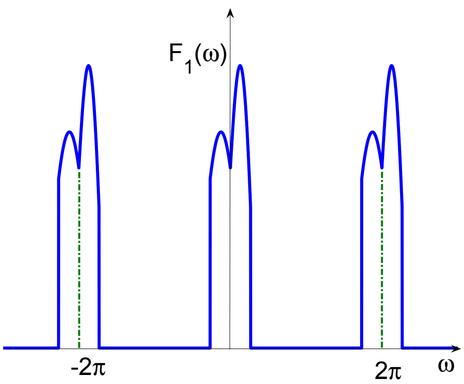

2.3.e: $F_1(\omega)$

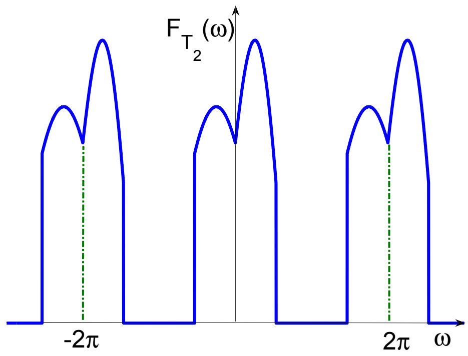

2.3.f: $F_{T2}(\omega)$

Figure 2.3: Spectra of the signals for the sample rate conversion system in Figure 2.2 for $L/M = 3/2$.

An example is the signals used for Ultra-Wide Band (UWB) radio communications which can have bandwidths up to several giga-Hertz [5, 37].

Shannon's sampling theorem tells us that aliasing is unavoidable when we sample a non-bandlimited signal. Thus whether such a signal can be perfectly reconstructed from its samples depends on what *a priori* information is available [38]. Suppose the signal can be represented by

$$f(x) = \sum_k c[k]\phi(x-k) \tag{2.8}$$

where ϕ is a known function. ϕ is called the *reconstruction* or *synthesis* function since $f(x)$ can be synthesized using (2.8). Given ϕ, $f(x)$ can be perfectly reconstructed from $c[k]$ if it belongs to the vector space spanned by $\{\phi(x-k)\}_{k\in\mathbb{Z}}$, denoted by

$$V^\phi = \left\{ h(x) = \sum_k c[k]\phi(x-k), \qquad \mathbf{c} \in \ell^2 \right\} \tag{2.9}$$

$\{\phi_k\}_{k\in\mathbb{Z}}$ is called a *frame* of V^ϕ [39]. In order for every $f(x) \in V^\phi$ to have a unique representation, the only restriction on the choice of ϕ is that the set $\{\phi(x-k)\}_{k\in\mathbb{Z}}$ satisfies the *Riesz condition* which states that for every finite scalar sequence $\{c[k]\}_{k\in\mathbb{Z}}$ the following admissibility condition must be satisfied [39]

$$A\|c[k]\|^2_{\ell^2} \leq \|\sum_k c[k]\phi(x-k)\|^2_{L^2} \leq B\|c[k]\|^2_{\ell^2} \tag{2.10}$$

where A and B are the Riesz bounds and $0 < A \leq B$. If $\{\phi(x-k)\}_{k\in\mathbb{Z}}$ satisfies (2.10), the set $\{\phi(x-k)\}_{k\in\mathbb{Z}}$ is admissible and is the *Riesz Basis* of the space V^ϕ. On the other hand, ϕ is referred as the *generating* function of V^ϕ.

The stability of the reconstruction in (2.8) is measured by the condition number α [8]. It is derived from the Riesz constants of ϕ

$$\alpha = \sqrt{\frac{B_\phi}{A_\phi}} \geq 1 \tag{2.11}$$

The smaller α is, the more stable the reconstruction process.

The way by which the samples $\{c[k]\}_{k\in\mathbb{Z}}$ in (2.8) are obtained depends on the properties of ϕ. The reconstruction process using (2.8) therefore also depends on ϕ and can be classified as [40] interpolation, quasi-interpolation or least square approximation.

2.2.1 Interpolation

A function ϕ is called a *Nyquist function* [41–43] if it satisfies

$$\phi(x) = \begin{cases} 1, & x = 0 \\ 0, & x = n, n \in \mathbb{Z}, n \neq 0 \end{cases} \tag{2.12}$$

Thus Nyquist functions have zero-crossings at integer values of x except for $x = 0$. An example is the *sinc* function used in Shannon's sampling theory. The samples $c[k]$ can be obtained by ideal sampling. That is,

$$c[k] = f(x)|_{x=k} \tag{2.13}$$

The continuous signal can be reconstructed from such samples by

$$\widetilde{f}(x) = \sum_{k} f[k]\phi(x-k) \tag{2.14}$$

This operation is bounded if $f(x)$ is sufficiently smooth [44]. It can be observed that $\widetilde{f}[k] = f[k]$ for all k.

2.2.2 Quasi-Interpolation

Quasi-interpolation relaxes the requirement on the integer crossing property of ϕ. A quasi-interpolating function ϕ of order $L = n+1$ is able to interpolate all polynomials up to order n [45]. A quasi-interpolant of order L must satisfy the Strang-Fix condition [46–48]. That is, the frequency response of ϕ must satisfy

$$\begin{cases} \Phi[2\pi k] = \delta[k] \\ \Phi^{(m)}[2\pi k] = 0, \quad k \in \mathbb{Z},\ m = 0, \cdots, L-1 \end{cases} \tag{2.15}$$

Here, the superscript m indicates the m-th derivative with respect to Ω. $\delta[k]$ is unit impulse sequence defined by

$$\delta[k] = \begin{cases} 1, & k = 0 \\ 0, & k \in \mathbb{Z}, k \neq 0 \end{cases} \tag{2.16}$$

The samples $c[k]$ can be obtained using ideal sampling, i.e. $c[k] = f(x)|_{x=k}$. The reconstructed signal $\widetilde{f}(x) = \sum_k f[k]\phi(x-k)$ satisfies $\widetilde{f}(x) = f(x)$ for all $f(x)$ that is a polynomial of order up to n.

2.2.3 Convolution Based Least Square

It has been shown in [39] that if $\{\phi(x-k)\}_{k\in\mathbb{Z}}$ form Riesz basis, then there exists a unique function ϕ_d such that for every pair of $\phi(x-k)$ and $\phi_d(x-k)$ for $k \in \mathbb{Z}$,

$$\langle \phi(x-l), \phi_d(x-m) \rangle = \delta[l-m] \qquad l, m \in Z \tag{2.17}$$

(2.17) is the *dual condition* and the functions ϕ and ϕ_d are said to be dual operator of each other. The set $\{\phi_d(x-k)\}_{k\in\mathbb{Z}}$ is also a Riesz basis for V^{ϕ}. For a generating function ϕ, let its sampled auto-correlation function be defined by

$$a_{\phi}[k] = \int \phi(x)\phi(x-k)dx \qquad k \in \mathbb{Z} \tag{2.18}$$

with Fourier transform

$$A_{\phi}(\omega) = \sum_k |\Phi(\Omega + 2k\pi)|^2 \tag{2.19}$$

Then the Fourier transform of ϕ_d is given by [49, 50]

$$\Phi_d(\Omega) = \frac{\Phi(\Omega)}{A_{\phi}(\omega)} \tag{2.20}$$

where $\omega = T\Omega$. If ϕ_d exists, then the signal has a unique representation in the space V^{ϕ}. An equivalent condition for this is that [51]

$$A \le A_{\phi}(\omega) \le B \quad \text{a.e.} \tag{2.21}$$

where a.e. means almost everywhere. Note that this is the same as the admissibility condition (2.10).

Figure 2.4 shows a block diagram of the sampling and reconstruction process with a general *sampling* or *acquisition* function φ and a *reconstruction* or *synthesis* function ϕ. The sequence of samples $\mathbf{c}$ are obtained by the inner product of the signal and $\varphi(x)$.

$$c[k] = \langle f(x), \varphi(x-k) \rangle \tag{2.22}$$

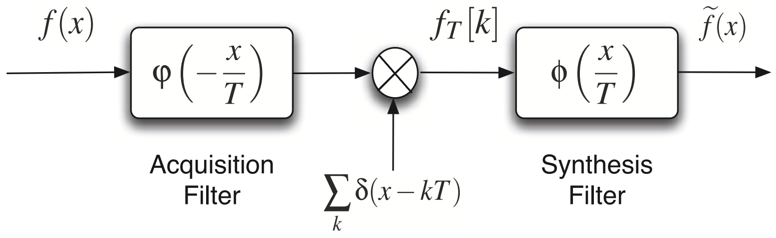

Figure 2.4: Block diagram of a sampling and reconstruction system with general acquisition and synthesis functions.

The reconstructed signal is therefore given by

$$\begin{aligned}\widetilde{f}(x) &= \sum_k c[k]\phi(x-k) \\ &= \sum_k \langle f(x), \varphi(x-k)\rangle\, \phi(x-k) \qquad (2.23)\end{aligned}$$

When $\varphi = \phi_d$, $\widetilde{f}(x)$ is a projection of the signal $f(x)$ onto V^ϕ [52–55]. If $f(x) \in V^\phi$, then $\widetilde{f}(x) = f(x)$ and the reconstruction is perfect.

So far we have assumed that the sampling interval is $T = 1$. A general formulation can be obtained by dilating the acquisition and synthesis function by the sampling interval. Therefore (2.22) and (2.23) can be rewritten as

$$\begin{aligned}c[k] &= \left\langle f(x), \varphi\left[\frac{1}{T}(x-kT)\right]\right\rangle \\ &= \left\langle f(x), \varphi\left(\frac{x}{T}-k\right)\right\rangle \qquad (2.24) \\ \widetilde{f}(x) &= \sum_k c[k]\phi\left[\frac{1}{T}(x-kT)\right] \\ &= \sum_k c[k]\phi\left(\frac{x}{T}-k\right) \qquad (2.25)\end{aligned}$$

Sampling performance is measured by how closely the reconstructed signal resembles the original signal. Quantitatively, it is given by $\|f(x) - \widetilde{f}(x)\|_{L^2}$. Intuitively, one would expect that reducing T will lead to a reduction in the reconstruction error. As $T \to 0$, the samples are taken almost continuously and therefore the reconstruction error vanishes.

The *approximation order* of a synthesis function measures the rate of decrease of the reconstruction error as $T \to 0$ [56, 57]. If the approximation order is L, then an upper bound on the reconstruction error is given by

$$\|f(x) - \widetilde{f}(x)\|_{L^2} \leq C \times T^L \tag{2.26}$$

where C is a positive constant. The approximation order of a function can be easily characterized [58]. One possible way to verify the approximation order is through the Strang-Fix condition defined by (2.15). Thus the condition is the same as for a quasi interpolation function of L.

More specifically, the performance for a given T can be quantitatively predicted by a formula in the frequency domain derived by [47, 59] as follows.

$$\eta_f(T) = \left[\frac{1}{2\pi}\int |F(\Omega)|^2 E_\phi(T\Omega)d\Omega\right]^{\frac{1}{2}} \tag{2.27}$$

where the error kernel $E_\phi(\Omega)$ is given by

$$E_\phi(\Omega) = \underbrace{1 - \frac{|\Phi(\Omega)|^2}{A_\phi(\omega)}}_{E_{\min}(\Omega)} + \underbrace{A_\phi(\omega)\,|\Psi(\Omega) - \Phi_d(\Omega)|^2}_{E_{\text{res}}(\Omega)} \tag{2.28}$$

$A_\phi(\omega)$ and $\Phi_d(\Omega)$ are given by (2.19) and (2.20) respectively.

When $\varphi = \phi_d$, the second term E_{res} of (2.28) is reduced to zero and the error is minimum. In this case, optimal reconstruction is achieved for a given ϕ and T. The reconstructed signal is the closest signal in V^ϕ to $f(x)$. It can be obtained by the solving the following minimization problem.

$$\arg_{\widetilde{f}(x)\in V_T^\phi} \min \left\| f(x) - \widetilde{f}(x) \right\|_{L^2} \tag{2.29}$$

The objective function is the L^2-norm which measures the reconstruction error in a mean squared sense since the difference is integrated over the whole x axis [60, 61]. Therefore it is a Mean Square Error (MSE). Other objective functions can be used. They are typically variations of the MSE which include Tikhonov regularization [62], normalized MSE [63], frequency weighted least square [64] and regularized least square [65]. A generalized L^P norm is studied in [66]. A criterion using the ℓ^2 norm of the difference between the samples of the original signal and of the reconstructed signal has also been proposed [67].

It is obvious that the sampling performance depends crucially on the choice of the acquisition and synthesis functions. Many functions have been studied thoroughly in relation to their potential applications in sampling. They include polynomials and rational functions [68, 69]. Spline functions which form a Riesz basis are systematically studied in [70]. Other functions such as the Gaussian function have also been used in sampling systems due to its efficiency in memory access and low computational complexity [71].

Besides reconstruction in the time domain, it is also possible to interpolate the frequency samples of a signal in the frequency domain. The spectral samples can be interpolated and then inverse transformed to obtain the time domain signal [72, 73]. Gabor representation has been used to reconstruct a signal from the samples of its windowed Fourier transform [74–77]. Chebyshev polynomials have been used to sample signals to their cosine transform [22, 78]. Signals can also be approached from the mixed time-frequency domain. This has been demonstrated by recent developments using wavelet functions [79, 80]. In this thesis, we concentrate on the use of B-splines and wavelet functions.

2.3 Special Acquisition and Synthesis Functions

2.3.1 Splines

Spline functions were first introduced in 1946, slightly ahead of Shannon's sampling theorem [81, 82]. However, it has only been intensively studied when mathematicians realized that these functions could be used to draw smooth curves. With the advent of digital computers, the use of splines has a tremendous impact on computer-aided design and computer graphics. It is mainly applied to the interpolation of samples of smooth functions [63, 68, 83–86]. More recently, it is also applied to signal processing [87–91].

Splines are smoothly connected piecewise continuous polynomials. For a spline of degree n, each segment is a polynomial of degree n. At the joints between segments, known as *knots*, the spline and its derivatives up to $(n-1)$-th order are continuous to ensure smoothness. Schoenberg [81] has found that splines $s(x)$ with uniform spacing are uniquely characterized by their B-spline expansion:

$$s(x) = \sum_{k \in \mathbb{Z}} c[k]\beta^n(x-k) \tag{2.30}$$

where $c[k]$ are the *B-spline coefficients* and $\beta^n(x)$ is the n-th order B-spline. The zero-th order B-spline is given by the rectangular function

$$\beta^0(x) = \begin{cases} 1, & |x| < \frac{1}{2} \\ 0, & \frac{1}{2} < |x| \end{cases} \tag{2.31}$$

as shown in Figure 2.5.a. The frequency response of $\beta^0(x)$ is given by

$$B^0(\Omega) = sinc\left(\frac{\Omega}{2\pi}\right) \tag{2.32}$$

The n-th order B-spline can be obtained recursively by

$$\beta^n(x) = \beta^0 * \beta^{n-1}(x) \qquad n \geq 1 \tag{2.33}$$

Using the convolution property of Fourier transform, the frequency response of the n-th order B-spline is given by

$$B^n(\Omega) = \left[B^0(\Omega)\right]^n = \left[sinc\left(\frac{\Omega}{2\pi}\right)\right]^n \tag{2.34}$$

B-splines up to the third order are shown in Figure 2.5. It can be observed that B-splines are symmetrical about y axis. Second and higher order B-splines have non-increasing bell shapes. Spline functions are of finite local support. An n-th order B-spline has support

$$\mathcal{B}_{\beta^n} = \left[-\frac{n+1}{2}, \frac{n+1}{2}\right] \tag{2.35}$$

B-splines of orders higher than 1 are non-Nyquist functions. Therefore if a signal can be represented as (2.30), its ideal samples $s[k] = s(x)|_{x=k}$ are not the same as the

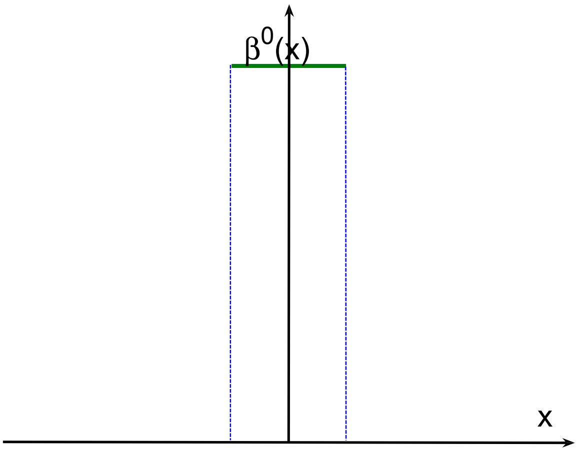

2.5.a: β^0

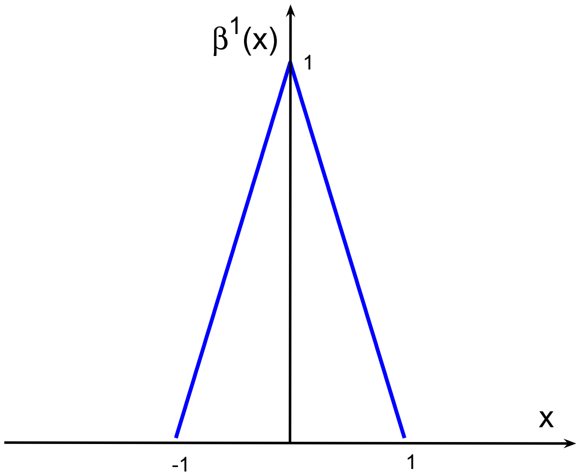

2.5.b: $\beta^1 = \beta^0 * \beta^0$

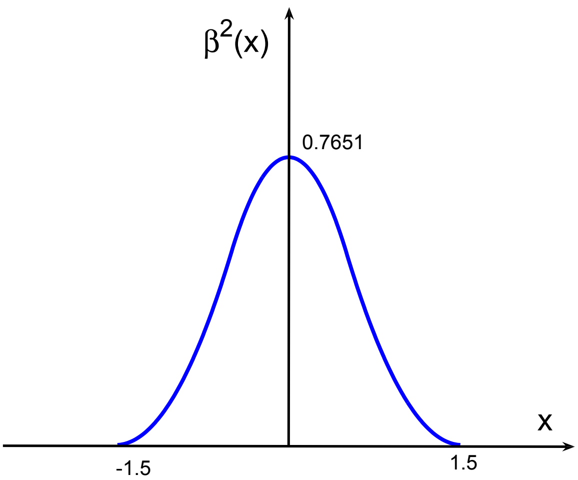

2.5.c: $\beta^2 = \beta^1 * \beta^0$

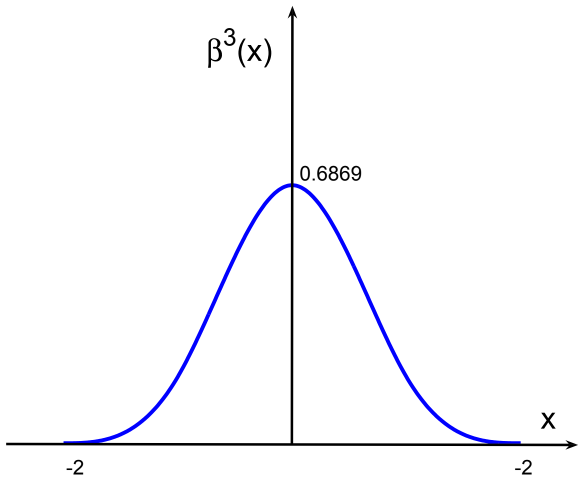

2.5.d: $\beta^3 = \beta^2 * \beta^0$

Figure 2.5: Zero-th to third order B-spline functions.

	ϕ	$B^n(\omega)$	$B^n(z)$	$A_{\beta^n}(\omega)$
$n=0$	β^0	1	1	1
$n=1$	β^1	1	1	$1-\frac{2}{3}\sin^2\left(\frac{\omega}{2}\right)$
$n=2$	β^2	$1-\frac{1}{2}\sin^2\left(\frac{\omega}{2}\right)$	$\frac{1}{8}(z+6+z^{-1})$	$1-\sin^2\left(\frac{\omega}{2}\right)+\frac{2}{15}\sin^4\left(\frac{\omega}{2}\right)$
$n=3$	β^3	$1-\frac{2}{3}\sin^2\left(\frac{\omega}{2}\right)$	$\frac{1}{6}(z+4+z^{-1})$	$1-\frac{4}{3}\sin^2\left(\frac{\omega}{2}\right)+\frac{2}{3}\sin^4\left(\frac{\omega}{2}\right)-\frac{4}{315}\sin^6\left(\frac{\omega}{2}\right)$

Table 2.1: Approximation of the frequency responses of B-spline up to order 3.

B-spline coefficients $c[k]$. Nevertheless, $c[k]$ can be obtained from $s[k]$ through the *Direct Transform* [92, 93]:

$$c[k] = \left((b^n)^{-1} * s\right)[k] \tag{2.36}$$

where $(\mathbf{b}^n)^{-1}$ denotes the convolution inverse of the discrete B-spline sequence $\mathbf{b}^n$. The discrete B-spline sequence is given by

$$b^n[k] = \beta^n(x)|_{x=k} \tag{2.37}$$

or in the frequency domain

$$B^n(\omega) = \sum_k b^n[k]e^{-j\omega} \tag{2.38}$$

and

$$(\mathbf{b}^n)^{-1} \qquad \xrightarrow{FT} \qquad \frac{1}{B^n(e^{j\omega})} \tag{2.39}$$

The frequency response of the discrete B-spline is also given by

$$B^n(\omega) = \sum_k B^n(\Omega + 2\pi k) \tag{2.40}$$

with $\omega = \Omega$. In [47], $B^n(\omega)$ can be approximated by the simple expressions listed Table 2.1 for $n \leq 3$. Alternatively, the values of $b^n[k]$ can be obtained by evaluating $\beta^n(x)$ at $x = k$. Thus the z transform of discrete B-splines can be obtained easily.

Substituting (2.36) into (2.30), $s(x)$ can be reconstructed from its ideal samples in the subspace V^{β^n} by

$$s(x) = \sum_{k\in\mathbb{Z}} \left((b^n)^{-1} * s\right)[k]\beta^n(x-k) \tag{2.41}$$

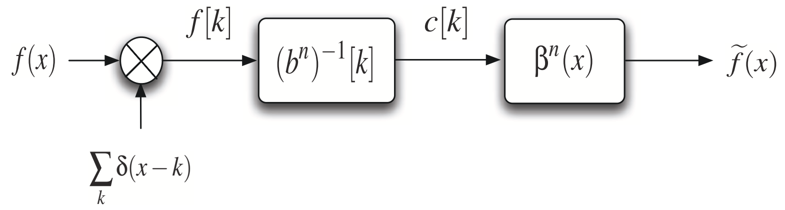

Figure 2.6: The sampling system using B-spline as synthesis filter

Thus a sampling system based on B-splines for sampling and reconstruction will have a structure as shown in Figure 2.6. The sampling function φ is the sequence $(\mathbf{b}^n)^{-1}$. Therefore its frequency response is given by

$$\Psi(\Omega) = \frac{1}{B^n(\omega)} \tag{2.42}$$

with $\Omega = \omega$. The synthesis function is $\phi = \beta^n$.

The performance of this sampling system can be derived from (2.28). It can be shown that the autocorrelation function $a_{\beta^n}[k]$ of β^n is related to $b^n[k]$ by

$$a_{\beta^n}[k] = b^{2n}[k] \tag{2.43}$$

Using the approximations of $B^n(\omega)$ given in Table 2.1, $A_{\beta^n}(\omega)$ can be derived accordingly. The values of $B^n(z)$ and $A_{\beta^n}(\omega)$ for $n \leq 3$ are also shown in Table 2.1.

There are several advantages in using splines for sampling systems. First, the order n of the splines is directly related to the approximation order L by $L = n+1$. Furthermore, the best kernels that are able to achieve minimum approximation error, i.e. minimum C in (2.26), can be expressed using derivatives of B-splines of approximation order L [40]. Thus splines are very good for approximating signals.

Second, it has been shown that among all the functions with the same order of approximation, spline functions have the minimum support [16, 94, 95]. These function are referred as Maximum Order Minimum Support (*MOMS*) functions. To compute the value of a signal at location x_k using an interpolation function of support $\mathcal{B} = [u, v]$, samples within the range $[x_k + u, x_k + v]$ are used. For a function of approximation order

L, the support of ϕ is lower bounded by $|\mathcal{B}| = |v - u| \geq L$ [48, 96]. From (2.35), we can see that the support of B-splines of approximation order $L = n + 1$ is equal to the lower bound L. Therefore splines are efficient in sampling and reconstruction computations.

Third, sampling using B-splines in the discrete domain is easy and straightforward [97, 98]. Since B-splines are symmetric with respect to $x = 0$, the discrete B-splines $\mathbf{b}^n$ are also symmetric. The inverse filter $(\mathbf{b})^{-1}$ can be easily implemented. Furthermore, differentiation and integration of a signal can be performed on its B-spline coefficients and processed in the digital domain efficiently [68, 87, 92, 93].

Many variations of B-splines have been used in the sampling literature. Cardinal splines is one of them [99–101]. The reconstruction process of (2.41) can be expressed as

$$\begin{aligned} s(x) &= \sum_{k \in \mathbb{Z}} \left((b^n)^{-1} * s\right)[k]\beta^n(x-k) \\ &= \sum_m s[m] \left(\sum_k (b^n)^{-1}[k]\beta^n(x-k)\right) \\ &= \sum_m s[m]\eta^n(x-m) \end{aligned} \tag{2.44}$$

where

$$\eta^n(x) = \sum_{k \in Z} (b^n)^{-1}[k]\beta^n(x-k) \tag{2.45}$$

is called the *cardinal splines*. Figure 2.7 shows a third order cardinal spline. All cardinal splines are Nyquist functions. As the order n increases, the cardinal splines behave more and more like the *sinc* function.

The univariate polynomial splines can be used to reconstruct signals in the weak Chebyshev space [102]. A combination of different splines can also be employed [42, 84, 103–105]. In [106], it has been demonstrated that the use of splines to minimize MSE when noise is present simulates the optimal Wiener filter. It can also be modified to suit a different coordinate system when applied to multidimensional systems. For instance, in [107] the splines are used to sample signals on a hexagonal grid instead of the rectilinear grid. They are also used in multidimensional spaces covered by polygons [108]. Other splines include cardinal polysplines [99].

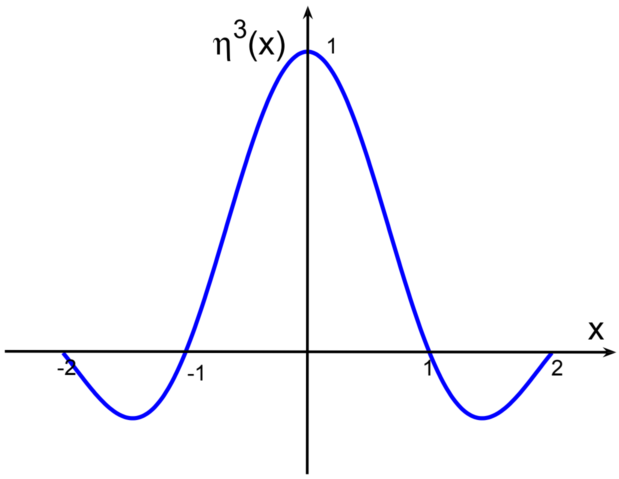

Figure 2.7: The sampling system using B-spline as synthesis filter

2.3.2 Wavelets

Similar to splines, wavelet functions also have local support. It has been used to perform time-frequency analysis by separating the signal into a range of time and frequency scales [109,110]. Based on a function $\phi(x) \in L^2(\mathbb{R})$, a wavelet frame $\{\phi_j^{a,b}\}_{j\in\mathbb{Z}}$ is composed of the functions

$$\begin{aligned} \phi_j^{a,b} &= (S_{kb}D_{a^{-j}}\phi)(x) && (2.46)\\ &= \frac{1}{a^{j/2}}\phi(a^j x - kb) \qquad j,k \in \mathbb{Z} && (2.47) \end{aligned}$$

Here, D_u denotes the dilation operation defined by

$$D_u\phi(x) = \phi\left(\frac{x}{u}\right) \tag{2.48}$$

and S denotes the shift operation

$$S_v\phi(x) = \phi(x - v) \tag{2.49}$$

The constants a and b are chosen such that the set of functions form a frame of its span. The term *mother wavelet* refers to the function ϕ for which the set $\{\phi_{j,k}\}$ of functions

$$\phi_{j,k}(x) = 2^{j/2}\phi(2^j x - k) \qquad j,k \in \mathbb{Z} \tag{2.50}$$

is an orthonormal basis for $L^2(\mathbb{R})$ [111, 112].

The sampling and reconstruction of signals using wavelets is carried out in a similar manner as the convolution least squares approach described in Section 2.2.3. The approximation power of wavelets is discussed in [113]. In [114], the conditions under which the underlying signals can be reconstructed from the wavelet samples are studied.

The wavelet transform is a powerful tool because it manages to represent both transient and stationary behaviors of a signal with only a few transform coefficients [115,116]. A distinctive property of the wavelet transform is its ability to analyze a signal at different resolution or scales. Let the space spanned by $\{S_k\phi\}_{k\in\mathbb{Z}}$ be denoted by V_0, where

$$V_0 = \left\{ h(x) \,\middle|\, h(x) = \sum_k c[k]\phi(x-k), \qquad \sum_k |c[k]|^2 < \infty \right\} \tag{2.51}$$

V_j is the span of $\{D_jS_k\phi\}_{k\in\mathbb{Z}}$ for $j \in \mathbb{Z}$. Multiresolution Analysis (MRA) [117] involves a sequence of closed subspaces V_j and a *scaling function* $\psi(x)$ such that

(i) $\cdots \subset V_{-1} \subset V_0 \subset V_1 \subset \cdots$

(ii) $\bigcup_{j\in\mathbb{Z}} V_j = L^2(\mathbb{R})$

(iii) $\bigcap_{j\in\mathbb{Z}} V_j = 0$

(iv) $f(x) \in V_j$ if and only if $f(2x) \in V_{j+1}$

(v) $\psi \in V_0$ and $\{\psi(x-k)\}_{k\in\mathbb{Z}}$ form an orthonormal basis for V_0

The *mother* wavelet ϕ is related to the scaling function ψ by

$$\phi(x) = \sum_k (\sqrt{2})\bar{c}[1-k](-1)^k\psi(2x-k) \tag{2.52}$$

where $\bar{c}$ denotes the complex conjugate of c. The coefficients $c[k]$ are obtained by the inner product

$$c[k] = \left\langle \psi(x), \sqrt{2}\psi(2x-k) \right\rangle \qquad k \in \mathbb{Z} \tag{2.53}$$

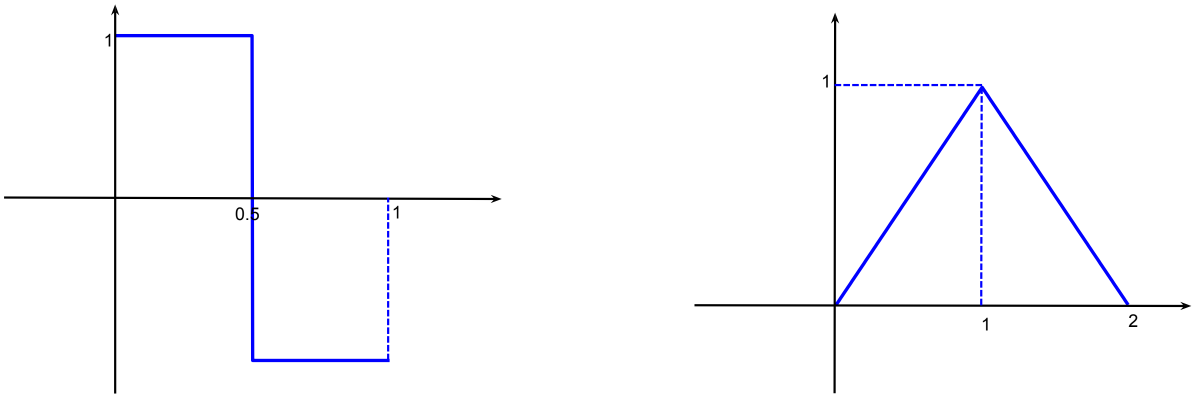

2.8.a: The Haar Mother Wavelet ϕ

2.8.b: The Franklin Mother Wavelet ϕ

Figure 2.8: The mother function for some well known wavelets

Common examples of mother wavelets include the Haar function and the Franklin wavelets as shown in Figure 2.8. Compared with Figure 2.5, the Haar and Franklin functions appear similar to the zero-th and first order splines respectively. This fact has inspired the development of spline induced wavelets [118, 119].

Wavelet transforms have found much application in data compression [112, 120, 121]. Large compression ratios can be achieved if the signal of interest contains unevenly spread frequency components [122]. Application of wavelet to sampling has been mainly via discrete wavelets [79, 80, 116, 121]. The nature of the wavelet transform also makes it easy to be extended to multirate system [123, 124].

2.4 Consistent Sampling

In Section 2.2.3, we said that if the acquisition function $\varphi = \phi_d$ is a dual function of the synthesis function ϕ, then perfect reconstruction can be achieved. However, there are cases when the acquisition function is given *a priori* and $\varphi \neq \phi_d$. In this case, the term E_{res} in (2.28) will not be zero due to reconstruction errors such as distortion and aliasing. This may lead to significant loss in sampling performance. A generalized sampling theory has been proposed to address this problem [4, 125, 126].

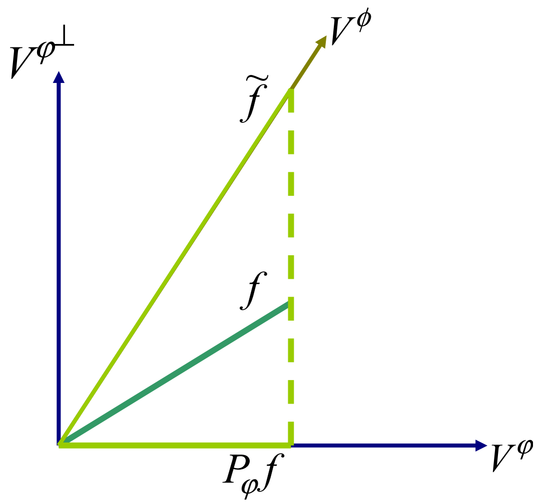

Figure 2.9: Geometric interpretation of the effect of the correction filter (taken from [1]).

This generalized sampling theory is based on the concept of *consistent sampling*. Since the original signal $f(x)$ is non-bandlimited, in general, the reconstructed signal $\widetilde{f}(x)$ will not be the same as $f(x)$. However, if $\widetilde{f}(x)$ is sampled by the same acquisition function φ as $f(x)$ and results in the same sampled sequence as that for $f(x)$, then we say that the sampling is consistent. In other words, we obtain the same set of measurements in the subspace V^{φ} from both $f(x)$ and $\widetilde{f}(x)$. Mathematically, consistent sampling requires that

$$\langle f(x), \varphi(x-k) \rangle = \left\langle \widetilde{f}(x), \varphi(x-k) \right\rangle \tag{2.54}$$

for all $k \in \mathbb{Z}$. Without loss of generality, we assume that the sampling period $T = 1$.

A geometric interpretation is provided by [1] and Figure 2.9 helps us to visualize what consistent sampling aims to achieve. Essentially, we want to obtain a $\widetilde{f}(x) \in V^{\phi}$ such that $\widetilde{f}(x)$ and $f(x)$ have the same orthogonal projection onto V^{φ}. For arbitrary acquisition and synthesis filters, a digital correction filter $q[n]$ is required to make this happen. A generic consistent resampling system has a structure as shown in Figure 2.10.

Using the notations in Figure 2.10, the reconstructed signal in V^{ϕ} is given by

$$\widetilde{f}(x) = \sum_{k} c_{2T}[k]\phi(x-k) \tag{2.55}$$

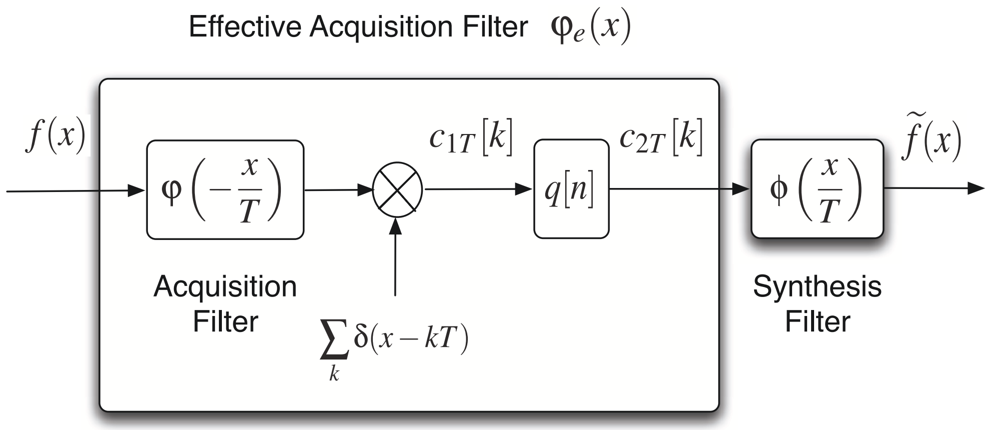

Figure 2.10: Generalized sampling and reconstruction.

where $\mathbf{c}_{2T}$ is obtained from the samples $\mathbf{c}_{1T}$ of $f(x)$ in V^{φ} by

$$c_{2T}[k] = (\mathbf{c}_{1T} * \mathbf{q})[k] \tag{2.56}$$

The correction filter transforms $\mathbf{c}_{1T}$ to $\mathbf{c}_{2T}$ such that the desired $\widetilde{f}(x)$ can be obtained.

Substituting (2.55) and (2.56) into (2.54), we have

$$\begin{aligned} c_{1T}[k] &= \left\langle \sum_m c_{2T}[m]\phi(x-m), \varphi(x-k) \right\rangle \\ &= \sum_m (\mathbf{c}_{1T} * \mathbf{q})[m] \langle \phi(x-m), \varphi(x-k) \rangle \end{aligned} \tag{2.57}$$

Let $a_{\phi\varphi}[k]$ denote the sampled cross correlation between the synthesis filter $\phi(x)$ and the acquisition filter $\varphi(x)$. It is given by

$$a_{\phi\varphi}[k] = \langle \phi(x-k), \varphi(x) \rangle \tag{2.58}$$

and (2.57) can be expressed as

$$\begin{aligned} c_{1T}[k] &= \sum_m (\mathbf{c}_{1T} * \mathbf{q})[m] a_{\phi\varphi}[k-m] \\ &= (\mathbf{c}_{1T} * \mathbf{q} * \mathbf{a}_{\phi\varphi})[k] \end{aligned} \tag{2.59}$$

which implies that

$$(\mathbf{q} * \mathbf{a}_{\phi\varphi})[k] = \delta[k] \tag{2.60}$$

In the frequency domain, (2.59) becomes

$$C_{1T}(\omega) = C_{1T}(\omega)Q(\omega)A_{\phi\varphi}(\omega) \tag{2.61}$$

Thus the frequency response of the correction filter is given by

$$Q(\omega) = A_{\phi\varphi}^{-1}(\omega) \tag{2.62}$$

Similar to condition (2.21) for Φ_d in (2.20), to ensure the existence and stability of the correction filter, the response $A_{\phi\varphi}(\omega)$ is required to satisfy

$$0 \leq M_1 \leq |A_{\phi\varphi}(\omega)| \leq M_2 < \infty \tag{2.63}$$

almost everywhere (a.e.), where M_1 and M_2 are two positive constants.

It can be proved that consistent sampling is optimal for arbitrary pairs of φ and ϕ [127, 128]. From (2.56),

$$\begin{aligned} c_{2T}[k] &= (\mathbf{c}_{1T} * \mathbf{q})[k] \\ &= \sum_n \langle f(x), \varphi(x-n) \rangle q[k-n] \\ &= \int f(x) \left(\sum_n \varphi(x-n) q[k-n] \right) dx \\ &= \langle f(x), \varphi_e(x-k) \rangle \end{aligned} \tag{2.64}$$

where

$$\varphi_e(x) = \sum_k q[k]\varphi(x-k) \tag{2.65}$$

is the effective acquisition filter which is a combination of the acquisition filter and the correction filter. The inner product of $\varphi_e(x-k)$, $\phi(x-m)$ is given by

$$\begin{aligned}
\langle \varphi_e(x-k), \phi(x-m)\rangle &= \left\langle \sum_n q[n]\varphi\left(x-n-k\right), \phi(x-m)\right\rangle \\
&= \sum_n q[n]\left\langle \varphi\left(x-n-k\right), \phi(x-m)\right\rangle \\
&= \sum_n q[n]a_{\phi\varphi}[m-n-k] \\
&= \left(\mathbf{q} * a_{\phi\varphi}\right)[m-k] \qquad (2.66)
\end{aligned}$$

Based on (2.60), (2.66) can be reduced to

$$\langle \varphi_e(x-k), \phi(x-m)\rangle = \delta[m-k] \qquad (2.67)$$

Therefore, φ_e and ϕ are dual functions and hence $\varphi_e = \phi_d$. Thus (2.64) is equivalent to

$$c_{2T}[k] = \langle f(x), \phi_d(x-k)\rangle \qquad (2.68)$$

Reconstructing $\widetilde{f}(x) \in V^{\phi}$ using $\mathbf{c}_{2T}$ reduces to the convolution based least square approach in Section 2.2.3. Therefore, consistent sampling achieves optimal performance for arbitrary φ and ϕ. When $\varphi = \delta(x)$ and $\phi = sinc(x)$, consistent sampling reduces to Shannon's unform sampling theory.

However, consistent sampling may no longer be optimal when noise is present. In [128–131], the effects of noise in a generalized sampling system is studied for signals that belong to a subspace $\mathcal{U}$. It has been shown that though consistent sampling achieves unbiased performance, i.e. the performance is independent of the input signal, the actual error is not necessarily small. It has been suggested that algorithms could be classified as *admissible* or *dominating* according to the performance metric used. An algorithm is said to dominate another if its performance as measured by the metric is never worse than the other. An algorithm that is not dominated by any other is said to be admissible.

An important result obtained from the analysis is that for bounded signals, the solution for the minimax problem

$$\mathbf{q} = \arg \inf_{\text{all possible } \mathbf{q}} \sup_{f \in \mathcal{U}} \|\widetilde{f} - f\|_{L^2} \tag{2.69}$$

is admissible and always achieves smaller actual error than any other approach. Therefore, the solution to this problem gives us the optimal correction filter. When sampling is free of noise, the solution of (2.69) is the consistent correction filter.

2.5 Sampling Signals with Finite Rates of Innovation

The sampling methods discussed in Sections 2.2 and 2.4 view Shannon's reconstruction formula

$$f(x) = \sum_n f_T[n] sinc\left(\frac{x}{T} - n\right) \tag{2.70}$$

as a special case with *sinc* as the synthesis function. $f(x)$ is projected onto the subspace generated by the *sinc* function. Another possible interpretation of (2.70) for a bandlimited signals is that it requires a minimum of $1/T$ number of samples per unit of time to uniquely define it. The degree of freedom per unit time for such a signal is therefore $1/T$. In [7], this is called the *rate of innovation* (RI) and is denoted by ρ. Shannon's sampling theory can therefore be viewed as a sampling theory for signals with an RI of $1/T$.

By allowing synthesis functions other than *sinc* in (2.70), signals with finite RI can be expressed as

$$\widetilde{f}(x) = \sum_k c[k]\phi\left[\frac{1}{T}(x - kT)\right] \tag{2.71}$$

as given by (2.25) in Section 2.2. Clearly the RI of this signal is $\rho = 1/T$ if ϕ is known. By allowing arbitrary delays x_k rather than periodic delays kT and denoting the coefficients by c_k instead, (2.71) becomes

$$f(x) = \sum_k c_k\phi\left[\frac{1}{T}(x - x_k)\right] \tag{2.72}$$

The only degrees of freedom of $f(x)$ are the x_k's and the c_k's. Let $C_f(x_a, x_b)$ be a counting function that indicates the degree of freedom within the time period $[x_a, x_b]$. Then RI can be formally defined as

$$\rho = \lim_{\tau \to \infty} \frac{1}{\tau} C_f\left(-\frac{\tau}{2}, \frac{\tau}{2}\right) \tag{2.73}$$

If $\rho < \infty$, then the signal has a finite RI.

Recently, a new sampling technique for signals with finite RI has been proposed [7, 132–137]. In this thesis, we shall refer to this method as *innovation sampling*.

In [7], the sampling of periodic analog signals such as streams of Diracs and its derivatives are considered. A periodic signal $f(x)$ can be expressed as a Fourier series.

$$f(x) = \sum_{m \in Z} F[m] e^{j(2\pi m x/\tau)} \tag{2.74}$$

It was shown that these signals can be reconstructed from their projections onto lowpass subspaces of appropriate dimensions. For example, consider a stream of Diracs:

$$f(x) = \sum_k c_k \delta(x - x_k) \tag{2.75}$$

If it is a stream of K Diracs with periodicity τ, then $c_{k+K} = c_k$ and $x_{k+K} = x_k + \tau$. Thus its RI is $\rho = 2K/\tau$. The signal can be represented as

$$f(x) = \sum_{k=0}^{K-1} c_k \sum_{n \in Z} \delta(x - x_k - n\tau) \tag{2.76}$$

From Poisson's summation formula, (2.76) can be rewritten as

$$\begin{aligned} f(x) &= \sum_{k=0}^{K-1} \frac{1}{\tau} \sum_{m \in Z} e^{j(2\pi m(x - x_k)/\tau)} \\ &= \sum_{m \in Z} \frac{1}{\tau} \left(\sum_{k=0}^{K-1} c_k e^{-j(2\pi m x_k/\tau)} \right) e^{j(2\pi m x/\tau)} \end{aligned} \tag{2.77}$$

Compare (2.77) with (2.74), we notice that

$$F[m] = \frac{1}{\tau} \left(\sum_{k=0}^{K-1} c_k e^{-j(2\pi m x_k/\tau)} \right) \tag{2.78}$$

are the Fourier series coefficients of $f(x)$.

To project $f(x)$ onto a lowpass subspace, choose the sampling kernel to be an ideal lowpass filter with impulse response

$$h_B(x) = Bsinc(Bx) \tag{2.79}$$

with $B \geq \rho$. Take N uniform samples at $x = nT$ where $N \geq 2\lfloor B\tau/2 \rfloor + 1$, we have

$$y_T[n] = \langle f(x), h_B(x - nT) \rangle \tag{2.80}$$

for $n = 0, \cdots, N-1$. Using (2.74), (2.80) becomes

$$\begin{aligned} y_T[n] &= \sum_m X[m] \left\langle h_B(x - nT), e^{j(2\pi m x/\tau)} \right\rangle \\ &= \sum_m X[m] \int h_B(x - nT) e^{j(2\pi m x/\tau)} dx \end{aligned} \tag{2.81}$$

The Fourier transform of h_B is given by

$$H_B(\Omega) = \int h_B(x) e^{-j2\pi\Omega x} dx \tag{2.82}$$

Let $\Omega = -m/\tau$, it becomes

$$H_B\left(-\frac{2\pi m}{\tau}\right) = \int h_B(x) e^{j2\pi m x/\tau} dx \tag{2.83}$$

Since $h_B(x)$ is a symmetric function, H_B is also symmetric and so

$$H_B(-\frac{2\pi m}{\tau}) = H_B(\frac{2\pi m}{\tau}) \tag{2.84}$$

Thus,

$$H_B\left(\frac{2\pi m}{\tau}\right) = \int h_B(x) e^{j2\pi m x/\tau} dx \tag{2.85}$$

Substituting (2.85) into (2.81), we obtain

$$\begin{aligned} y_T[n] &= \sum_m X[m] H_B\left(\frac{2\pi m}{\tau}\right) e^{j(2\pi m n T/\tau)} \\ &= \sum_{m=-M}^{M} X[m] e^{j(2\pi m n T/\tau)} \end{aligned} \tag{2.86}$$

since H_B defines a low pass filter with a bandwidth of $[-B/2, B/2]$. When T is a divisor of τ and the N equations are of rank $2M+1$, this system of equations is invertible and $\mathbf{y}_T$ is simply the inverse Discrete Time Fourier Transform (DTFT) of $F[m]$. Therefore $F[m]$ can be obtained by taking the DTFT of the N samples of $\mathbf{y}_T$.

The key part of the reconstruction of $f(x)$ using $\mathbf{y}_T$ (or equivalently $F[m]$) is to identify the innovative parts, x_k and c_k, of the signal from these samples. This can be solved by an annihilation filter, which is well known in the field of spectral analysis. Denote a finite annihilation filter by

$$A(z) = \sum_{m=0}^{K} a[m] z^{-m} \tag{2.87}$$

such that

$$A(z) = \prod_{k=0}^{K-1} \left(1 - e^{-j(2\pi x_k/\tau)} z^{-1}\right) \tag{2.88}$$

$A(z)$ has zeros at $u_k = e^{-j(2\pi x_k/\tau)}$. Now, $F[m]$ in (2.78) is a summation of K exponentials. Each of these exponentials can be zeroed out by one of the roots of $A(z)$. Hence

$$\sum_m a[m] * \sum_m F[m] = 0 \tag{2.89}$$

Consequently, a Yule-Walker system can be formulated to solve for $a[m]$. Using $A(z)$ in the form given by (2.88), the K locations $\{x_k\}_{k=0}^{K-1}$ can be identified from the roots u_k.

The weights c_k can be obtained from $F[m]$ and u_k. For $m = 0, \ldots, K-1$, (2.78) can be expressed in matrix form as

$$\begin{bmatrix} F[0] \\ F[1] \\ \vdots \\ F[K-1] \end{bmatrix} = \frac{1}{\tau} \begin{bmatrix} 1 & 1 & \cdots & 1 \\ u_0 & u_1 & \cdots & u_{K-1} \\ \vdots & \vdots & \cdots & \vdots \\ u_0^{K-1} & u_1^{K-1} & \cdots & u_{K-1}^{K-1} \end{bmatrix} \begin{bmatrix} c_0 \\ c_1 \\ \vdots \\ c_{K-1} \end{bmatrix} \tag{2.90}$$

which is a Vandermonde system that can be solved for the c_k's. With x_k and c_k, $f(x)$ can be perfectly reconstructed from the uniform samples $\mathbf{y}_T$.

This reconstruction process involves root finding and solving a Yule-walker system and a Vandermonde system. When noise is present, one or more of these systems can become ill-conditioned and therefore the solutions obtained may not be stable or accurate. The effects of noise in the system is studied in [133] and a more robust method with better numerical conditioning in the presence of noise is proposed.

In [134, 136], the use of sampling kernels with finite support is studied. The authors argued that the sampling kernel h_B in (2.79) is of infinite support and usually non-realizable. Infinite support of the kernel also leads to high complexity and instablity of the reconstruction scheme. The use of wavelets in innovation sampling has also been explored in [137].

An independent approach similar to innovation sampling is presented in [138]. The authors suggested that it is possible to sample a certain groups of the signals in the same way as suggested by innovation sampling: the sampling kernel is $h_B = BsincBx$ and the rate $1/T = 1/B$. Instead of periodic signals, the group of perfect reconstructible signals is defined to be to sample a certain group of signals whose frequency response is in the form

$$F(\Omega) = G(T\Omega)S(T\Omega) \tag{2.91}$$

where $G(\Omega)$ is periodic and $S(\Omega)$ is a slow varying function where for all $\lambda > 0$,

$$\lim_{\Omega \to +\infty} \frac{S(\lambda\Omega)}{S(\Omega)} = 1 \tag{2.92}$$

The signal is first modulated by $e^{j2\pi xa}$. If a is big enough, the samples contain necessary information to reconstruct $f(x)$. The reconstruction procedure varies depending on the the property of $S(\Omega)$. Nevertheless, the principle underlying this approach is similar to that of Innovation sampling. It has been shown that when $a \to \infty$, the reconstruction error approaches to 0.

However, there are two problems associated with innovation sampling that remain unsolved. The first one is related to the RI of a signal. The RI of a signal in the form of

(2.72) can be obtained if we have exact knowledge of ϕ. This is generally not true for an arbitrary signal. The second problem is that although the lower bound on the sampling rate is specified by the RI, it is unclear how a proper acquisition function (sampling kernel) should be chosen. These two problems are tackled in Chapter 6.

In the discussions above, the sequence of Diracs in (2.76) is treated as a continuous signal. The response of the signal is given by

$$\begin{aligned} F(\Omega) &= \int f(x)e^{-i\Omega x}dx \\ &= \sum_{k}^{K-1} c_k \sum_{n} e^{-j\Omega(x_k+n\tau)} \end{aligned} \tag{2.93}$$

Therefore, the signal is of non-bandlimited response. On the other hand, this signal can be considered as a modulated signal of the sequence $\{f[x_k]\}_{k\in\mathbb{Z}}$ where $f[x_k] = c_k$ for all k. The sampling process described by innovation sampling can in turn be interpreted as an interpolation of the sequence by $h_B(x)$ and then resampled uniformly to produce the output $\mathbf{y}_T$. Therefore, it can be viewed as a resampling process of non-bandlimited signals. Since $\mathbf{f}[x_k]$ is reconstructed from $\mathbf{y}_T$, a general guideline to design resampling process can be drawn from the innovation sampling: the original sequence shall be able to be recovered from its resampled sequence.

2.6 Resampling Non-bandlimited Signals

As discussed earlier in Section 2.1.2, resampling is essentially a two-step process [139]. In the first step, the discrete input is interpolated to a continuous signal and in the second step, this continuous signal is resampled at the desired locations and at the desired sampling rate to produce a discrete output. In this section, we lift the restriction of band-limitation on the signals and functions involved.

2.6.1 Performance of Resampling

As discussed in Section 2.2, a signal that is non-bandlimited can be sampled by an acquisition function $\varphi \in \mathcal{H}$. Let

$$c(x) = f(x) * \varphi(-x) \tag{2.94}$$

The samples are given by $c[k] = c(x)|_{x=kT}$ for all $k \in \mathbb{Z}$ assuming that $T = 1$. The frequency response $c(x)$ is therefore given by

$$C(\Omega) = F(\Omega)\overline{\Psi}(\Omega) \tag{2.95}$$

and that of $c[k]$ is given by

$$C(\omega) = \sum_k C\left(\Omega + \frac{2k\pi}{T}\right)\bigg|_{\omega=\Omega T} \tag{2.96}$$

Since $C(\Omega)$ is not assumed to be bandlimited, sampling $c(x)$ would inevitably cause aliasing and $C(\omega)$ contains overlapped copies of $C(\Omega)$. Therefore, it is inappropriate to compare the spectra of the input and output signals to gauge the performance of resampling when the signals involved are non-bandlimited [140, 141].

There are other ways to directly or indirectly measure the performance of a resampling system or process. They can be classified are two main groups of performance metrics depending on whether the entire resampling process or only the interpolation process is to be considered. Those metrics that include the whole resampling process are usually application dependent. For example, for most image processing application, the Peak Signal to Noise Ratio (PSNR) is commonly used. PSNR is defined by

$$PSNR = 10 \cdot \log_{10} \frac{MAX^2}{MSE} \tag{2.97}$$

where

$$MSE = \frac{1}{mn} \sum_{i=0}^{m} \sum_{j=0}^{n} \| I(i,j) - K(i,j) \|_{\ell^2}^2 \tag{2.98}$$

and MAX denotes the maximum pixel value of the $(m \times n)$ image. Here, I and K denote the original image and processed image respectively. Instead of the ℓ^2 norm, sometimes the ℓ^∞ norm is used [43]. Some care must be taken when using this kind of metrics to compare different resampling algorithms for images. For instance, the size of the processed image has to be identical to that of the original image. Thus they are not very robust and are not applicable to a lot of cases, e.g. when the resizing factor is not an integer.

Another example of this group of metrics is the Bit Error Rate (BER) used in digital communication systems where the sampled signals are usually resampled [142, 143]. The better a resampling scheme, the lower its BER with the same signal-to-noise ratio (SNR). This method can become very complicated since the relationship between BER and SNR varies depending on the modulation scheme used. Extensive research has been done to work out these relationships for different modulations schemes [143–147]. As far as resampling is concerned, in order to draw valid conclusions, resampling algorithms should be compared using the same modulation scheme.

Since the metrics in this group are very application specific, comparisons between resampling algorithms from different fields are practically impossible. For example, it is impossible to compare the performance of a denoising system for image processing and one for mobile channel detection. Since resampling is widely applied in almost all fields, it is essential that a unified metric can be used to compare the performance of different resampling algorithms.

The second group of metrics addresses this issue by considering the performance of the interpolation process only [38, 148, 149]. Thus it measures only the interpolation error [150, 151]. Those metrics discussed earlier in Section 2.2 for sampling and reconstruction are all applicable.

Many functions have been used for interpolation in resampling. The most widely used include nearest neighbour (β^0), linear (β^1) [152], quadratic interpolators [153], cubic B-splines (β^3) [94] and cubic convolution [95, 101, 154]. Besides the B-splines and the polynomial families, other interpolating functions considered include the fractal interpolating function [155], Gabor filters [41, 156], Taylor series interpolation [157], the Gaussian function and its derivatives [158] and de Boor-Ron interpolation filters [12]. There is also a study on the use of rational filters which shows that the information of the input sequence can be preserved with great fidelity at low computational cost [159].

In addition, some non-linear methods have been devised specifically for resampling. In [160], the signal is expressed in terms of the synthesis function. The optimally reconstructed signal is obtained by solving a set of separable partial differential equations such that the MSE is minimized. A similar approach can be found in the research for scalable video coding [10]. The upsampling and downsampling of the discrete signals are modeled and solved via differential equations. In [161–164], classic interpolation techniques are employed in conjunction with estimation of edges. If the image is locally smooth, the edge orientation of the image can be computed from local pixels. The interpolation error can then be reduced around the edges. Adaptive interpolating filters are used in [165,166] to minimize the MSE for each individual estimated sample. A generalized approach is proposed in [167] that makes use of kernel regression methods to obtain the coefficients of the spline functions that minimize the MSE.

Other methods are based on the underlying principles used for consistent sampling. In [168, 169], the consistent sampling technique is directly applied to image resizing and rotation. Two major techniques, oblique interpolation and quasi interpolation, have been developed in these papers.

2.6.2 Oblique Interpolation Method

Oblique interpolation is the direct application of consistent sampling to image processing [170]. The original image $\mathbf{f}$ is assumed to be obtained by sampling a continuous signal on a uniform grid using the function $\varphi = \beta^0$. This discrete image is interpolated by a Nyquist function ϕ to obtain the continuous image $\widetilde{f}$. To resize an image by a factor of

a, the continuous image is scaled to $g(x) = \widetilde{f}(x/a)$. The resized image $\mathbf{g}$ is obtained by sampling $g(x)$ using φ. Oblique interpolation requires that

$$\widetilde{g} = \sum_m g[m]\phi(x - m) \tag{2.99}$$

which is the interpolated continuous image of $\mathbf{g}$ and $g(x)$ are consistent with respect to φ. That is,

$$\left\langle \widetilde{g}, \beta^0(x-k) \right\rangle = \left\langle g, \beta^0(x-k) \right\rangle \tag{2.100}$$

In order to achieve consistency, a correction filter is incorporated into the resampling system.

Suppose cardinal splines of order n defined in (2.45) are used for interpolation, then $\phi = \eta^n$. From (2.58), the sampled cross correlation of φ and ϕ is given by

$$\begin{aligned} a_{\phi\varphi}[k] &= \left\langle \beta^0(x-k), \sum_k (b^n)^{-}1[l]\beta^n(x-l) \right\rangle \\ &= \left((b^n)^{-1} * b^{n+1}\right)[k] \end{aligned} \tag{2.101}$$

Hence the correction filter can be obtained from (2.62) and is given by

$$\begin{aligned} Q(\omega) &= \frac{1}{A_{\phi\varphi}(\omega)} \\ &= \frac{B^n(\omega)}{B^{n+1}(\omega)} \end{aligned} \tag{2.102}$$

2.6.3 Quasi Interpolation Method

If the resampling performance is measured by the performance of its embedded interpolation process, the performance of the image applications can be analyzed by the formula given by (2.27):

$$\eta_f(T) = \left[\frac{1}{2\pi}\int |F(\Omega)|^2 E_\phi(T\Omega)d\Omega\right]^{\frac{1}{2}} \tag{2.103}$$

Assuming $T = 1$, the error kernel $E_\phi(\Omega)$ is given by

$$E_\phi(\Omega) = \underbrace{1 - \frac{|\Phi(\Omega)|^2}{A_\phi(\omega)}}_{E_{\min}(\Omega)} + \underbrace{A_\phi(\omega)\,|\Psi(\Omega) - \Phi_d(\Omega)|^2}_{E_{\text{res}}(\Omega)} \tag{2.104}$$

$E_{\min}(\Omega)$ is the lower bound of $E_\phi(\Omega)$, which is optimal but unattainable since $F(\Omega)$ is unknown. The quasi interpolation method proposed that ϕ should be chosen such that $E_{\min}(\Omega)$ is minimized [171]. For images which are essentially lowpass, $E_{\min}(\Omega)$ is required to be as close to zero as possible around $\Omega = 0$. More specifically,

$$E_{\min}(\Omega) = O(\Omega^{2L}) \tag{2.105}$$

where the integer L should be as large as possible. This is equivalent to the Strang-Fix condition in (2.15) for ϕ to have an approximation order of L [46].

On the other hand, as discussed in Section 2.3.1, the support of a function of approximation order L is $\mathcal{B} \geq L$. L has to be small so that the computational cost is kept reasonably low. Following the discussions in Section 2.3.1, ϕ can be chosen among the B-splines since for a given approximation order L, the support of B-splines attains the lower bound L.

Once ϕ is chosen, a correction filter is used to ensure that $E_{\text{res}}(\Omega)$ is arbitrarily small and

$$E_\phi(\Omega) \approx E_{\min}(\Omega) \tag{2.106}$$

Quasi interpolation requires that the residue error satisfies

$$E_{\text{res}}(\Omega) = O(\Omega^N) \tag{2.107}$$

where $N \geq 2L + 1$. According to (2.104), this amounts to requiring that

$$\Psi(\Omega) = \Phi_d(\Omega) + O(\Omega^M) \tag{2.108}$$

with $M \geq \frac{N}{2} \geq L + 1$. If the resampling function is $\psi = \delta(x)$, then the correction filter for quasi interpolation is given by

$$Q(\omega) = \Phi_d(\Omega) + O(\Omega^M) \tag{2.109}$$

with $\omega = T\Omega = \Omega$. Note that $Q(\omega)$ is not unique. Hence the correction filter can be designed to suit particular applications. For example, the lowest order correction filter can be used so that the computational cost is kept to a minimum.

It has been shown that the resampling performs better using oblique and quasi interpolation methods. However, when Janssen and Kalker analyzed the performance of de-interlacing using the techniques derived for consistent sampling, results contradictory to common sense arose [9]. Deinterlacing and their observations will be described in Section 2.7. What this reveals is that optimal resampling cannot be obtained from optimal sampling for non-bandlimited signals. Therefore, although consistent sampling is optimal for sampling without noise, oblique and quasi interpolation methods are not guaranteed to achieve optimal resampling performance.

2.7 De-interlacing

The *interlaced* video format is heavily used in television broadcasting. It consists of two types of fields – one with only the odd scan lines and the other with only the even scan lines. These two types of fields are transmitted in an interlaced fashion so that only half of the information changes at any one time at the receiver. The received video frames need to be de-interlaced (the opposite of interlacing) before the images can be displayed on the video monitor. This is because the monitors typically utilize a *progressive* scanning approach that displays both odd and even scan lines in order from top to bottom for a single frame. Thus de-interlacing involves interpolation. Since the fields consist of pixels and are discrete, de-interlacing is essentially a resampling process [172].

While it is trivial to obtain interlaced signals from non-interlaced ones, the reverse process requires much more effort. Figure 2.11 illustrates the difference between interlaced and deinterlaced signals. The input of a deinterlacing system consists of interlaced fields containing samples of either the odd or the even scan lines. Let n be the index of the field and $\vec{x} = (x, y)$ denote the samples along scan line y. The interlaced field is

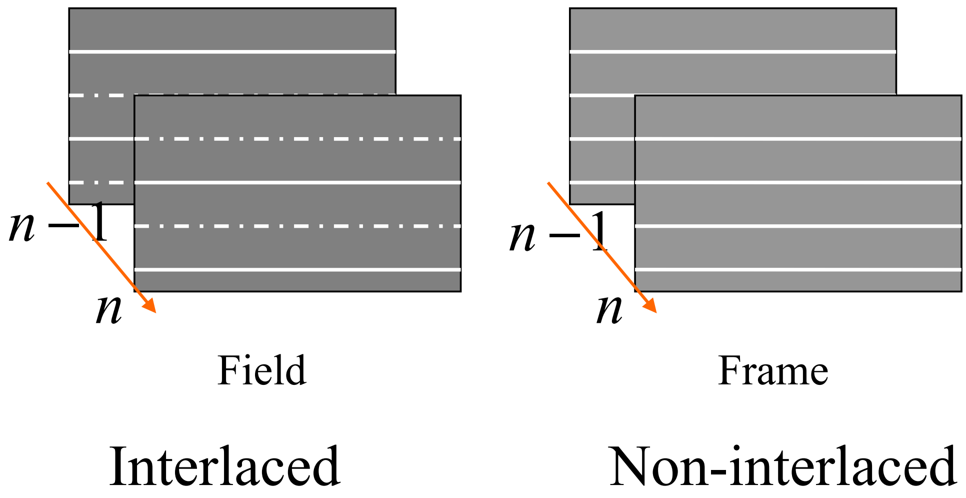

Figure 2.11: Interlaced and de-interlaced signals.

represented by $F(\vec{x}, n)$ where only the lines $(y \mod 2) = (n \mod 2)$ are defined. The output frame can be expressed as

$$F_o(\vec{x}, n) = \begin{cases} F(\vec{x}, n), & (y \mod 2) = (n \mod 2) \\ F_i(\vec{x}, n), & \text{Otherwise} \end{cases} \tag{2.110}$$

where $F_i(\vec{x}, n)$ are the interpolated fields.

The interpolated fields are obtained from the preceding and/or succeeding fields. In terms of resampling, the problem of de-interlacing is one of up-sampling. The process is complicated by the fact that the process of interlacing is essentially sub-sampling without prefiltering, which is a violation of the Nyquist rate criteria. As a result, some error will be present in the interlaced signal. This error can only be reduced by making assumptions and prediction about the motion of the objects in the video picture. A number of techniques are used, the suitability of each depends on the characteristics of the images involved.

The simpler deinterlacing algorithms are linear, with the interpolated fields $F_i(\vec{x}, n)$ obtained by

$$F_i(\vec{x}, n) = \sum_k F(\vec{x} + k\vec{u}_y, n + m)h(k, m) \tag{2.111}$$

for $k, m \in \mathbb{Z}$ and $(k+m) \mod 2 = 1$. $h(k, m)$ is the impulse response of the filter defined in the vertical-temporal (VT) domain and $\vec{u}_y = (0\ 1)^T$. The choice of $h(k, m)$ determines whether it is a spatial (intrafield), temporal (interfield), or spatial-temporal filter. For example,

$$h(0, -1) = \begin{cases} 1, & k = -1 \\ 0, & \text{otherwise} \end{cases} \tag{2.112}$$

is a temporal filter. In this case, every line y in field n is copied from line y of the previous field $n-1$. Consequently, there is no degradation for stationary video scenes. The linear approach was common for televisions until the end of the 1970's.

In 1990's, motion compensation (MC) has been proposed and the most advanced deinterlacing algorithms all employ MC. To detect motion, the differences between two (or more) pictures are calculated and a motion vector for each pixel is estimated. The motion vectors should reflect the true motion of the objects. Given the motion vectors, MC methods try to interpolate in the direction with the highest correlation. It allows us to virtually convert a moving a sequence into a stationary one. Therefore, methods that perform better for stationary than moving scenes, such as linear temporal filtering, will profit from MC. Incorporating MC, (2.111) becomes

$$F_i(\vec{x}, n) = \sum_k F(\vec{x} + m\vec{d}(\vec{x}, n) + k\vec{u}_y, n + m)h(k, m) \tag{2.113}$$

where $\vec{d}(\vec{x}, n)$ is the motion vector for the pixel $(\vec{x}, n)$.

The time-recursive (TR) de-interlacing algorithm [173] suggested that once a deinterlaced image and the motion vectors are available, resampling can be applied to deinterlace the current field by

$$F_o(\vec{x}, n) = \begin{cases} F(\vec{x}, n), & (y \mod 2) = (n \mod 2) \\ F_o(\vec{x} - \vec{d}(\vec{x}, n), n-1), & \text{Otherwise} \end{cases} \tag{2.114}$$

The interpolated samples depend on the previous as well as the current field samples as illustrated in Figure 2.12. The previous original samples are shifted in the direction

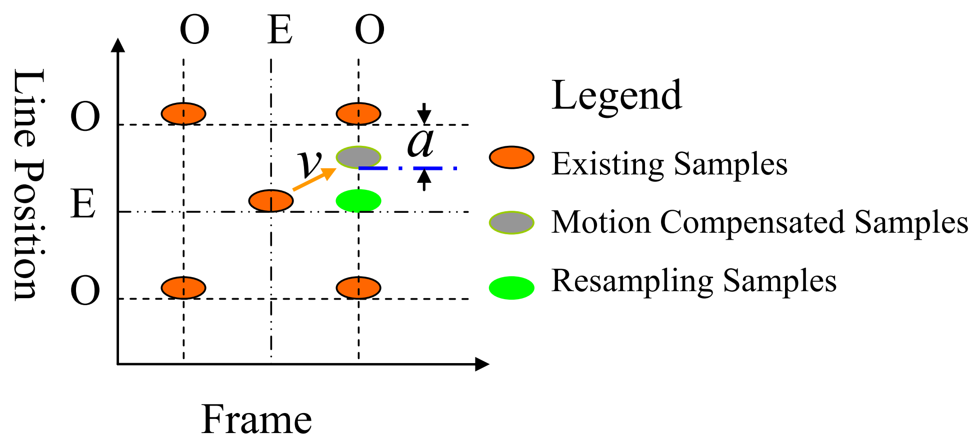

Figure 2.12: The de-interlacing process. The horizontal axis denotes the input fields while the vertical axis denotes the scan lines. The motion vector a relates to the velocity of the scene by $a = 1 - v$.

of the motion vector toward the current field in order to create two independent sets of samples valid at the same temporal instant. Let a denote the distance between the motion compensated sample and the existing sample, as shown in Figure 2.12. De-interlacing can be viewed as the resampling of $f[2k]$ and $f[2k+a]$, for $0 \leq a < 1$, to uniformly spaced samples $\hat{f}[k]$ [9]. When $a = 1$, $f[2k+1]$ can be obtained by copying the sample from the previous field. Thus the performance of the resampling system is optimal in this case.

Janssen and Kalker [9] analyzed the performance of de-interlacing using the stability measure defined in (2.11). The Resampling performance is computed as a function of a and it shows that the optimal performance is achieved when $a = \sqrt{\frac{2}{3}}$ instead of the intuitive $a = 1$. The authors argued that while reconstruction is a process of $\ell^2 \to L^2$, the process of resampling is one of $\ell^2 \to \ell^2$. Therefore the performance of interpolation is not an appropriate measure of the performance of resampling and an optimal sampling system does not automatically lead to an optimal resampling system. This motivated us to develop a theory for resampling without bandlimited constraints and an associated performance metric which can be used to measure resampling performance with fidelity.

Chapter 3

Noiseless Consistent Resampling

In this chapter, a new generalized theory for the resampling of discrete-time signals with non-bandlimited frequency responses is developed. In Section 3.1, the problem of resampling is formulated using the framework of generalized sampling discussed in Section 2.4. Then a generalized theory of resampling is developed in Section 3.2 which is based on the new concept of *consistent resampling*. The idea originates from consistent sampling introduced in Section 2.4. But it is more than a simple extension since measuring the difference between the input and output is very different for a resampling system compared to a sampling/reconstruction system. Consistent resampling is achieved by incorporating a correction filter into the resampling system so that the choice of sampling, resampling and interpolating functions are decoupled from each other. In Section 3.3, the problem of de-interlacing discussed in Section 2.7 is tackled using consistent resampling to show that our theory generates the correct results. Consistent resampling is also applied to the demodulation of UWB signals and to image processing in Section 3.4.1 and Section 3.4.2 respectively. It is shown that a consistent resampling system results in superior performance when high frequency components are processed compared with methods based on bandlimited signal processing theory,

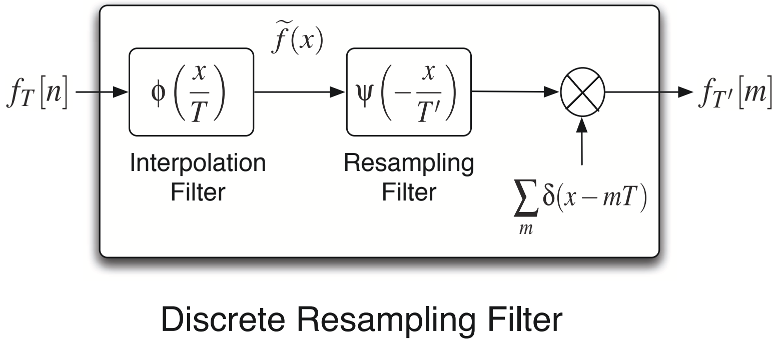

Figure 3.1: A resampling system with generalized interpolating and resampling functions.

3.1 Problem Formulation

3.1.1 Mathematical Model

Let the input discrete signal of a resampling system be $\{f_T[n]\}_{n\in\mathbb{Z}}$ with a sampling period of T. Let $\{f_{T'}[m]\}_{m\in\mathbb{Z}}$ denote the output discrete signal with sampling period T' which may or may not be the same as T. Suppose the synthesis function and the resampling functions are $\phi(\frac{x}{T})$ and $\psi(\frac{x}{T'})$ respectively. Then the time-domain approach to resampling discussed in Section 2.6 can be described by Figure 3.1. The signals and functions involved are assumed to be elements of the Hilbert space. The conventional SRC system is a specific example where $\phi = sinc(x/T)$ and $\psi = \delta(x)$.

In general, the argument of ψ should be $(x - x_0)/T'$ where x_0 is a constant. This is because in some applications such as image rotation, the resampling interval is the same as the original (i.e. $T' = T$) but the locations at which the samples taken are different.

Taking this into account, the intermediate continuous signal is obtained from the input signal by

$$\widetilde{f}(x) = \sum_n f_T[n]\phi\left(\frac{x}{T} - n\right) \tag{3.1}$$

The output of the resampling system is therefore given by

$$\begin{aligned} f_{T'}[m] &= \left\langle \sum_n f_T[n]\phi\left(\frac{x}{T}-n\right), \psi\left(\frac{x-x_0}{T'}-m\right)\right\rangle \\ &= \sum_n f_T[n]\left\langle \phi\left(\frac{x}{T}-n\right), \psi\left(\frac{x-x_0}{T'}-m\right)\right\rangle \end{aligned} \tag{3.2}$$

Let $\psi'(x) = \psi(x-x_0)$ and $\psi\left(\frac{x-x_0}{T'}-m\right)$ in (3.2) can be replaced by $\psi'(x/T')$.

If $\{\psi_k = \psi(x-k)\}_{k\in\mathbb{Z}}$ form a Riesz Basis of the space V^{ψ}, then ψ satisfies the admissibility condition of (2.10), or its equivalent form in the frequency domain (2.21). Let $\psi'(x) = \psi(x-x_0)$ and $\psi\left(\frac{x-x_0}{T'}-m\right)$ in (3.2) be replaced by $\psi'(x/T')$. The Fourier transform of ψ' is given by

$$\Psi'(\Omega) = e^{-j\Omega x_0}\Psi(\Omega) \tag{3.3}$$

Since

$$\begin{aligned} \|\Psi'(\Omega+2\pi k)\|^2 &= \|e^{-j[\Omega+2\pi k]x_0}\|^2\|\Psi(\Omega+2\pi k)\|^2 \\ &= \|\Psi(\Omega+2\pi k)\|^2 \end{aligned} \tag{3.4}$$

Φ in (2.21) can be replaced by Ψ'. This implies that $\{\psi_k = \psi(x-k)\}_{k\in\mathbb{Z}}$ is also a Riesz basis for $V^{\psi'}$. Hence omitting x_0 will not affect the stability and uniqueness of the resampling operation. For the sake of conciseness, we shall do so for the rest of this thesis.

In summary, the resampling process is characterized by the discrete and time varying resampling filter:

$$h(n,m) = \left\langle \phi\left(\frac{x}{T}-n\right), \psi\left(\frac{x}{T'}-m\right)\right\rangle \tag{3.5}$$

where $h(n,m)$ specifies the relationship between the nth input to the mth output. Thus resampling is an operation of $\ell^2 \to \ell^2$.

3.1.2 Consistent Resampling Defined

When the signal and the sequences are bandlimited and ideal sampling is used to obtain the samples, the performance of resampling can be concluded by comparing the spectra of the input and output of the resampling process, as discussed in Section 2.1.2. Provided that the resampling rate $1/T'$ is higher than twice the bandwidth of the reconstructed signal, the spectrum of the input signal is preserved. However, when non-ideal samplers are employed to sample non-bandlimited signals, the output will be aliased.

The generalized sampling theory for non-bandlimited signals [4, 125] introduced another criterion to compare the input and output of a sampling-reconstruction system. It is called consistent resampling and has been described in Section 2.4. The basic idea is to compare the input signal and the reconstructed signal by projecting them onto the acquisition space. Sampling is said to be consistent if they produce the same set of measurements. A similar idea can be used for resampling.

We shall say that resampling is *consistent* if the output discrete signal appears to be the same as the input discrete signal as far as the synthesis function is concerned. In other words, to the synthesis function, both input and output signals describe the same analog signal. This concept can be defined formally using frame theory.

Definition 3.1.1. *(Consistent Resampling) Consider a resampling system as shown in Figure 3.1. Let the set of vectors* $\left\{\phi\left(\frac{x}{T}-n\right)\right\}_{n\in\mathbb{Z}}$ *form a Riesz basis, i.e.*

$$0 < A \leq \sum_{n\in Z} \left|\phi\left(\frac{x}{T}-n\right)\right|^2 \leq B < \infty \tag{3.6}$$

where A *and* B *are the Riesz bounds. The resampling system is said to be consistent if and only if* $\widetilde{f}(x) = \widehat{f}(x)$ *where*

$$\widetilde{f}(x) = \sum_{n} f_T[n]\phi\left(\frac{x}{T}-n\right) \tag{3.7}$$

$$\widehat{f}(x) = \sum_{m} f_{T'}[m]\phi\left(\frac{x}{T'}-m\right) \tag{3.8}$$

are the continuous functions reconstructed from $\{f_T[n]\}_{n\in\mathbb{Z}}$ *and* $\{f_{T'}[m]\}_{m\in\mathbb{Z}}$ *respectively using* ϕ*.*

3.1.3 Physical Justification

To view the signals $\widetilde{f}(x)$ and $\widehat{f}(x)$ in frequency domain, we first decompose the signals into forms of convolution:

$$\begin{aligned} \widetilde{f}(x) &= f_T(x) * \phi\left(\frac{x}{T}\right) && (3.9) \\ \widehat{f}(x) &= f_{T'}(x) * \phi\left(\frac{x}{T'}\right) && (3.10) \end{aligned}$$

where $f_T(x)$ and $f_{T'}(x)$ are the modulated signals of $\mathbf{f}_T$ and $\mathbf{f}_{T'}$ respectively, defined by

$$\begin{aligned} f_T(x) &= \sum_n f_T[n]\delta(x - nT) \\ f_{T'}(x) &= \sum_m f_{T'}[n]\delta(x - mT') \end{aligned}$$

It is worth pointing out that $f_T(x)$ is a continuous signal while $\mathbf{f}_T$ is discrete. The response of $f_T(x)$ can be directly evaluated from FT:

$$\begin{aligned} F_T(\Omega) &= \int_x f_T(x)e^{-j\Omega x}dx \\ &= \int_x \sum_n f_T[n]\delta(x - nT)e^{-j\Omega x}dx \\ &= \sum_n f_T[n]e^{-j\Omega nT} && (3.11) \end{aligned}$$

Since

$$\begin{aligned} F_T(\Omega + 2\pi/T) &= \sum_n f_T[n]e^{-j(\Omega+2\pi/T)nT} \\ &= \sum_n f_T[n]e^{-j\Omega nT} \\ &= F_T(\Omega) && (3.12) \end{aligned}$$

F_T is of period $2\pi/T$. Similarly, the response of $f_{T'}$ is given by

$$F_{T'}(\Omega) = \sum_m f_{T'}[m]e^{-j\Omega mT'} \quad (3.13)$$

and its period is $2\pi/T'$.

On the other hand, from the scaling property of FT, the response of $\phi\left(\frac{x}{T}\right)$ and $\phi\left(\frac{x}{T'}\right)$ as in (3.9) and (3.10) are given by $T\Phi(T\Omega)$ and $T'\Phi(T'\Omega)$ respectively.

Following the convolution property of FT, the response of $\widetilde{f}$ and $\widehat{f}(x)$ is given by

$$\widetilde{F}(\Omega) = F_T(\Omega)T\Phi(T\Omega) \tag{3.14}$$

$$\widehat{F}(\Omega) = F_{T'}(\Omega)T'\Phi(T'\Omega) \tag{3.15}$$

To view consistent resampling in frequency domain, we have

$$\widetilde{F}(\Omega) = \widehat{F}(\Omega) \tag{3.16}$$

Substitute (3.14) and (3.15) into (3.16),

$$F_T(\Omega)T\Phi(T\Omega) = F_{T'}(\Omega)T'\Phi(T'\Omega) \tag{3.17}$$

By rearrangement, the response of the output signal is given by

$$F_{T'}(\Omega) = F_T(\Omega)\frac{T\phi(T\Omega)}{T'\phi(T'\Omega)} \tag{3.18}$$

An analysis of (3.18) provides an insightful view of consistent resampling theory in frequency domain. On one hand, to evaluate $F_T(\Omega)\phi(T\Omega)$, since $F_T(\Omega)$ is of period $2\pi/T$, we only need to concern one period defined in the range $\Omega \in [2(k-1)\pi/T, 2k\pi/T)$. During this period, $\Phi(T\Omega)$ is evaluated in the range $T\Omega \in [2(k-1)\pi, 2k\pi)$. It is equivalent to evaluate $\Phi(\Omega)$ in the range of $\Omega \in [2(k-1)\pi, 2k\pi)$. Define

$$F_{T_c}(\Omega) = \begin{cases} F_T(\Omega/T) & \Omega \in [-\pi, \pi) \\ 0 & \text{otherwise} \end{cases} \tag{3.19}$$

For consecutive intervals of 2π, $\widetilde{F}(\Omega)$ is obtained by evaluating $\Phi(\Omega)$ manipulated by the signal $F_{T_c}(\Omega - 2k\pi)$.

On the other hand, to consider $\phi(T'\Omega)$ in the intervals $[2(k-1)\pi, 2k\pi)$, the value of Ω is taken in the range of $\Omega \in 2((k-1)\pi/T', 2k\pi/T']$. Since $F_{T'}$ is of period $2\pi/T'$, define

$$F_{T'_c}(\Omega) = \begin{cases} F_{T'}(\Omega/T') & \Omega \in [-\pi, \pi) \\ 0 & \text{otherwise} \end{cases} \tag{3.20}$$

It can be similarly argued that for consecutive intervals of 2π, $\widehat{F}(\Omega)$ is obtained by evaluating $\Phi(\Omega)$ manipulated by the signal $F_{T'_c}(\Omega - 2k\pi)$.

Hence, the consistent resampling theory requires $F_{T'_c}(\Omega) = F_{T_c}(\Omega)$. From (3.19) and (3.20), we can observe that it is equivalent to state that $F_{T'}(\Omega)$ resembles a dilated version of $F_T(\Omega)$, just as $\Phi(T'\Omega)$ is a dilated version of $\Phi(T\Omega)$.

3.2 Consistent Resampling Systems

3.2.1 Correction Filter

In general, for any arbitrary ϕ and ψ, a resampling system will not be *consistent*, i.e. it does not conform to Definition 3.1.1. However, a digital correction filter $q[n]$ can be incorporated into the system in the way shown in Figure 3.2 to achieve consistent resampling. The following proposition provides a formula for the design of this correction filter.

Before we proceed, we consider the frequency response of a time-variant sequence. From its definition, the response of a discrete sequence, or the Discrete Time Fourier Transform (DTFT) is derived from the FT for continuous signal. Conventionally, the sampling is defined by convolve the signal with the ideal impulse train,

$$\Delta_T(x) = T \sum_n \delta(x - nT) \tag{3.21}$$

and the samples of a signal $f(x)$ is defined by $f[n] = f(x)|_{xT}$. To work out its frequency response, we first modulate the sequence by the Diracs function

$$f_T(x) = T \sum_n f(nT)\delta(x - nT) \tag{3.22}$$

which is a continuous function and its response is given by FT:

$$\begin{aligned} F_T(\Omega) &= \int f_T(x)e^{-j\Omega x}dx \\ &= \sum_n Tf(nT)\int \delta(x-nT)e^{-j\Omega x}dx \\ &= \sum_n Tf(xT)e^{-j\Omega nT} \end{aligned} \tag{3.23}$$

With the association $\omega = \Omega T$, the DTFT is hence defined by

$$F(\omega) = \sum_n f_T(n)e^{-j\omega n} \tag{3.24}$$

Let the cross correlation of $\phi\left(\frac{x}{T}-n\right)$ and $\psi\left(\frac{x}{T'}-m\right)$ be defined by

$$c_{\phi\psi}[n,m] = \int_x \phi\left(\frac{x}{T}-n\right)\psi\left(\frac{x}{T'}-m\right)dx \tag{3.25}$$

The sequence can be obtained by sampling the signal

$$c^n_{\phi\psi}(x) = \phi\left(\frac{x}{T}-n\right) * \psi\left(-\frac{x}{T'}\right) \tag{3.26}$$

at period T'. For one particular n, the response of the sequence $c^n_{\phi\psi}(x)|_{x=mT'}$ is given by

$$\begin{aligned} C^n_{\phi\psi}(\omega) &= \sum_m c^n_{\phi\psi}(x)\int \delta(x-mT')e^{j\Omega x}dx \\ &= c_{\phi\psi}[n,m]e^{j\Omega mT'} \end{aligned} \tag{3.27}$$

With the association of $\omega = \Omega T'$, the DTFT of $c^n_{\phi\varphi}[m]$ is given by

$$C^n_{\phi\psi}(\omega) = \sum_m c_{\phi\psi}[n,m]e^{j\omega m} \tag{3.28}$$

On the other hand, the function $\phi\left(\frac{x}{T}-n\right)$ can be rewritten as

$$\phi\left(\frac{x}{T}-n\right) = \phi\left(\frac{x-nT}{T}\right) \tag{3.29}$$

The shifting property of Fourier transform states that

$$f(x) \overset{FT}{\to} F(\Omega) \Rightarrow f(x-n) \overset{FT}{\to} e^{-j\Omega n} \tag{3.30}$$

To take into consideration of the shift n, for a given n the shifting factor is $e^{-j\Omega nT}$. Therefore, the response of the sequence $c_{\phi\psi}[n,m]$ is given by

$$C_{\phi\psi}(\omega) = \sum_{n,m} c_{\phi\psi}[n,m] e^{j\omega m} e^{-j\Omega nT} \tag{3.31}$$

Since $\omega = \Omega T'$ and $\Omega = \omega/T'$, the above equation can be reformed into

$$C_{\phi\psi}(\omega) = \sum_{n,m} c_{\phi\psi}[n,m] e^{j\omega(m-nT_r)} \tag{3.32}$$

where $T_r = T/T'$.

We can see that this definition is of the same form of the response of a filter bank, as seen in [8].

We proceed to the next proposition on the design of the digital correction filter:

Proposition 3.2.1. *Let*

$$C_{\phi\psi}(\omega) = \sum_{m,n} c_{\phi\psi}[n,m] e^{j\omega(m-nT_r)} \tag{3.33}$$

be the frequency response of the sampled cross correlation $\{c_{\phi\psi}[n,m]\}_{m,n\in\mathbb{Z}}$ *of* $\phi(\frac{x}{T})$ *and* $\psi(\frac{x}{T'})$ *where*

$$c_{\phi\psi}[n,m] = \int_x \phi\left(\frac{x}{T} - n\right) \psi\left(\frac{x}{T'} - m\right) dx \tag{3.34}$$

with $T_r = T/T'$*. Similarly, let* $C_{\phi\phi_d}(\omega)$ *be the frequency response of* $\{c_{\phi\phi_d}[n,m]\}_{m,n\in\mathbb{Z}}$*, the sampled cross correlation of* $\phi(\frac{x}{T})$ *and* $\phi_d(\frac{x}{T'})$*, the dual operator of* $\phi(\frac{x}{T'})$*, given by*

$$c_{\phi\phi_d}[n,m] = \int_x \phi\left(\frac{x}{T} - n\right) \phi_d\left(\frac{x}{T'} - m\right) dx \tag{3.35}$$

Then the resampling system in Figure 3.2 is consistent if the frequency response of the digital correction filter is

$$Q(\omega) = \frac{C_{\phi\phi_d}(\omega)}{C_{\phi\psi}(\omega)} \tag{3.36}$$

Proof. The output of the system in Figure 3.2 is given by

$$f_{T'}[m] = \sum_s \sum_n f_T[n] \left\langle \phi\left(\frac{x}{T} - n\right), \psi(\frac{x}{T'} - s)\right\rangle q[m-s] \tag{3.37}$$

Substituting (3.37) into (3.8), we have

$$\begin{aligned}\widehat{f}(x) &= \sum_m \left(\sum_s \sum_n f_T[n] \left\langle \phi\left(\frac{x}{T} - n\right), \psi(\frac{x}{T'} - s)\right\rangle q[m-s] \right) \phi\left(\frac{x}{T'} - m\right) \\ &= \sum_{m,n} f_T[n] \sum_s \int_x \phi\left(\frac{x}{T} - n\right) \psi(\frac{x}{T'} - s) dx q[m-s] \cdot \phi\left(\frac{x}{T'} - m\right) \end{aligned} \tag{3.38}$$

With the cross correlaiton $c_{\phi\psi}[n,m]$ as defined by (3.34), (3.38) can be expressed as

$$\widehat{f}(x) = \sum_n f_T[n] \sum_s c_{\phi\psi}[n,s] \sum_m q[m-s] \phi\left(\frac{x}{T'} - m\right) \tag{3.39}$$

Since $\phi_d(\frac{x}{T'})$ and $\phi(\frac{x}{T'})$ are duals of each other, we have

$$\left\langle \phi_d(\frac{x}{T'}), \phi(\frac{x}{T'} - n)\right\rangle = \delta[n] \tag{3.40}$$

Using this condition, if we sample $\widehat{f}(x)$ using $\phi_d(\frac{x}{T'})$, we obtain

$$\begin{aligned}\widehat{f}_{T'}[k] &= \sum_n f_T[n] \sum_s c_{\phi\psi}[n,s] \sum_m q[k-s] \\ &= \mathbf{f}_T * \mathbf{c}_{\phi\psi} * \mathbf{q} \end{aligned} \tag{3.41}$$

Since

$$\begin{aligned} c_{\phi\psi}[n,s] &= \int_x \phi\left(\frac{x}{T} - n\right) \psi\left(\frac{x}{T'} - s\right) dx \\ &= \int_x \phi\left(\frac{x}{T}\right) \psi\left(\frac{x}{T'} - s + nT_r\right) dx = c_{\phi\psi}[0, s - nT_r] \end{aligned} \tag{3.42}$$

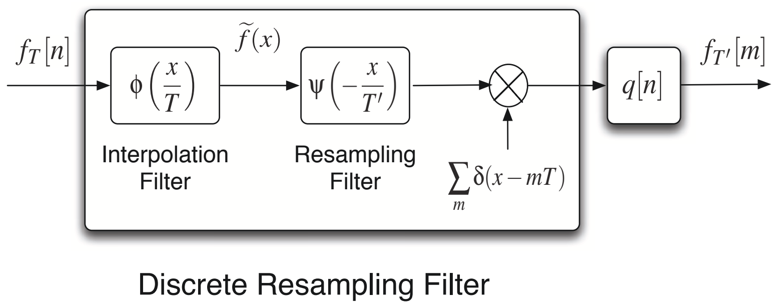

Figure 3.2: The consistent resampling system with the correction filter.

with $T_r = T/T'$. The response of the 2D sequence $\mathbf{c}_{\phi\psi}$ can be calculated as

$$C_{\phi\psi}(\omega) = \sum_{n,s} c_{\phi\psi}[n,s]e^{-j\omega(s-nT_r)} \tag{3.43}$$

Taking the Fourier transform of (3.41), we have

$$\widehat{F}_{T'}(\omega) = F_T(\omega)C_{\phi\psi}(\omega)Q(\omega) \tag{3.44}$$

On the other hand, sampling $\widetilde{f}(x)$ as expressed in (3.7) using $\phi_{T'_d}$ we have

$$\begin{aligned} \widetilde{f}_{T'}[v] &= \sum_n f_T[n]c_{\phi\phi_d}[n,v] \\ &= \mathbf{f}_T * \mathbf{c}_{\phi\phi_d} \end{aligned} \tag{3.45}$$

where $c_{\phi\phi_d}$ is given by (3.35). It can be expressed in the Fourier domain as

$$\widetilde{F}_{T'}(\omega) = F_T(\omega)C_{\phi\phi_d}(\omega) \tag{3.46}$$

In order that the resampling system is consistent as defined by Definition 3.1.1, we need to have $\widetilde{f}(x) = \widehat{f}(x)$, or alternatively $\widehat{F}_{T'}(\omega) = \widetilde{F}_{T'}(\omega)$. Thus, using (3.44) and (3.46), we require

$$F_T(\omega)C_{\phi\psi}(\omega)Q(\omega) = F_T(\omega)C_{\phi\phi_d}(\omega) \tag{3.47}$$

This condition will hold if the frequency response of the discrete correction filter is given by

$$Q(\omega) = \frac{C_{\phi\phi_d}(\omega)}{C_{\phi\psi}(\omega)} \tag{3.48}$$

□

Given (3.36), we assume that the sequence $\{c_{\phi\psi}[n,m]\}_{n,m\in\mathbb{Z}}$ is invertible, from (2.63), it is stable and reversible if

$$M_1 \le |C_{\phi\psi}(\omega)| \le M_2 \tag{3.49}$$

almost everywhere (a.e.) where M_1 and M_2 are two positive constants. This condition also ensures the existence and stability of the inverse filter, which is defined by $\mathbf{c}_{\phi\psi}^{-1}$ and

$$\frac{1}{C_{\phi\psi}(\omega)} \xrightarrow{IFT} \mathbf{c}_{\phi\psi}^{-1} \tag{3.50}$$

3.2.2 Optimality

It turns out that consistent resampling has a very desirable property that is described by the following proposition.

Proposition 3.2.2. *Consider a consistent resampling system as shown in Figure 3.2 with the correction filter $Q(\omega)$ given by (3.36). Let a_ϕ denote the sampled autocorrelation function of ϕ such that $a_\phi[k] = \langle \phi(x), \phi(x-k) \rangle$. If a_ϕ is invertible, then the input signal $f_T[n]$ can be reconstructed from the output by*

$$f_T[n] = \left\langle \sum_m f_{T'}[m]\phi\left(\frac{x}{T'} - m\right), \phi_d\left(\frac{x}{T} - n\right) \right\rangle \tag{3.51}$$

where ϕ_d is the dual operator of ϕ satisfying condition (2.17).

Proof. If the resampling is consistent, then

$$\begin{aligned} \widetilde{f}(x) &= \sum_n f_T[n]\phi\left(\frac{x}{T} - n\right) \\ &= \sum_m f_{T'}[m]\phi\left(\frac{x}{T'} - m\right) \end{aligned} \tag{3.52}$$

Sampling $\widetilde{f}(x)$ using ϕ_d, we get

$$c_T[n] = \left\langle \widetilde{f}(x), \phi_d(\frac{x}{T} - n) \right\rangle \tag{3.53}$$

Interpolating $c_T[n]$ with $\phi(\frac{x}{T'})$, we obtain the continuous signal

$$\widetilde{f}_c = \sum_n c_T[n]\phi\left(\frac{x}{T} - n\right) \tag{3.54}$$

Substituting (3.53) into (3.54), we have

$$\widetilde{f}_c = \widetilde{f} \sum_n \left\langle \phi\left(\frac{x}{T} - n\right), \phi_d(\frac{x}{T} - n) \right\rangle \tag{3.55}$$

Since ϕ_d and ϕ are a dual pair, this simplifies to $\widetilde{f}_c = \widetilde{f}$.

The frequency response of $\mathbf{a}_\phi$ is given by

$$A_\phi(\omega) = \sum_k |\Phi(\Omega + 2\pi k)|^2 \tag{3.56}$$

with $\omega = \Omega$. If $\mathbf{a}_\phi$ is invertible, then the condition (2.63) gives us

$$M_1 \leq \sum_k |\Phi(\Omega + 2\pi k)|^2 \leq M_2 \tag{3.57}$$

Hence ϕ satisfies the Riesz Condition. This implies that for any signal $\widetilde{f} \in V_T^\phi$, there exists a unique sequence $f_T[n]$ representing it in V_T^ϕ . Therefore $f_T[n] = c_T[n]$ and it can be reconstructed from $f_{T'}[m]$ using (3.53). $\square$

Since it is possible to reverse the resampling process if it is consistent, the information contained in the input sequence is preserved in the output through the synthesis function. Thus consistent resampling is informationally lossless and hence optimal. Furthermore, this proposition shows that optimal resampling can be achieved regardless of the choice of the resampling function.

Note that a similar strategy has been proposed in [164]. The authors suggest that upsampling can be viewed as the inverse of downsampling. So when the upsampled sequence is downsampled, the original sequence should be recovered. The theory of consistent resampling generalizes the situation to any sample rate conversion and is not restricted to upsampling. Furthermore, the sampling and resampling functions are not limited to the ideal sampler and the sampling interval ratio T/T' need not be rational as required in other literature [164, 174, 175].

3.2.3 Correction Filter Implementation

The frequency response of the correction filter is given by (3.36) which is

$$Q(\omega) = \frac{C_{\phi\phi_d}(\omega)}{C_{\phi\psi}(\omega)} \tag{3.58}$$

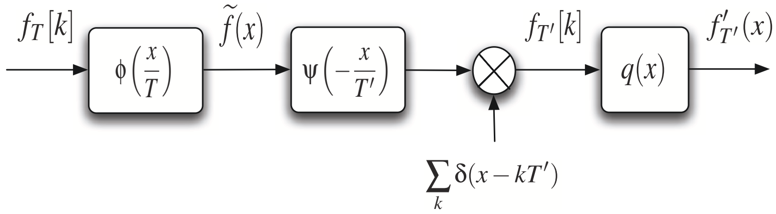

Figure 3.3: The resampling system with continuous correction filter.

with

$$C_{\phi\psi}(\omega) = \sum_{n,m} c_{\phi\psi}[n,m]e^{j\omega(m-nT_r)} \tag{3.59}$$

$$C_{\phi\phi_d}(\omega) = \sum_{n,m} c_{\phi\phi_d}[n,m]e^{j\omega(m-nT_r)} \tag{3.60}$$

Since $T_r = T/T'$ is generally not an integer, $(m - nT_r)$ is also typically a non-integer. Therefore, the conventional impulse invariant approach cannot be used to obtain the impulse response $\mathbf{q}$ of the correction filter.

We approach this problem by deriving the impulse response of a continuous correction filter $q(x)$ which achieves consistent resampling. The resampling system becomes the one in Figure 3.3 with the discrete correction filter replaced by a continuous one. The frequency response $Q(\Omega)$ of this filter should approximate $Q(\omega)$ in (3.58). Then the digital correction filter can be derived from $q(x)$.

From Figure 3.3, the resampling output is given by

$$f'_{T'}(x) = \sum_k f_{T'}[k]q(x - kT') \tag{3.61}$$

Now if $f'_{T'}(x)$ is filtered by $\phi(\frac{x}{T'})$, we obtain

$$\widehat{f}'(x) = \left[f'_{T'} * \phi\left(\frac{x}{T'}\right)\right](x) \tag{3.62}$$

Since the continuous signal reconstructed from the discrete input signal is given by $\widetilde{f}(x) = \sum_n f_T[n]\phi\left(\frac{x}{T} - n\right)$, by definition, consistent resampling is achieved when $\widehat{f}'(x) = \widetilde{f}(x)$.

Proposition 3.2.3. *The system in Figure 3.3 is consistent if the frequency response of correction filter $q(x)$ satisfies:*

$$Q(\Omega) = \frac{\Phi_d(\Omega)}{\Psi(\Omega)} \tag{3.63}$$

where $\phi_d(x)$ is the dual operator of ϕ as defined in (2.20).

Proof. From Figure 3.3,

$$f_{T'}[k] = \left\langle \widetilde{f}(x), \psi\left(\frac{x}{T'} - k\right)\right\rangle \tag{3.64}$$

Substituting (3.64) into (3.61), the output of the system can be expressed as

$$f'_{T'}(x) = \sum_m \left\langle \widetilde{f}(x), \psi\left(\frac{x}{T'} - m\right)\right\rangle q(x - mT') \tag{3.65}$$

Filtering this signal by $\phi(\frac{x}{T'})$ as in (3.62), we have

$$\widehat{f'}(x) = \sum_m \left\langle \widetilde{f}(x), \psi\left(\frac{x}{T'} - m\right)\right\rangle q(x - mT') * \phi\left(\frac{x}{T'}\right) \tag{3.66}$$

If the resampling is consistent, then $\widehat{f'}(x) = \widetilde{f}(x)$.

Sample $\widehat{f'}(x)$ by $\phi_d\left(\frac{x}{T'}\right)$, the dual function of $\phi\left(\frac{x}{T'}\right)$, at rate T'. The sampled values are given by

$$\begin{aligned}
\widehat{f}'_{T'}[n] &= \left\langle \widehat{f'}(x), \phi_d\left(\frac{x}{T'} - n\right)\right\rangle \\
&= \sum_m \left\langle \widetilde{f}(x), \psi\left(\frac{x}{T'} - m\right)\right\rangle q(x - mT') * \phi\left(\frac{x}{T'}\right) * \phi_d\left(-\frac{x}{T'}\right)|_{x=nT'} \\
&= \sum_m \left\langle \widetilde{f}(x), \psi\left(\frac{x}{T'} - m\right)\right\rangle q(x - mT')|_{x=nT'} \\
&= \left\langle \widetilde{f}(x), \left[\sum_m q([n-m]\,T')\psi\left(\frac{x}{T'} - m\right)\right]\right\rangle
\end{aligned} \tag{3.67}$$

due to the duality property

$$\left\langle \phi\left(\frac{x}{T'} - m\right), \phi_d\left(\frac{x}{T'} - v\right)\right\rangle = \delta[m - v] \tag{3.68}$$

On the other hand, the sample values of $\widetilde{f}(x)$ are given by

$$\widehat{f}'_{T'}[k] = \left\langle \widetilde{f}(x), \phi_d\left(\frac{x}{T'} - k\right)\right\rangle \tag{3.69}$$

If $\widetilde{f}(x) = \widehat{f}'(x)$, the two sequences in (3.67) and (3.69) are the same. This amounts to requiring

$$\phi_d\left(\frac{x}{T'}\right) = \sum_m q(mT')\psi\left(\frac{x}{T'} - m\right) \tag{3.70}$$

Let

$$q_{T'}(x) = \sum_m q_{T'}[m]\delta(x - mT') \tag{3.71}$$

where $q_{T'}[m] = q(mT')$. Then (3.70) can be expressed as

$$\phi_d\left(\frac{x}{T'}\right) = q_{T'}(x) * \psi\left(\frac{x}{T'}\right) \tag{3.72}$$

In the Fourier domain, this equation becomes

$$\begin{aligned} &\Phi_d(T'\Omega) = Q_{T'}(\Omega)\Psi(T'\Omega) \\ \Rightarrow\quad &Q_{T'}(\Omega) = \frac{\Phi_d(T'\Omega)}{\Psi(T'\Omega)} \end{aligned} \tag{3.73}$$

where $Q_{T'}(\Omega)$ is the Fourier transform of $q_{T'}(x)$. The frequency response of $q(x)$ is therefore given by

$$Q(\Omega) = Q_{T'}\left(\frac{\Omega}{T'}\right) \tag{3.74}$$

$$\qquad = \frac{\Phi_d(\Omega)}{\Psi(\Omega)} \tag{3.75}$$

□

Proposition 3.2.3 derives the continuous correction filter according to the consistent resampling principle. The impulse response of the digital correction filter can now be obtained by the impulse invariant method. By sampling $q(x)$ at rate T', we have $q'_T[m] = q(x)|_{x=T'}$. The frequency response $Q(\omega)$ of the digital correction filter is identical to $Q_{T'}(\Omega)$ given by (3.73). Therefore, according to Proposition 3.2.3, this digital filter enforces consistent resampling.

3.3 De-interlacing Revisited

We follow the model discussed in Section 2.7 to analyze the de-interlacing system using consistent resampling. Suppose the first order B-spline which is defined by

$$\beta^1(x) = \begin{cases} 1-|x|, & 0 \le |x| < 1 \\ 0, & \text{otherwise} \end{cases} \tag{3.76}$$

is chosen to be the interpolation function of the de-interlacing system. Then the existing samples $f[2k]$, the resampled samples $f[2n+1]$ and the motion compensated $f[2m+a]$ in Figure 2.12 are related by

$$f[2m+a] = \left(\sum_k f[2k]\beta^1(x-2k) + \sum_n f[2n+1]\beta^1(x-2n-1) \right) \Bigg|_{x=2m+a} \tag{3.77}$$

for $k, n, m \in \mathbb{N}$. Since $\beta^1(x)$ is non-zero only in interval $x \in [-1, 1]$ and $0 < a \le 1$, $\beta^1(a+2(m-k))$ and $\beta^1(a+2(n-k)-1)$ are zero for all k and n, except when $k = n = m$. Hence (3.77) can be reduced to

$$f[2k+a] = (1-a)f[2k] + af[2k+1] \tag{3.78}$$

Rearranging, we have

$$f[2k+1] = \frac{1}{a} f[2k+a] - \frac{1}{a}(1-a)f[2k] \tag{3.79}$$

Expressing (3.79) in the matrix form, the input and output sequences of the de-interlacing system are related by

$$\begin{bmatrix} f[2k] \\ f[2k+1] \end{bmatrix} = \underbrace{\frac{1}{a} \begin{bmatrix} a & 0 \\ a-1 & 1 \end{bmatrix}}_{\mathbf{D}} \begin{bmatrix} f[2k] \\ f[2k+a] \end{bmatrix} \tag{3.80}$$

where the transfer matrix of the system is denoted by $\mathbf{D}$. The stability of the resampling system is measured by the condition number as discussed in Section 2.4.

$$\alpha = \mathbf{D}^T\mathbf{D} = \frac{1}{a^2} \begin{bmatrix} a^2 + (a-1)^2 & a-1 \\ a-1 & 1 \end{bmatrix} \tag{3.81}$$

In this case, it can be equivalently measured as the square root of the ratio of the maximum and minimum eigenvalues of the system matrix [8]. Thus

$$\alpha = \sqrt{\frac{\lambda_{\max}}{\lambda_{\min}}} = \sqrt{\frac{1 + a^2 - a + (1-a)\sqrt{1+a^2}}{1 + a^2 - a - (1-a)\sqrt{1+a^2}}} \tag{3.82}$$

It can be easily verified that α is minimum when $(1 - a) = 0$ or when $a = 1$.

We proceed to analyze the effect of the consistent resampling in de-interlacing system. Denote the existing samples by $\mathbf{f}_{0,i} = \{f[2k]\}_{k\in\mathbb{Z}}$ and the motion compensated samples by $\mathbf{f}_{1,i} = \{f[2m + a]\}_{m\in\mathbb{Z}}$ which are the inputs to the de-interlacing system. Let the resampled output be $\mathbf{f}_{1,o} = \{f[2n + 1]\}_{n\in\mathbb{Z}}$. The complete output consists of the samples $\mathbf{f}_{0,o} = \mathbf{f}_{0,i} = \{f[2k]\}_{k\in\mathbb{Z}}$ and the resampled sequence $\mathbf{f}_{1,o}$.

If the system is consistently resampling, then according to Definition 3.1.1 the output and input must both approximate the same analog signal in the space of V^{β^1}. That is,

$$\begin{aligned} & \sum_k f[2k]\beta^1(x - 2k) + \sum_m f[2m + a]\beta^1(x - 2k - a) \\ = \; & \sum_k f[2k]\beta^1(x - 2k) + \sum_n f[2n + 1]\beta^1(x - 2n - 1) \end{aligned} \tag{3.83}$$

Taking samples of the signals on the left and right hand sides of (3.83) at $x = 2l$ (even positions) where $k, l, m, n \in \mathbb{Z}$, we have

$$\begin{aligned} & \sum_k f[2k]\beta^1(2(l - k)) + \sum_m f[2m + a]\beta^1(2(l - m) - a) \\ = \; & \sum_k f[2k]\beta^1(2(l - k)) + \sum_n f[2n + 1]\beta^1(2(l - n) - 1) \end{aligned} \tag{3.84}$$

This simplifies to

$$f[2l] + (1 - a)f[2l + a] = f[2l] \tag{3.85}$$

Similarly, sampling (3.83) at the odd positions where $x = 2l + 1$, we have

$$\begin{aligned} & \sum_k f[2k]\beta^1(2(l - k) + 1) + \sum_m f[2m + a]\beta^1(2(l - m) + 1 - a) \\ = \; & \sum_k f[2k]\beta^1(2(l - k) + 1) + \sum_n f[2n + 1]\beta^1(2(l - n)) \end{aligned} \tag{3.86}$$

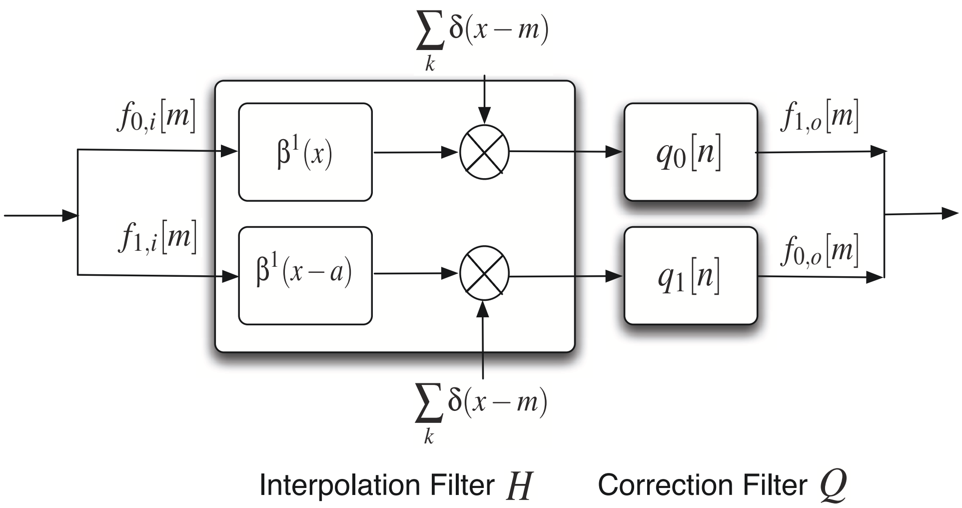

Figure 3.4: De-interlacing system modeled as a multichannel system.

which simplifies to

$$af[2l+a] = f[2l+1] \tag{3.87}$$

Using (3.85) and (3.87), the de-interlacing system can be represented by the matrix equation

$$\begin{bmatrix} 1 & 1-a \\ 0 & a \end{bmatrix} \begin{bmatrix} f[2l] \\ f[2l+a] \end{bmatrix} = \begin{bmatrix} 1 & 0 \\ 0 & 1 \end{bmatrix} \begin{bmatrix} f[2l] \\ f[2l+1] \end{bmatrix} \tag{3.88}$$

The de-interlacing system can be modelled as a multichannel system. The number of channels is two since there are two sets of input – existing samples $\mathbf{f}_{0,i}$ and motion compensated samples $\mathbf{f}_{1,i}$. This two-channel system is shown in Figure 3.4. The displacement between the two channels are modelled by a corresponding displacement between the interpolation functions $\phi_1 = \beta(x)$ and $\phi_2 = \beta(x-a)$. The first subscript denotes the channel number, and the second subscript indicates the input and output.

Denote the multichannel interpolation filter and the multichannel correction filter by $\mathbf{H}$ and $\mathbf{Q}$ respectively. The input-output relationship of this multichannel system is therefore given by

$$\mathbf{F}_o = \mathbf{QHF}_i \tag{3.89}$$

where

$$\begin{aligned} \mathbf{F}_o &= \begin{bmatrix} f_{0,o} \\ f_{1,o} \end{bmatrix} \\ \mathbf{F}_i &= \begin{bmatrix} f_{0,i} \\ f_{1,i} \end{bmatrix} \end{aligned} \tag{3.90}$$

Using (3.89) and (3.90), (3.88) can be expressed as

$$\begin{aligned} \begin{bmatrix} 1 & 1-a \\ 0 & a \end{bmatrix} \mathbf{F}_i &= \begin{bmatrix} 1 & 0 \\ 0 & 1 \end{bmatrix} \mathbf{F}_o \\ &= \begin{bmatrix} 1 & 0 \\ 0 & 1 \end{bmatrix} \mathbf{QHF}_i \end{aligned} \tag{3.91}$$

The resampling process can be described by the matrix

$$\mathbf{QH} = \begin{bmatrix} 1 & 1-a \\ 0 & a \end{bmatrix} \tag{3.92}$$

The stability of the resampling process is evaluated by the condition number $\alpha = \sqrt{\frac{\lambda_{\max}(A)}{\lambda_{\min}(A)}}$ where A is the matrix

$$A = (\mathbf{QH})^T \mathbf{QH} \tag{3.93}$$

$$= \begin{bmatrix} 1 & (1-a) \\ (1-a) & a^2 + (1-a)^2 \end{bmatrix} \tag{3.94}$$

It can be verified that

$$\alpha = \sqrt{\frac{\lambda_{\max}(A)}{\lambda_{\min}(A)}} = \sqrt{\frac{a^2 - a + 1 + |a-1|\sqrt{a^2+1}}{a^2 - a + 1 - |a-1|\sqrt{a^2+1}}} \tag{3.95}$$

α has the minimum value of 1 when $\lambda_{\max} = \lambda_{\min}$. This is achieved if $a = 1$. Therefore, using consistent resampling, results consistent with intuition is obtained. This is not achievable by applying the generalized sampling theory to de-interlacing as discussed previously in Section 2.7.

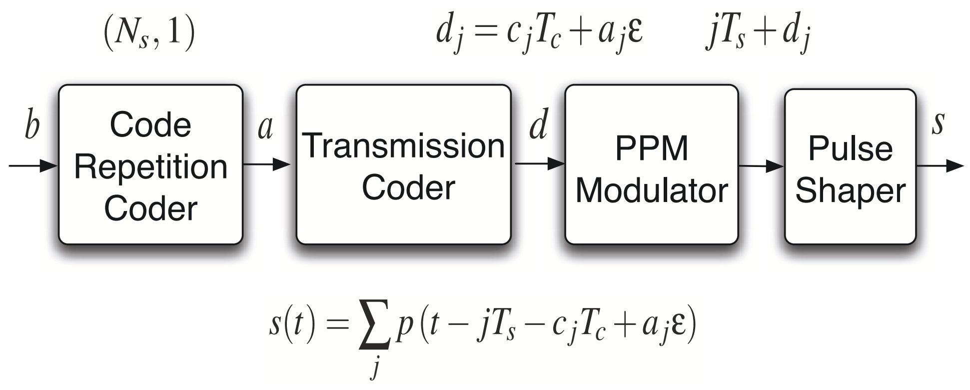

Figure 3.5: Transmission scheme for a PPM-UWB signal.

3.4 Applications

3.4.1 Demodulation of UWB Signals

We demonstrate the lossless property of consistent resampling by considering the problem of demodulation of Impulse Radio UWB signals.

Time-hopping impulse radio has been proposed as a simple UWB wireless communication technique. It transmits a stream of pulse-position modulated (PPM) impulses that are of very short (sub-nanosecond) duration [5, 176]. A typical impulse radio transmitter consists of (1) a channel coder to introduce redundancy, (2) a transmission coder to scramble and code the sequence, (3) a PPM modulator to produce modulated pulses and (4) a pulse shaper [177]. It is illustrated in Figure 3.5.

Given a binary sequence $\mathbf{b} = \{\ldots, b_0, b_1, \ldots, b_k, \ldots\}$ to be transmitted, the code repetition coder produces a sequence $\mathbf{a} = \{\ldots, a_0, a_1, \ldots, a_k, \ldots\}$ where $a_j = \{b_j, b_j, \ldots, b_j\}$ which is a repetition of the symbol b_j N_s times. The transmission coder then adds an integer valued code $\mathbf{c} = \{\ldots, c_0, c_1, \ldots, c_k, \ldots\}$ to the binary sequence $\mathbf{a}$ and generates a new sequence $\mathbf{d}$. Each pulse in $\mathbf{d}$ is modulated by the pulse-position modulator and shaped by a pulse shaping function $p(t)$. The signal $s(t)$ that is transmitted is given by

$$s(t) = \sum_j p(t - jT_s - c_j T_c - a_j \epsilon) \tag{3.96}$$

where T_s is the symbol rate, T_c is the chip rate and $c_j T_c + \epsilon < T_s$ for all c_j.

Demodulating such signals involves an estimation of the position of each pulse [178–180]. For our purposes, it suffices to combine the various time shifts into a single variable t_j. Thus

$$s(t) = \sum_j p(t - t_j \epsilon) \tag{3.97}$$

Since the duration of the pulses are short and strictly non-overlapping [181, 182], we can assume that $s(t)$ is a sequence of Diracs:

$$x(t) = \sum_{k \in [1,2,\cdots]} c_k \delta\left(t - t_k\right) \qquad \forall t_k \geq 0 \tag{3.98}$$

The pulses can be viewed as nonuniform samples of an underlying continuous signal. Consistent resampling can be applied to convert this non-uniformly sampled sequence to a uniformly resampled one. The original pulse positions can then be deduced from the uniformly sampled sequence.

If we interpolate the stream of pulses in (3.98) using $\beta_m^n(t)$, we have

$$\widehat{f}(t) = \sum_k c_k \beta_m^n(t - t_k) \tag{3.99}$$

where $\beta_m^n(t)$ is the dilated B-spline of order n, $t \in R$ which is defined by

$$\beta_m^n(t) = \sum_{j=0}^{n+1} \frac{(-1)^j}{n!} \left(\begin{array}{c} n+1 \\ j \end{array} \right) \cdot \left(\frac{t}{m} + \frac{n+1}{2} - j \right)^n \mu \left(\frac{t}{m} + \frac{n+1}{2} - j \right) \tag{3.100}$$

and $\mu(x)$ is the step function where $\mu = 1$ for $x \geq 0$ and zero otherwise. It can be observed from (3.100) that

$$\beta_m^n(t) = 0 \text{ when } |t| \geq \tfrac{(n+1)m}{2} \tag{3.101}$$

The dilation level m is chosen such that the width of the support of β_m^n, $\mathcal{B} = [-\frac{(n+1)m}{2}, \frac{(n+1)m}{2}]$ is smaller than the minimum distance between the pulses,

$$(n+1)m < \min_k (t_{k+1} - t_k) \tag{3.102}$$

Therefore $\widehat{f}$ contains non-overlapping weighted shifts of β_m^n. Without loss of generality, assume that $m = 1$.

The first derivative of the B-spline is given by [92]

$$\frac{d\beta^n(t)}{dt} = \beta^{n-1}\left(t + \frac{1}{2}\right) - \beta^{n-1}\left(t - \frac{1}{2}\right) \tag{3.103}$$

Therefore the derivative of (3.99) is

$$\frac{d\widehat{f}(t)}{dt} = \sum_k c_k \left[\beta^{n-1}\left(t + \frac{1}{2} - t_k\right) - \beta^{n-1}\left(t - \frac{1}{2} - t_k\right)\right] \tag{3.104}$$

We shall assume that $n > 1$.

Note that c_k and t_k are independent parameters of the signal. We shall show that $\widehat{f}(t)$ contains all the information we need to estimate c_k and t_k.

Proposition 3.4.1. *Let the set* $\Gamma = \{t_c\}$ *contains all the roots of (3.104) such that*

$$\left.\frac{d\widehat{f}(t)}{dt}\right|_{t_c} = 0 \tag{3.105}$$

Then all the values of t_k *in (3.99) can be found in* Γ.

Proof. When $t = t_k$, (3.104) becomes

$$\frac{d\widehat{f}(t)}{dt} = \sum_k c_k \left[\beta^{n-1}\left(\frac{1}{2}\right) - \beta^{n-1}\left(-\frac{1}{2}\right)\right] \tag{3.106}$$

Since B-splines are symmetric and $\beta^{n-1}(t) = \beta^{n-1}(-t)$, we have $d\widehat{f}(t)/dt = 0$ and therefore $t_k \in \Gamma$. □

Proposition 3.4.2. *All* t_k *in (3.99) can be identified from the set* Γ *as defined in Proposition 3.4.1.*

Proof. Let $t = t_c$ in (3.104). Since t_k is unique and the pulses are strictly non-overlapping, (3.105) implies that $\forall k$

$$\beta^{n-1}\left(t_c - t_k + \frac{1}{2}\right) = \beta^{n-1}\left(t_c - t_k - \frac{1}{2}\right) \tag{3.107}$$

There are two possibilities to consider in solving this equation:

(i) $\beta^{n-1}\left(t_c - t_k + \frac{1}{2}\right) = \beta^{n-1}\left(t_c - t_k - \frac{1}{2}\right) \neq 0$;

(ii) $\beta^{n-1}\left(t_c - t_k + \frac{1}{2}\right) = \beta^{n-1}\left(t_c - t_k - \frac{1}{2}\right) = 0$

We consider the two cases inidvidually. In the first case, since β^{n-1} is symmetric, (3.107) requires that

$$t_c - t_k + \frac{1}{2} = t_c - t_k - \frac{1}{2} \qquad \text{or} \qquad -\left(t_c - t_k - \frac{1}{2}\right) \tag{3.108}$$

This gives us

$$t_c = t_k \tag{3.109}$$

In the second case, since $\beta^{n-1}\left(t_c - t_k + \frac{1}{2}\right) = 0$ and $\beta^{n-1}\left(t_c - t_k - \frac{1}{2}\right) = 0$, from (3.101) we have

$$\left|t_c - t_k + \frac{1}{2}\right| \geq \frac{n}{2} \tag{3.110}$$

$$\left|t_c - t_k - \frac{1}{2}\right| \geq \frac{n}{2} \tag{3.111}$$

The inequality (3.110) is reduced to

$$t_c - t_k \geq \frac{n}{2} - \frac{1}{2} \qquad \text{or} \qquad t_c - t_k \leq -\frac{n}{2} - \frac{1}{2} \tag{3.112}$$

Similary, (3.111) is equivalent to

$$t_c - t_k \geq \frac{n}{2} + \frac{1}{2} \qquad \text{or} \qquad t_c - t_k \leq -\frac{n}{2} + \frac{1}{2} \tag{3.113}$$

Since $n > 0$, combining (3.112) and (3.113), we have

$$t_c - t_k \geq \frac{n}{2} + \frac{1}{2} \tag{3.114}$$

or

$$t_c - t_k \leq -\frac{n}{2} - \frac{1}{2} \tag{3.115}$$

Therefore,

$$|t_c - t_k| \geq \frac{n+1}{2} \tag{3.116}$$

Thus the set Γ contains $t_c = t_k$ (from the first case) and $|t_c - t_k| \geq \frac{n+1}{2}$ (from the second case). To identify t_k, notice that when $t = t_c$ and $|t_c - t_k| \geq \frac{n+1}{2}$, then $\widehat{f} = 0$. This is because in (3.99), if $t = t_c$, then $|t_c - t_k| \geq \frac{n+1}{2}$ and $\beta^n(t_c - t_k) = 0$ for all k, giving $\widehat{f} = 0$. It is therefore possible to identify t_k from the set Γ by checking the value of $\widehat{f}(t_c)$. When $\widehat{f}(t_c) \neq 0$, we have $t_k = t_c$. □

The proof given above provides us with a method to determine t_k. Once the values of t_k are available, the coefficients can be obtained by $c_k = \widehat{f}(t)|_{t=t_k}$. All information of $x(t)$ are preserved and stored in the continuous signal $\widehat{f}(t)$. $x(t)$ can be reconstructed from $\widehat{f}(t)$.

Based on Proposition 3.4.2, we apply consistent resampling to the demodulation of impulse radio signals. Consider $x(t)$ to be a modulated discrete sequence $\mathbf{c}$ at positions $\mathbf{t}$, it approximates $\widehat{f}(x)$ in the space generated by β^n. Let a sequence $\mathbf{g}_T$ satisfy

$$\sum_m g_T[m]\beta^n\left(\frac{x}{T} - m\right) = \sum_k c_k \beta^n(t - t_k) \tag{3.117}$$

i.e. $\mathbf{g}_T$ is the consistently resampled sequence of $x(t)$ in V^{β^n}. From Proposition 3.4.2, $\widehat{f}(t)$ contains all information required to reconstruct $x(t)$. Since $\mathbf{g}_T$ approximates $\widehat{f}$, $x(t)$ can be obtained from $\mathbf{g}_T$ as well.

Note that we have not yet discussed the conditions on the resampling interval T such that consistent resampling can be achieved. We shall do so in Section 6.2.2. In the mean time, we shall assume that the resampling rate is sufficient to achieve consistent resampling.

We shall now use β^2 as an example. Since the main purpose is to localize the pulses, we shall assume that $c_k = 1$ for all k. Let a sequence of pulses consists of eight distinct pulses in a time segment of length 128. The pulses are generated randomly and their positions

	t_1	t_2	t_3	t_4	t_5	t_6	t_7	t_8
original	9	15	19	32	57	62	82	105
estimated	9	15	19	32	57	62	82	105

Table 3.1: The desired and the estimated values of t_k.

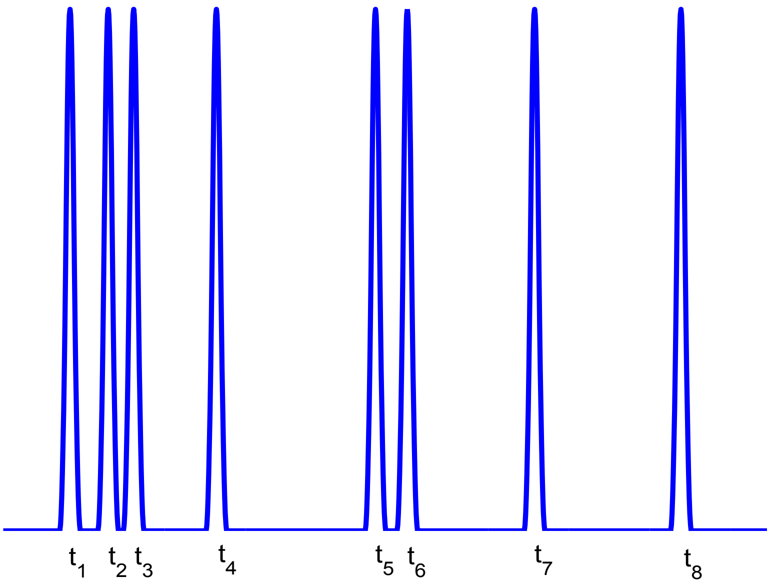

Figure 3.6: The modulated signal $\widehat{f}(t)$.

are shown in the first row of Table 3.1. The minimum distance between neighboring pulses is $D = t_3 - t_2 = 4$. Since the width of the support of β^2 is $2\left(\frac{2+1}{2}\right) < 4$, $\widehat{f}$ contains non-overlapping modulated pulses, as shown in Figure 3.6.

The first order derivative of $\widehat{f}(t)$ is shown in Figure 3.7. Note that the pulse locations t_k are at the zero-crossings of $d\widehat{f}/dt$ with the t axis. Using Proposition 3.4.2, t_k can be identified as those points where $d\widehat{f}/dt = 0$ and $\widehat{f} \neq 0$.

This process can also be performed in the discrete domain. The B-spline coefficients $g[k]$ of a signal can be obtained through a direct transform [87, 92, 93]. The process is shown in Figure 3.8. Sampling $\widehat{f}(t)$ at $t = mk$ gives us $y_m[k]$ and the B-spline coefficients are given by

$$g[k] = (b_m^n)^{-1} * y_m[k] \tag{3.118}$$

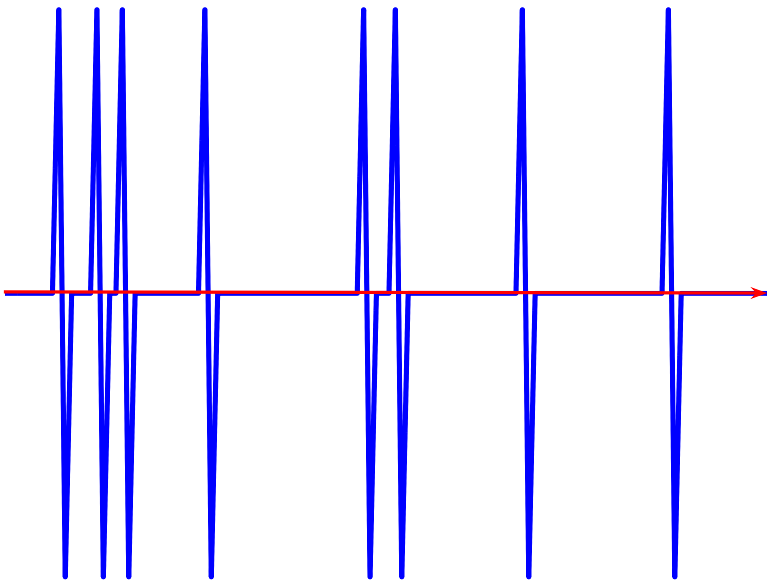

Figure 3.7: First order differentiation of $\widehat{f}(t)$.

The filter $(b_m^n)^{-1}$ is the inverse of the discrete B-spline filter with coefficients

$$b_m^n[k] = \beta^n \left(\frac{k}{m}\right) \tag{3.119}$$

The derivative is obtained by applying the difference operator $\mathbf{d} = \delta(k) - \delta(k-1)$ to $\{g[k]\}$ followed by a shifted discrete B-spline filter $\mathbf{c}_m^{n-1}$, as shown in Figure 3.9, where

$$c_m^{n-1}[k] = \beta^{n-1} \left(\frac{k}{m} + \frac{1}{2}\right) \tag{3.120}$$

Here, m is the sampling interval used in the system. The output $\mathbf{h}$ is the ideally sampled sequence of $\frac{df(t)}{dt}$ at rate m. Thus,

$$h[k] = \left.\frac{df(t)}{dt}\right|_{t=km} \tag{3.121}$$

In this example, $b_m^2[k] = \beta^2\left(\frac{k}{m}\right)$ and $c_m^1[k] = \beta^1\left(\frac{k}{m} + \frac{1}{2}\right)$. Since c_m^1 is shifted from the B-spline by $\frac{1}{2}$, choose $m = \frac{1}{2}$. The ideal samples $\mathbf{y}$ and the output sequence $\mathbf{h}$ obtained are shown in Table 3.2 and Table 3.2 respectively. Based on Proposition 3.4.2, we choose k such that $y[k] \neq 0$ and $h[k] = 0$. Since the sequence is sampled at $m = \frac{1}{2}$, the exact locations are given by $k/2$. The results are shown in the second row of Table 3.1. It shows that our method demodulates $x(t)$ accurately.

To summarize, the steps to demodulate UWB signal in the digital domain is to

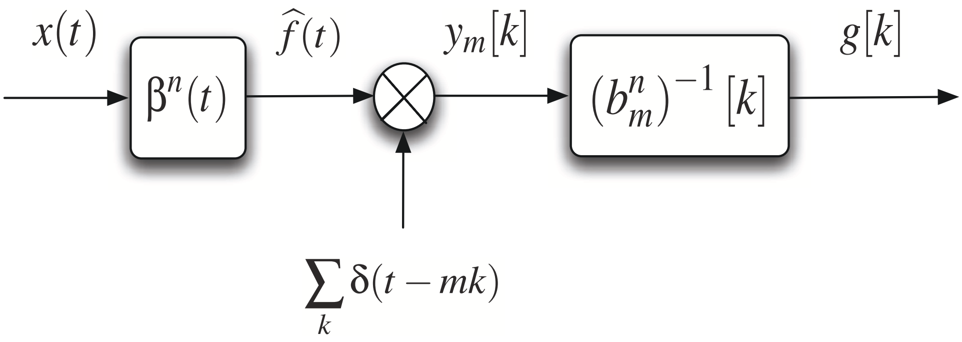

Figure 3.8: Direct Transform to obtain the B-spline coefficients of signal $x(t)$.

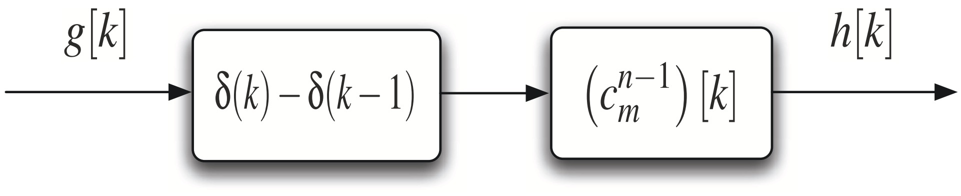

Figure 3.9: Differentiate a discrete sequence using B-spline..

k	$y[k]$							
$16-23$	0.1239	0.4545	0.7438	0.6198	0.2314	0	0	0
$24-31$	0	0	0	0	0.1239	0.4545	0.7438	0.6198
$32-39$	0.2314	0	0	0	0.1239	0.4545	0.7438	0.6198
$40-47$	0.2314	0	0	0	0	0	0	0
$60-67$	0	0	0.1239	0.4545	0.7438	0.6198	0.2314	0
$68-75$	0	0	0	0	0	0	0	0
$112-119$	0.1239	0.4545	0.7438	0.6198	0.2314	0	0	0
$120-127$	0	0	0.1239	0.4545	0.7438	0.6198	0.2314	0
$156-163$	0	0	0	0	0	0	0.1239	0.4545
$164-171$	0.7438	0.6198	0.2314	0	0	0	0	0
$208-215$	0.1239	0.4545	0.7438	0.6198	0.2314	0	0	0
$216-223$	0	0	0	0	0	0	0	0

Table 3.2: Value of $y[k]$. All other elements of $y[k]$ are zero.

k	$h[k]$															
$16-31$	0	1	0	-1	0	0	0	0	0	0	0	0	0	1	0	-1
$32-47$	0	0	0	0	0	1	0	-1	0	0	0	0	0	0	0	0
$60-75$	0	0	0	1	0	-1	0	0	0	0	0	0	0	0	0	0
$112-127$	0	1	0	-1	0	0	0	0	0	0	0	1	0	-1	0	0
$156-171$	0	0	0	0	0	0	0	1	0	-1	0	0	0	0	0	0
$208-223$	0	1	0	-1	0	0	0	0	0	0	0	0	0	0	0	0

Table 3.3: Value of $h[k]$. All other elements of $h[k]$ are zero.

(i) Find the B-spline coefficient of the sequences;

(ii) differentiate the B-spline coefficients;

(iii) Compare two discrete sequences

Assume that the number of pulses of the UWB signal is N. The first step is to linear process the sequence. The filter length depends on the choice of B-spline function. However the complexity of this step is $O(N)$ since only linear processing is involved. Similarly, to differentiate the sequence is of complexity $O(N)$.

The major part is the third step which performs a comparison between 2 discrete sequence. The size of the sequence depends on the sparsity of the original UWB sequence. In our case, there are 8 pulses in the period of 124. The minimum distance between the neighboring pulses is 4 and the resampling rate is 2Hz. Therefore the size of the sequence is $N = 2 \times 128 = 256$. To compare two sequence of size N, the complexity is at most $O(N^2)$. An in-depth analysis shows that the comparison is carried out to locate the positions in the sequence such that one is zero ($h[k] = 0$) and the other is not ($y[k] \neq 0$), it would simply result in worst case scenario of linear complexity. Therefore, the complexity of the demodulation algorithm is $O(N)$, although the factor depends on the order of the B-spline and the sparsity of the sequence and can be large.

There is one limitation of our algorithm that it is sensitive to noise. In real life, the UWB signals are inevitably corrupted by noise and our method will result in false positive pulses. A possible solution is that the UWB signal is first to go through a de-noising process. An effective way to do so is to correlate the UWB signal with its pulse function. The output signal is free of Gaussian-like white noise and our algorithm can be used to demodulate the sequence.

3.4.2 Image Resizing

Now we consider the application of consistent resampling to image resizing. Usually, the quality of an image will degrade when it is zoomed in and out several times. In our experiments, an image is either enlarged by a factor of 1.25 or reduced to 0.8 of its size. These factors are chosen arbitrarily and other factors could have been chosen instead.

Four different resampling techniques are considered. They are

(i) classic interpolation

(ii) oblique interpolation [170]

(iii) quasi interpolation [171]

(iv) consistent resampling

In order to obtain a fair comparison, the interpolating function used by all four techniques is the first order B-spline β^1. Recall that

$$\beta^1(x) = \begin{cases} 1 - |x|, & |x| \leq 1 \\ 0, & \text{otherwise} \end{cases} \tag{3.122}$$

Since β^1 is a Nyquist function, the B-spline coefficients are the same as the samples obtained by ideal sampling.

The function 'imresize' from the image processing toolbox of MATLAB is used to obtain the results of classic resampling. This function treats the 2D image as separable and operations are carried out along each axis. The 'METHOD' is set to be 'bilinear' for interpolation using β^1. For a resizing factor of 1.25, the resampling interval is $T' = 0.8$. Let I denote the input image. Then the output image, denoted as K, is given by

$$\begin{aligned} K[m] &= \sum_i I[i]\beta^1(x-i)|_{x-mT'} \\ &= \sum_i I[i]\beta^1(0.8m-i) \end{aligned} \tag{3.123}$$

where $i, m \in \mathbb{Z}$. Since $\beta^1(x)$ is zero for $|x| \geq 1$, only the samples $I[i]$ whose indices fall in the range $|0.8m - i| < 1$ are used to obtain $K[m]$. Thus the possible values of i are

$$\begin{aligned} & 0.8m - 1 < i < 0.8m + 1 \\ \Rightarrow \quad & i = \lfloor 0.8m \rfloor \;\text{ or }\; i = \lceil 0.8m \rceil \end{aligned} \tag{3.124}$$

where $\lfloor x \rfloor$ represents the largest integer not greater than x and $\lceil x \rceil$ is the smallest integer not less than x. So for $x \notin \mathbb{Z}$, $\lfloor x \rfloor + 1 = \lceil x \rceil$. Thus when $0.8m$ is not an integer, (3.123) becomes

$$\begin{aligned} K[m] &= I\left[\lfloor 0.8m \rfloor\right]\beta^1(\lfloor 0.8m \rfloor - 0.8m) + I\left[\lceil 0.8m \rceil\right]\beta^1\left(\lceil 0.8m \rceil - 0.8m\right) \\ &= I\left[\lfloor 0.8m \rfloor\right]\left(\lceil 0.8m \rceil - 0.8m\right) + I\left[\lceil 0.8m \rceil\right]\left(0.8m - \lfloor 0.8m \rfloor\right) \end{aligned} \tag{3.125}$$

When $0.8m$ is an integer, we only need to consider $i = 0.8m$ and (3.123) is reduced to

$$K[m] = I[0.8m] \tag{3.126}$$

Since the classic interpolation method does not require any correction filter, $Q(z) = 1$.

Oblique interpolation has been described in Section 2.4. The correction filter required is specified in (2.102). Since we are now using β^1 as the interpolating function, $n = 1$. From Table 2.1 we have

$$B^1(z) = 1 \tag{3.127}$$

$$B^2(z) = \frac{1}{8}\left(z + 6 + z^{-1}\right) \tag{3.128}$$

Substituting (3.127) into (2.102), we have the transfer function of the correction filter which is given by

$$Q(z) = \frac{8}{z + 6 + z^{-1}} \tag{3.129}$$

For quasi interpolation, as discussed in Section 2.6.3, the correction filter $Q(z)$ is designed such that the effective sampling filter approximates the dual function of the interpolation filter. In this case, the sampling function is the Dirac impulse $\delta(x)$ and the sampling interval $T = 1$. From (2.65) the effective sampling function is given by

$$\psi_e(x) = \sum_k q[k]\delta\left(x - k\right) \tag{3.130}$$

with the Fourier transform

$$\Psi_e(\Omega) = Q(\omega) \tag{3.131}$$

where $\omega = \Omega T = \Omega$. When the interpolation function is $\beta^1(x)$, the order of approximation is $L = 2$ and $N = L + 1 = 3$, (2.108) amounts to requiring

$$\begin{aligned} & Q(\omega) - B_d^1(\Omega) = O(\Omega^3) \\ \Rightarrow \quad & Q(\omega) = B_d^1(\Omega) + O(\Omega^3) \end{aligned} \tag{3.132}$$

where $B_d^1(\Omega)$ is the frequency response of the dual function of $\beta^1(x)$. From (2.20), the dual function β_d^1 is approximated by

$$\begin{aligned} B_d^1(\Omega) &= \frac{B_1(\Omega)}{A_\beta^1(\omega)} \\ &= \frac{1}{1 - \frac{2}{3}sin^2\left(\frac{\Omega}{2}\right)} \end{aligned} \tag{3.133}$$

Using Taylor's expansion on $A_\beta^1(\omega)$, we have

$$B_d^1(\Omega) = \frac{1}{1 - \frac{1}{12}\Omega^2 + O(\Omega^4)} \tag{3.134}$$

Let $P(\omega) = Q^{-1}(\omega)$. From (3.132),

$$\begin{aligned} P(\omega) &= \frac{1}{B_d^1(\Omega) + O(\Omega^3)} \\ &= \frac{1}{B_d^1(\Omega)} + \left(\frac{1}{B_d^1(\Omega) + O(\Omega^3)} - \frac{1}{B_d^1(\Omega)} \right) \\ &= \frac{1}{B_d^1(\Omega)} + \frac{O(\Omega^3)}{B_d^1(\Omega)[B_d^1(\Omega) + O(\Omega^3)]} \end{aligned} \tag{3.135}$$

When $\Omega \to 0$, $B_d^1(\Omega) \to 1$ and $B_d^1(\Omega) + O(\Omega^3) \to 1$. Therefore

$$P(\omega) = \frac{1}{B_d^1(\Omega)} + O(\Omega^3) \tag{3.136}$$

Substituting (3.134) into this equation, we have

$$P(\omega) = 1 - \frac{1}{12}\Omega^2 + O(\Omega^3) + O(\Omega^4) \tag{3.137}$$

When $\Omega \to 0$, $O(\Omega^4) = O(\Omega^3)$. Thus the equation is reduced to

$$\begin{aligned} P(\omega) &= 1 - \frac{1}{12}\Omega^2 + O(\Omega^3) \\ &= 1 - \frac{1}{12}\omega^2 + O(\omega^3) \end{aligned} \tag{3.138}$$

since $\omega = \Omega$ when $T = 1$. Ignoring the higher order terms and assuming that P is symmetrical up to order 1, let

$$P(\omega) = a + b(e^{j\omega} + e^{-j\omega}) = a + 2b\cos(\omega) \tag{3.139}$$

Using Taylor's expansion for the cosine function, we have

$$\begin{aligned} P(\omega) &= a + 2b(1 - \frac{\omega^2}{2} + O(\omega^4)) \\ &= (a + 2b) - b\omega^2 + O(\omega^4) \end{aligned} \tag{3.140}$$

Compare with (3.138), we obtain $b = \frac{1}{12}$ and $a = \frac{5}{6}$. Therefore,

$$Q(\omega) = \frac{1}{P(\omega)} = \frac{12}{e^{j\omega} + 10 + e^{-j\omega}} \tag{3.141}$$

with the corresponding transfer function in z domain given by

$$Q(z) = \frac{12}{z + 10 + z^{-1}} \tag{3.142}$$

The correction filter for consistent resampling is obtained by (3.36) in Proposition (3.2.1). It is implemented by sampling the continuous correction filter $q(x)$ defined by Proposition 3.2.3 at rate T'. Since $\psi(x) = \delta(x)$ and $\Psi(\Omega) = 1$, from (3.58), $Q(\Omega) = \Phi_d(\Omega)$. The frequency response of the dual function is specified in (2.20),

$$B_d^1(\Omega) = \frac{B^1(\Omega)}{A_{\beta^1}(\omega)} \tag{3.143}$$

From (2.34),

$$B^1(\Omega) = sinc^2\left(\frac{\Omega}{2}\right) \tag{3.144}$$

$A_\beta^1(\omega)$ can be looked up in Table 2.1. With $\omega = \Omega$,

$$Q(\Omega) = B_d^1(\Omega) = \frac{sinc^2\left(\frac{\Omega}{2}\right)}{1 - \frac{2}{3}\sin^2\left(\frac{\Omega}{2}\right)} \tag{3.145}$$

To sample $q(x)$ at T', the frequency response of the sequence $\mathbf{q}_{T'}$, $Q(\omega)$ is related to $Q(\Omega)$ by setting $\Omega = \frac{\omega}{T'}$, therefore

$$\begin{aligned} Q(\omega) &= Q(\Omega)|_{\Omega=\omega/T'} \\ &= \frac{sinc^2\left(\frac{\omega}{2T'}\right)}{1 - \frac{2}{3}\sin^2\left(\frac{\omega}{2T'}\right)} \end{aligned} \tag{3.146}$$

To find the impulse response $q[n]$ of the digital correction filter whose response satisfies (3.146), we adopt the same approach used in quasi interpolation. Note that the length of the correction filters in both oblique and quasi interpolation are IIR filters of length 3. In order to compare the performance at the same computational cost, we set the length of $q[n]$ to be 3 such that $Q(\omega) = [a + b(e^{j\omega} + e^{-j\omega})^{-1}]$ for some constants a and b. From Taylor's expression,

$$\begin{aligned} sinc(x) &= \frac{sinc(x)}{x} = \frac{x - \frac{x^3}{3!} + \frac{x^5}{5!} - \cdots}{x} \\ &= 1 - \frac{x^2}{3!} + \frac{x^4}{5!} - \cdots \end{aligned} \tag{3.147}$$

Table 3.4: The correction filters and their frequency responses.

Resampling Technique	$Q(z)$	$Q(\omega)$
Classic Resampling	1	1
Oblique Resampling	$\left[\frac{1}{4}z^{-1} + \frac{3}{4} + \frac{1}{4}z\right]^{-1}$	$\left[\frac{3}{4} + \frac{1}{2}\cos(\omega)\right]^{-1}$
Quasi Resampling	$\left[\frac{1}{12}z^{-1} + \frac{5}{6} + \frac{1}{12}z^{1}\right]^{-1}$	$\left[\frac{10}{12} + \frac{1}{12}\cos(\omega)\right]^{-1}$
Consistent Resampling (Zoom in)	$\left[\frac{4}{75}z + \frac{67}{75} + \frac{4}{75}z^{-1}\right]^{-1}$	$\left[\frac{67}{75} + \frac{8}{75}\cos(\omega)\right]^{-1}$
Consistent Resampling (Zoom out)	$\left[\frac{25}{592}z + \frac{542}{592} + \frac{25}{592}z^{-1}\right]^{-1}$	$\left[\frac{542}{592} + \frac{25}{296}\cos(\omega)\right]^{-1}$

When $T' = 0.8$, $Q(\omega)$ can be approximated by

$$\begin{aligned} Q(\omega) &= \frac{1 - \frac{(\omega/2T')^2}{3!} + \frac{(\omega/2T')^4}{5!} - \cdots}{1 - \frac{2}{3}\left[\omega/2T' - \frac{(\omega/2T')^3}{3!} + \cdots\right]^2} \\ &= \frac{1}{1 - \frac{4}{75}\omega^2 + O(\omega^4)} \end{aligned} \tag{3.148}$$

This yields $b = \frac{4}{75}$ and $a = \frac{67}{75}$. $Q(\omega)$ is given by

$$Q(\omega) = \frac{75/4}{e^{j\omega} + 67/4 + e^{-j\omega}} \tag{3.149}$$

with a corresponding z domain transfer function

$$Q(z) = \frac{75/4}{z + 67/4 + z^{-1}} \tag{3.150}$$

For zooming out, $T = 1$ and $T' = 1.25$. The correction filter has a frequency response given by

$$Q(\omega) = \frac{592/25}{e^{j\omega} + 542/25 + e^{-j\omega}} \tag{3.151}$$

and a corresponding transfer function

$$Q(z) = \frac{592/25}{z + 542/25 + z^{-1}} \tag{3.152}$$

The digital correction filters used in each resampling method and the corresponding frequency responses are listed in Table 3.4. Note that apart from classic interpolation methods, all other techniques involve IIR filters with symmetric structures. In [87], a fast implementation is developed for such filters. A filter with symmetric IIR form can be decomposed as

$$
\begin{aligned}
Q(z) &= \frac{A}{z+B+z^{-1}} && (3.153)\\
&= A\left(\frac{1}{1-z_1z^{-1}}\right)\left(\frac{-z_1}{1-z_1z}\right) && (3.154)
\end{aligned}
$$

where z_1 is the root of $z^2+B+1=0$ with the constraint $|z_1|<1$. The filtering processing is shown in Figure 3.10, where the input and output are related by

$$
\begin{aligned}
c^+[k] &= \quad s[k]+z_1c^+[k-1] && k=1,\cdots,N-1\\
c^-[k] &= \; z_1\left(c^-[k+1]-c^+[k]]\right) && k=N-2,\cdots,0
\end{aligned}
$$

For an image of size $M\times N$, the additional computational requirement due to the extra correction filtering stage is $4MN$ compared with classic techniques.

The four test images used in our experiment are shown in Figure 3.11. They are:

(i) the "Rays" image which is an artificial image with high frequency components;

(ii) the "Lena" image which is a portrait;

(iii) the "Peppers" image which consists of natural objects; and

(iv) the "CT-scanned Head" image which is a medical image where the details are of great importance.

The images are each enlarged by a factor of 1.25 eight consecutive times. Subsequently, the enlarged image is reduced to 0.8 of its size eight consecutive times so the resulting image has the same size as the original. The pixel signal-to-noise ratio (PSNR) of the resulting images defined by (2.97) are shown in Table 3.5. Figures 3.12 to 3.15 show the resulting images. Overall, consistent resampling produces the best visual results and the highest PSNR among the four techniques considered.

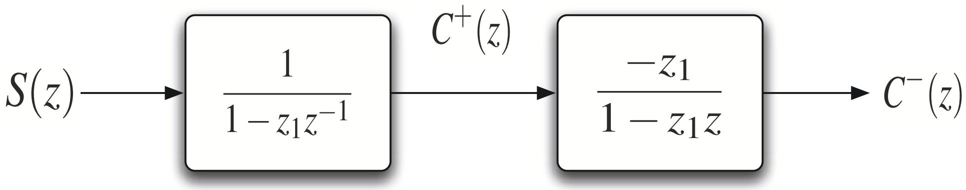

Figure 3.10: Causal and anti-causal implementation of IIR filter.

Table 3.5: PSNR for image zoomed out by 1.25 for 8 consecutive times, followed by zoomed in by 0.8 for 8 consecutive times.

PSNR	Rays	Lena	Pepper	Head
Classic	17.24	59.20	54.17	42.59
Oblique	24.71	61.21	54.62	50.58
Quasi	23.87	65.93	55.25	53.20
Consistent	29.96	66.01	56.17	55.64

When an image is zoomed in and out several times, artifacts are created due to aliasing and blurring, especially for the high frequency components. The Rays image in Figure 3.11.a contains mainly high frequency components. Using classic interpolation, the details are completely missing near the lower left corner (see Figure 3.12.a). This is because, according to (3.125), the value of each pixel in the resultant image $K[m]$ is obtained by the weighted average of its two neighboring pixels in the original image. Since the sum of these weights is 1, the intensity (sum of all pixel values) of the image does not change. Constant intensity plus the averaging effect ultimately leads to the disappearance of the details after a few resizing operations.

The details better preserved by oblique interpolation can be observed from Figure 3.12.b. However, the effect of overshoot, i.e. increased contrast, is particularly evident near the borders of the image. At $\omega = 0$, the sum of the coefficients of the correction filter given by (3.129) is

$$|Q| = \frac{3}{4} + \frac{1}{2} > 1 \tag{3.155}$$

Thus the pixel values in I are magnified. The dark gray pixels with values near the

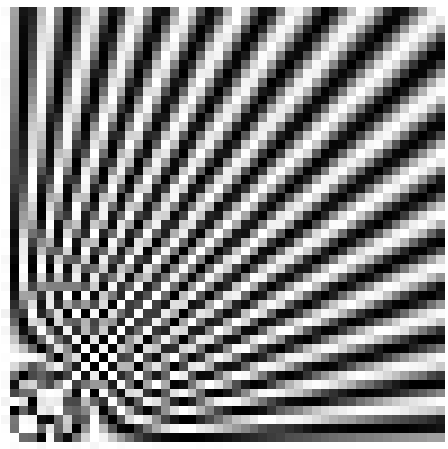

3.11.a: Rays

3.11.b: Lena

3.11.c: Peppers

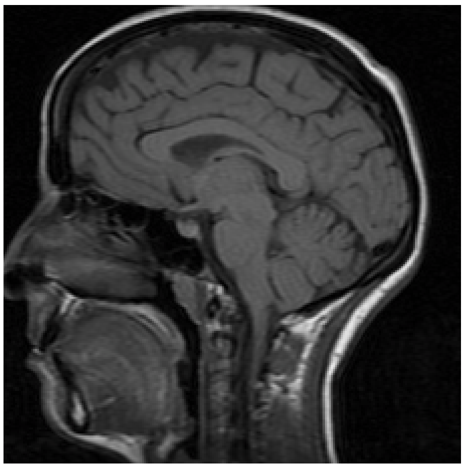

3.11.d: Head

Figure 3.11: The original test images.

maximum in I are turned into black pixels in K. Similarly, the light pixels with values near zero in I are turned into white pixels in K. This leads to the disappearance of the check pattern in the image.

The quasi interpolation method does not preserve the high frequency components as well as oblique interpolation. As shown in Figure 3.12.c, on one hand, details at the left lower corner has partly disappeared and the check pattern is invisible. On the other hand, the right upper corner which consists of lower high frequency components are better preserved. The blurred area is significant less than that obtained by classic interpolation.

Consistent resampling outperforms the other three techniques in preserving high frequency components. As shown in Figure 3.12.d, the check pattern is well recognizable. The contrast and intensity of the image is unchanged as well. Similar conclusion can be drawn by comparing the high frequency components in the other test images. For example, in Lena, the high frequency components are present in the hair and the edge of the hat, as shown in Figure 3.13. In Figure 3.14, the lower middle part of the image and the nose have particularly high frequency components.

For images like Peppers which consist mainly of low frequency components, the differences between the four methods are small as shown in Figure 3.15.

Note that a 3-tap correction filter is used for consistent resampling in order to make the comparisons fair. If a higher order filter is used, then the high frequency components of the images will be even better preserved by consistent resampling. Figure 3.16 shows the result obtained by using a 5-tap correction filter on the Rays image. The resultant PSNR is 43.22dB which more than doubled the improvement made by a 3-tap filter over the classic technique.

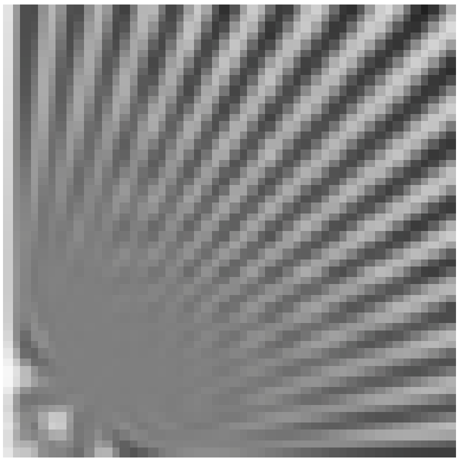

3.12.a: Classic Interpolation

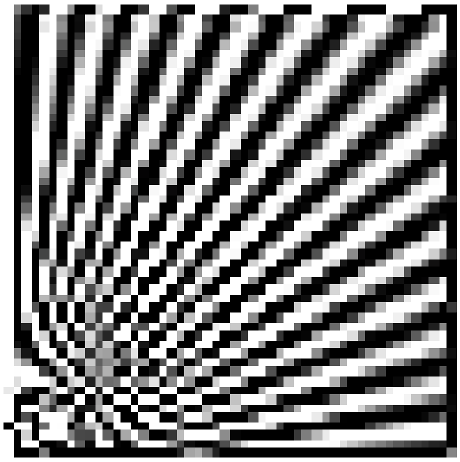

3.12.b: Oblique Interpolation

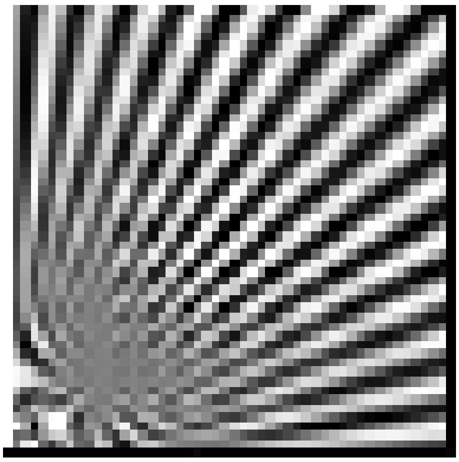

3.12.c: Quasi Interpolation

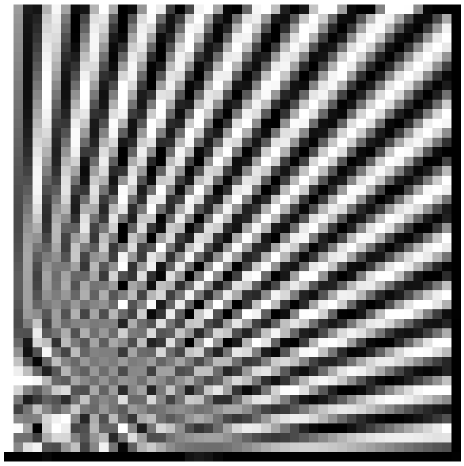

3.12.d: Consistent Resampling

Figure 3.12: The Rays image after eight consecutive enlargements followed by eight consecutive reductions.

3.13.a: Classic Interpolation

3.13.b: Oblique Interpolation

3.13.c: Quasi Interpolation

3.13.d: Consistent Resampling

Figure 3.13: The Lena image after eight consecutive enlargements followed by eight consecutive reductions.

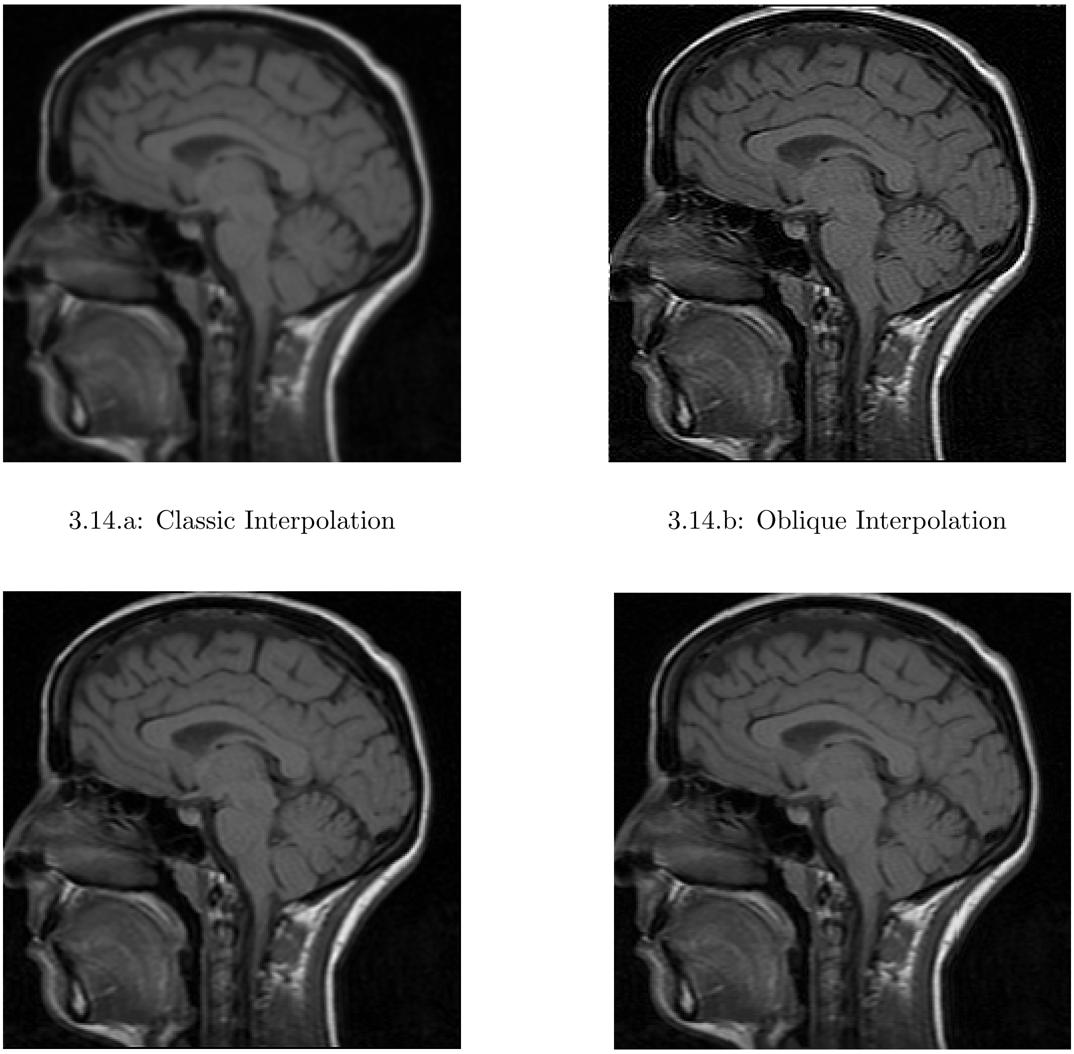

3.14.a: Classic Interpolation

3.14.b: Oblique Interpolation

3.14.c: Quasi Interpolation

3.14.d: Consistent Resampling

Figure 3.14: The Head image after eight consecutive enlargements followed by eight consecutive reductions.

3.15.a: Classic Interpolation

3.15.b: Oblique Interpolation

3.15.c: Quasi Interpolation

3.15.d: Consistent Resampling

Figure 3.15: The Peppers image after eight consecutive enlargements followed by eight consecutive reductions.

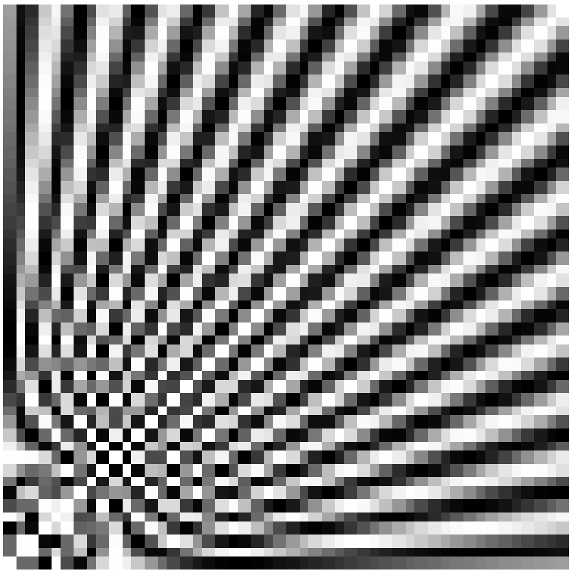

Figure 3.16: Using a 5th order correction filter on the Rays image.

3.4.3 Image Rotation

Image rotation by an angle θ anti-clockwise is usually performed by multiplying the image with the rotation matrix

$$R(\theta) = \begin{bmatrix} \cos\theta & -\sin\theta \\ \sin\theta & \cos\theta \end{bmatrix} \tag{3.156}$$

and then resampled. A typical implementation of the procedure is found in the function "imrotate" in MATLAB. Our experiments here involve comparing the outputs after rotating an image several times using this function and those produced using consistent resampling.

The conventional approach to image rotation is non-separable and therefore is a 2-D process. Hence the correction filter should also be a 2-D filter. Unfortunately the filter implementation becomes more complex as the filter order becomes higher. Fortunately, (3.156) can be factorized as

$$R(\theta) = ABA = \begin{bmatrix} 1 & -\tan\frac{\theta}{2} \\ 0 & 1 \end{bmatrix} \begin{bmatrix} 1 & 0 \\ \sin\theta & 1 \end{bmatrix} \begin{bmatrix} 1 & -\tan\frac{\theta}{2} \\ 0 & 1 \end{bmatrix} \tag{3.157}$$

Thus the multiplication with the rotation matrix $R(\theta)$ can be separated into three sequential steps – multiplication by matrices A, B and A. For a pixel at coordinates (m, n) in the original image, after the first step its new coordinates (m', n') are given by

$$\begin{aligned} \begin{bmatrix} m' \\ n' \end{bmatrix} &= A \begin{bmatrix} m \\ n \end{bmatrix} \\ &= \begin{bmatrix} 1 & -\tan\frac{\theta}{2} \\ 0 & 1 \end{bmatrix} \begin{bmatrix} m \\ n \end{bmatrix} \\ &= \begin{bmatrix} m - n\tan\frac{\theta}{2} \\ n \end{bmatrix} \end{aligned} \tag{3.158}$$

That is, the row index m is translated by $-n \tan\theta/2$ while the column index n is unchanged. This is a 1-D process. Similarly, in the second step, multiplication by matrix B leaves the row index unchanged while the column index is translated by $m \sin\theta$. Finally the last step is similar to the first. Thus the whole transformation process can be decomposed into a sequence of 1-D translations, as shown in Figure 3.17.

Existing methods for rotation based on this three-step process are focussed on the design appropriate translation algorithms [90, 169, 183]. We interpret the decomposed rotation process from a new angle. Assume that the size of the image is $R \times C$ pixels as shown in Figure 3.17.a. After the first step, each column is translated and so the image becomes what is shown in Figure 3.17.b. Therefore, each row in the original image is effectively resized by a the factor of $L_1 = C'/C = \sqrt{1 + \tan^2\theta/2}$. Assuming that the sampling period of the original signal is $T = 1$, the resampling period is given by $T' = 1/L_1$. Similarly, in the second step each column is resized from R_1 to R_1' as shown in Figure 3.17.c. The resizing factor is $L_2 = R_1'/R_1 = \sqrt{1 + \sin^2\theta}$ and the corresponding resampling period is $T' = 1/L_2$. In the third step, the columns of the image in Figure 3.17.c is translated in the same way as in the first step. The resizing factor is $L_1 = C_2'/C_2$.

Since the rotation process has now been formulated as a sequence of resizing operations, we can make use of our consistent resampling system to perform the rotation. For a given interpolation function ϕ and the parameters T and T', a consistent correction

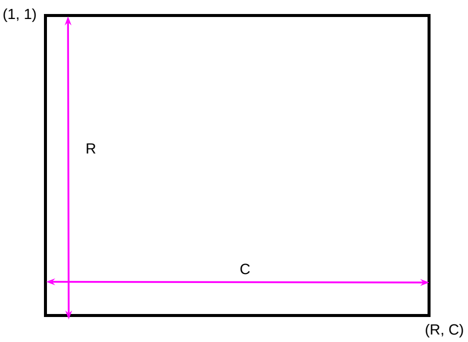

3.17.a: Original Figure

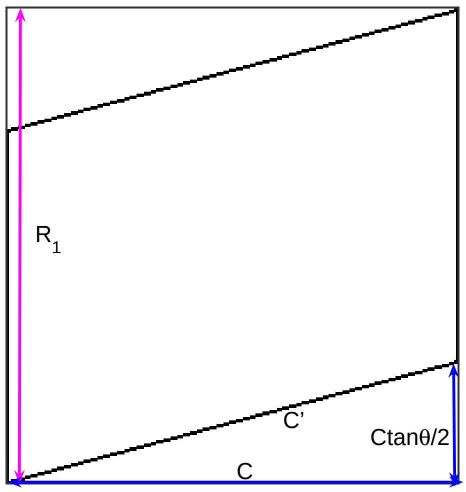

3.17.b: Step 1: Column-wise Translation

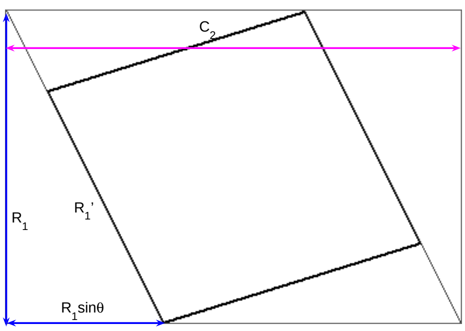

3.17.c: Step 2: Row-wise Translation

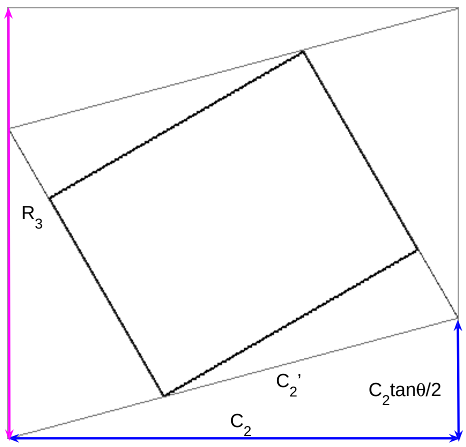

3.17.d: Step 3: Column-wise Translation

Figure 3.17: Illustration of decomposed rotation process.

filter can be designed in a similar way to what we have done in Section 3.4.2. Note that resizing factors L_1 and L_2 are functions of θ only and does not depend on the size of the image, the correction filters are applicable to images of any size. The procedure for rotating an image I of size $R \times C$ anti-clockwise by θ are as follows.

(i) Create a matrix K_1 of size $R1 \times C$ where $R_1 = R + C \tan\theta/2$ since the size of the image is changed to $R_1 \times C$ after the first step (see Figure 3.17.b).

(ii) A pixel $I(m, n)$ in the original image is mapped to $K_1(m', n')$ by

$$\begin{bmatrix} m' \\ n' \end{bmatrix} = \begin{bmatrix} m - n\tan\frac{\theta}{2} \\ n \end{bmatrix} \tag{3.159}$$

$$\Rightarrow \begin{bmatrix} m \\ n \end{bmatrix} = \begin{bmatrix} m' + n'\tan\frac{\theta}{2} \\ n' \end{bmatrix} \tag{3.160}$$

for $m' \in [1, R_1]$, $n' \in [1, C]$. For out of bound indices where

$$m = m' + n'\tan\theta/2 - C\tan\theta/2 < 1$$

let $K_1(m', n') = 0$. Note that m can be non-integer valued and $I[m - C\tan\theta/2, n]$ is obtained through interpolation.

(iii) Design a consistent correction filter $\mathbf{q}_1$ for interpolation function ϕ, sampling period $T = 1$ and resampling period $T' = 1/L_1$ using the procedure described in Section 3.4.2. Apply $\mathbf{q}_1$ to each row of K_1.

(iv) Create a matrix K_2 of size $R_1 \times C_2$ for the resulting image after step 2 shown in Figure 3.17.c with $C_2 = C_1 + R_1 \sin\theta$.

(v) Each pixel $K_1(m', n')$ is mapped to $K_2[m'', n'']$ by

$$\begin{aligned} \begin{bmatrix} m'' \\ n'' \end{bmatrix} &= B \begin{bmatrix} m' \\ n' \end{bmatrix} \\ &= \begin{bmatrix} m' \\ m'\sin\theta + n' \end{bmatrix} \\ \Rightarrow \begin{bmatrix} m' \\ n' \end{bmatrix} &= \begin{bmatrix} m'' \\ n'' - m''\sin\theta \end{bmatrix} \end{aligned} \tag{3.161}$$

for $m'' \in [1, R_1]$ and $n'' \in [1, C_2]$. Similarly, for non-integer values of n', $K_1(m', n')$ is obtained through interpolation.

Table 3.6: PSNR (dB) after 12 rotations of 30°.

	Lenna	Barbara	Baboon	Boat	Camera
Classic Resampling	57.9	45.97	39.55	49.83	46.82
Consistent Resampling	64.53	54.16	49.07	60.08	51.26

(vi) Design the consistent correction filter $\mathbf{q}_2$ with parameters ϕ, $T = 1$ and $T' = 1/L_2$. Apply $\mathbf{q}_2$ to each column of K_2.

(vii) Repeat (i) to (iii) on K_2 for the third rotation step to obtain an image as shown in Figure 3.17.d. The final image is of size $R_3 \times C_2$, where $R_3 = R_1 + C_2 \tan\theta/2$.

Five different images – Lena, Barbara, Baboon, Boat and Camera, are each rotated 30° anti-clockwise twelve times. Figure 3.18 shows the results obtained using the conventional method for rotation as implemented by the "imrotate" function in MATLAB. The interpolation method chosen is 'bilinear'. For a fair comparison, we use β^1 as the interpolation function for consistent resampling. Figure 3.19 shows the results obtained using correction filtering. It is obvious that the fine details of the image are highly preserved since consistent resampling does not assume a bandlimited signal. PSNR values are shown in Table 3.6. In each case, consistent resampling produces better results.

The consistent resampling approach to image resizing and rotation is simple and flexible. It simply involves computing the resampling factor and then obtaining the correction filter based on the interpolator chosen. The computational complexity grows linearly with the size of the image and the order of the correction filter.

3.4.4 On comparison of Consistent Resampling Theory and Other Techniques

In Section 3.4.2 and Section 3.4.3 we compared Quasi Interpolation, Oblique Interpolation and our Consistent resampling methods experimentally. The Quasi interpolation method, as discussed in Section 2.6.3, considers how a continuous signal is sampled and

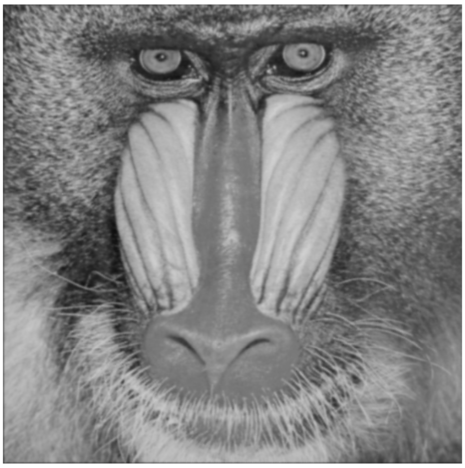

3.18.a: Baboon

3.18.b: Barabra

3.18.c: Boat

3.18.d: Lena

Figure 3.18: After twelve rotations of 30° by classic resampling.

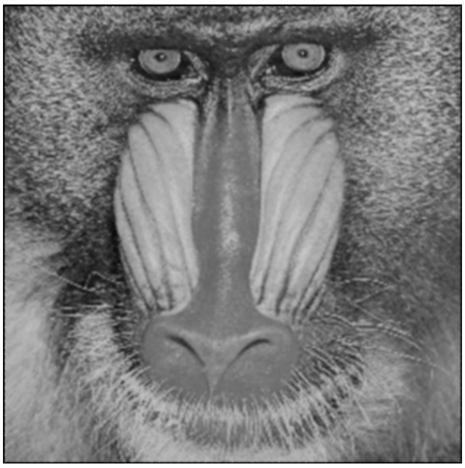

3.19.a: Baboon

3.19.b: Barbara

3.19.c: Boad

3.19.d: Lena

Figure 3.19: After twelve rotations of 30° by consistent resampling.

reconstructed. In case of image resizing, it ensures an arbitrary signal $f(x)$ can be optimally reconstructed using the interpolation function. In other words, it considers only the first step of the resampling process.

The Oblique method as presented in Section2.6.2 approaches image resizing by optimizing the sampling of $\widetilde{f}(x)$, which is reconstructed from the input sequence. It is equivalent to consider only the second step of the resampling process. Both of the methods are constrained by the fact that they are derivations of the consistent sampling theory and only one sample rate can exist in the system.

The consistent resampling theory, on the other hand, is designed for resampling system and inherently allows different sampling rates residing in the system. It considers both steps of a resampling process and targets to optimize the whole resampling performance. This explains the improvement of performance achieved by our consistent resampling theory.

It is noteworthy that in most image and video signals, low frequency components play a dominant part. Still consistent resampling theory outperform current resampling technologies as observed from Table 3.5 and Table 3.6. It can be concluded that the consistent resampling theory is ideal to process signals of low frequency response as well. It is because the ideal interpolation for low bandwidth signals, *sinc* is never used in practical applications due to its slow convergent property. Instead, other function of local support are used. The consistent resampling theory tackle the non-idealness of the interpolation function by deploying the principle of consistency. Therefore, the consistent resampling theory provides an optimal solution to resample signals of low or high frequency component.

3.5 Summary

In this chapter, the theory of consistent resampling is developed for any pair of synthesis and resampling filters. There is no restriction that the signals be bandlimited. Consistent resampling is achieved by a digital correction filter. Consistent resampling is shown to be optimal in the sense that the input sequence can be obtained from the output. We showed that when it is applied to the video de-interlacing problem, results consistent with intuition is obtained. This is not achievable through the generalized sampling theory proposed earlier. The practical usefulness of this theory is demonstrated by applying it to UWB impulse radio demodulation, image resizing and image rotation.

Chapter 4

Performance Metric for Sequences in ℓ^2

As discussed in Chapter 3, consistent resampling is optimal in the sense that the input sequence can be reconstructed from the output, i.e. the process is lossless. Unfortunately, the consistent resampling is not achievable when, for instance, noise is present in the resampling systems. This motivated us to look for a metric to quantitatively assess the performance of resampling systems. Furthermore, a suitable metric can be used to guide the design of resampling system for specific purposes. Given the diversity of applications of resampling, it is crucial to properly measure the performance of resampling system effectively so that the correction filters can be designed accordingly. It is also desirable to have a unified performance metric so that different resampling algorithms can be compared.

While the closeness of two continuous signals can be easily evaluated by the L^2 norm, it is not as simple when two discrete signals are involved. One may be tempted to use the ℓ^2 norm as a distance measure. There are two main reasons why this is not an appropriate measure. First, we require that the sampling intervals of the two signals be the same. In other words, they must belong to the same space $[V]_T$. Second, the samples may be obtained by using different sampling functions or sampled at different sets of points in the domain. A direct comparison between the sample values is therefore not a proper measure of the closeness of two sequences in general.

Various indirect measures have been used which are specific to the particular application to which the resampling system is applied. For example, in image processing, PSNR is commonly used. Thus it is difficult to compare resampling algorithms developed for different applications.

In this chapter we propose a new distance metric to compare discrete signals in ℓ^2 in a Mean Square Error (MSE) sense within the framework of resampling. The metric is based on the theory for consistent resampling developed in Chapter 3. The properties of the distance metric will be established.

4.1 The Distance Metric and Its Properties

Let $\mathbf{f}_T$ and $\mathbf{f}'_{T'}$ be the input and output sequences of a resampling system and ϕ be the synthesis (interpolating) function. Then consistent resampling requires that

$$\widetilde{f}(x) = \sum_n f_T[n]\phi\left(\frac{x}{T} - n\right) \tag{4.1}$$

and

$$\widehat{f}(x) = \sum_m \widetilde{f}_{T'}[m]\phi\left(\frac{x}{T'} - m\right) \tag{4.2}$$

be the same. When resampling is not completely consistent, the output $\mathbf{f'}_{T'}$ will be different from the consistently resampled output $\mathbf{f}_{T'}$. The distance between these two discrete signals can be obtained by the ℓ^2 norm

$$d_1 = \|\mathbf{f}'_{T'} - \mathbf{f}_{T'}\|_{\ell^2} \tag{4.3}$$

Since ϕ is a generating function for the space V^ϕ, $\mathbf{f}_{T'}$ uniquely approximate $\widehat{f}(x)$ in $V^\phi_{T'}$. The signal reconstructed from the non-consistently resampled output $\mathbf{f}'_{T'}$ is given by

$$\widehat{f}'(x) = \sum_m f'_{T'}[m]\phi\left(\frac{x}{T'} - m\right) \tag{4.4}$$

and $\widehat{f}'(x) \neq \widehat{f}(x)$. The distance between these two signals is measured by the L^2 norm d_2, from Schwartz Inequality,

$$\begin{aligned} d_2 &= \|\widehat{f}'(x) - \widehat{f}(x)\|_{L^2} && (4.5) \\ &= \left\| \sum_m f'_{T'}[m]\phi\left(\frac{x}{T'} - m\right) - \sum_m \widetilde{f}_{T'}[m]\phi\left(\frac{x}{T'} - m\right) \right\|_{L^2} \\ &\leq d_1 \left\| \phi\left(\frac{x}{T'}\right) \right\|_{L^2} && (4.6) \end{aligned}$$

Since $\left\|\phi\left(\frac{x}{T'}\right)\right\|_{L^2}$ is non-negative, d_2 is a monotonically increasing function of d_1. Thus the smaller d_1 is, the smaller its corresponding d_2. Replace $\widehat{f}(x)$ by $\widetilde{f}(x)$ in (4.5), we have

$$\begin{aligned} d_3 &= \left\|\widehat{f}'(x) - \widetilde{f}(x)\right\|_{L^2} \\ &= \left\| \sum_m f'_{T'}[m]\phi\left(\frac{x}{T'} - m\right) - \sum_n f_T[n]\phi\left(\frac{x}{T} - n\right) \right\|_{L^2} && (4.7) \end{aligned}$$

It measures the distance between the reconstructed signals using the input and output of resampling.

Definition 4.1.1. *For a resampling system shown in Figure 3.1 with finite energy input and output signals $\boldsymbol{f}_T[n]$, $\widetilde{\boldsymbol{f}}_{T'}[m] \in l^2$. The distance between the input and output with respect to the synthesis function $\phi(x) \in L^2(R)$ is defined by*

$$d_\phi\left(\boldsymbol{f}_T, \widetilde{\boldsymbol{f}}_{T'}\right) = \left\| \sum_n f_T[n]\phi\left(\frac{x}{T} - n\right) - \sum_m \widetilde{f}_{T'}[m]\phi\left(\frac{x}{T'} - m\right) \right\|_{L^2} \quad (4.8)$$

We shall show that this distance measure satisfies the basic requirements of a distance metric. It also possesses other appealing properties.

4.1.1 Positiveness

Since $\mathbf{f}_T$, $\widetilde{\mathbf{f}}_{T'} \in l^2$ and $\phi(x) \in L^2$, by the Schwarz inequality, the signals $\widetilde{f}(x)$ and $\widehat{f}(x)$ are also continuous and belong to L^2. From (4.8), $d_\phi(\mathbf{f}_T, \widetilde{\mathbf{f}}_{T'}) = \|\widetilde{f} - \widehat{f}\|_{L^2}$. Since the L^2 norm is always non-negative, so is d_ϕ.

However, note that although the L^2 norm defines a metric space, $d_\phi(\mathbf{f}_T, \widetilde{\mathbf{f}}_{T'})$ is a pseudo metric. By that we mean that even when $d_\phi(\mathbf{f}_T, \widetilde{\mathbf{f}}_{T'}) = 0$, the discrete sequences $\mathbf{f}_T$ and $\widetilde{\mathbf{f}}_{T'}$ are not necessarily element-by-element equal. A zero distance only implies that $\mathbf{f}_T$ and $\widetilde{\mathbf{f}}_{T'}$ appear the same to the properly dilated interpolating function. From the definition of consistent resampling, zero distance means that one sequence is a consistently resampled version of the other. The uniqueness of such sequence in $V_{T'}$ is guaranteed by the assumption that ϕ satisfies the Riesz condition. For every $\mathbf{f}_T$ there exists one and only one $\widetilde{\mathbf{f}}_{T'}$ such that $d_\phi(\mathbf{f}_T, \widetilde{\mathbf{f}}_{T'}) = 0$ for given interpolation function ϕ.

4.1.2 Symmetry

It is obvious that $d_\phi(\mathbf{f}_T, \widetilde{\mathbf{f}}_{T'}) = d_\phi(\widetilde{\mathbf{f}}_{T'}, \mathbf{f}_T)$ and the metric is symmetrical with respect to its arguments. When we have consistent resampling, $d_\phi(\mathbf{f}_T, \widetilde{\mathbf{f}}_{T'}) = 0$ and so $d_\phi(\widetilde{\mathbf{f}}_{T'}, \mathbf{f}_T) = 0$. Thus $\widetilde{\mathbf{f}}_{T'}$ is a consistently resampled version of $\mathbf{f}_T$ and vice versa. That is, we can obtain one sequence from the other.

When consistent resampling is not achieved, $d_\varphi(\mathbf{f}_T, \widetilde{\mathbf{f}}_{T'}) \neq 0$. A quantitative bound can be derived for the distance between $\widetilde{\mathbf{f}}_{T'}$ and its resampled sequence at rate T.

Proposition 4.1.2. *Let*

$$\widetilde{f}_{T'}[m] = \widetilde{f}(x)|_{x=mT'} \tag{4.9}$$

where

$$\widetilde{f}(x) = \sum_n f_T[n]\phi\left(\frac{x}{T} - n\right) \tag{4.10}$$

for some discrete signal $\mathbf{f}_T \in \ell^2$ *and* $\phi \in L^2$. *Also, let*

$$f'_T[k] = \widehat{f}(x)|_{x=kT} \tag{4.11}$$

where

$$\widehat{f}(x) = \sum_m \widetilde{f}_{T'}[m]\phi\left(\frac{x}{T'} - m\right) \tag{4.12}$$

Then

$$\left| d_\phi(\widetilde{\boldsymbol{f}}_{T'}, \mathbf{f}'_T) - d_\phi(\mathbf{f}_T, \widetilde{\mathbf{f}}_{T'}) \right| \leq D \left| \frac{\sum_{m,s} \left[\delta[m-k] - \phi\left(\frac{sT}{T'} - m\right)\right]}{\sum_{n,m} \left[\delta[n-m] - \phi\left(\frac{mT'}{T} - n\right)\right]} \right| \tag{4.13}$$

for $d_\phi(\mathbf{f}_T, \widetilde{\mathbf{f}}_{T'}) = D$.

Proof. From (4.8),

$$d_\phi(\widetilde{\mathbf{f}}_{T'}, \mathbf{f}\,'_T) = \left\| \sum_n \widetilde{f}_{T'}[m]\phi\left(\frac{x}{T'} - m\right) - \sum_k f'_T[k]\phi\left(\frac{x}{T} - k\right) \right\|_{L^2} \tag{4.14}$$

Substitute (4.11) and (4.12) into (4.14), we have

$$d_\phi(\widetilde{\mathbf{f}}_{T'}, \mathbf{f}'_T) = \left\| \widehat{f}(x) - \sum_k \widehat{f}(kT)\phi\left(\frac{x}{T} - k\right) \right\|_{L^2} \tag{4.15}$$

Using the Schwarz inequality,

$$d_\phi(\widetilde{\mathbf{f}}_{T'}, \mathbf{f}'_T) \leq \|\widehat{f}(x)\|_{L^2} \left| \sum_{m,s} \left[\delta[m-k] - \phi\left(\frac{kT}{T'} - m\right)\right] \right| \tag{4.16}$$

Similarly,

$$\begin{aligned} d_\phi(\mathbf{f}_T, \widetilde{\mathbf{f}}_{T'}) &= D && (4.17)\\ &\leq \left\|\widetilde{f}(x)\right\|_{L^2} \left| \sum_{n,m} \left[\delta[n-m] - \phi\left(\frac{mT'}{T} - n\right)\right] \right| && (4.18) \end{aligned}$$

Thus

$$\left\|\widetilde{f}(x)\right\|_{L^2} \geq \frac{D}{\left|\sum_{n,m} \left[\delta[n-m] - \phi\left(\frac{mT'}{T} - n\right)\right]\right|} \tag{4.19}$$

Since $\left\|\widetilde{f}(x) - \widehat{f}(x)\right\|_{L^2} = D$, $\left\|\widehat{f}(x)\right\|_{L^2}$ is bounded by

$$\left| D - \left\|\widetilde{f}(x)\right\|_{L^2} \right| \leq \left\|\widehat{f}(x)\right\|_{L^2} \leq D + \left\|\widetilde{f}(x)\right\|_{L^2} \tag{4.20}$$

Combining (4.19) and (4.20), we have

$$\left\|\widehat{f}(x)\right\|_{L^2} \leq D\left(1 + \frac{1}{\left|\sum_{n,m} \left[\delta[n-m] - \phi\left(\frac{mT'}{T} - n\right)\right]\right|}\right) \tag{4.21}$$

Substituting (4.21) into (4.16) and we obtain (4.13). □

Note that the bound in (4.13) is tight. We shall explore this further in Section 4.2.

4.1.3 Triangle Inequality

Proposition 4.1.3. $d_\phi(\mathbf{f}_T, \mathbf{f}_{T''}) + d_\varphi(\mathbf{f}_{T''}, \widetilde{\mathbf{f}}_{T'}) \geq d_\phi(\mathbf{f}_T, \widetilde{\mathbf{f}}_{T'})$ *for* $\mathbf{f}_T, \mathbf{f}_{T'}, \mathbf{f}_{T''} \in l^2$.

Proof. From the definition (4.8),

$$
\begin{aligned}
& d_\phi(\mathbf{f}_T, \mathbf{f}_{T''}) + d_\phi(\mathbf{f}_{T''}, \widetilde{\mathbf{f}}_{T'}) \\
= \; & \left\| \sum_n f_T[n] \phi\left(\frac{x}{T} - n\right) - \sum_k f_{T''}[k] \phi\left(\frac{x}{T''} - k\right) \right\|_{L^2} \\
& + \left\| \sum_n f_{T''}[s] \phi\left(\frac{x}{T''} - k\right) - \sum_m f_{T'}[m] \phi\left(\frac{x}{T'} - m\right) \right\|_{L^2}
\end{aligned}
$$

From the Schwarz inequality,

$$
\begin{aligned}
& d_\phi(\mathbf{f}_T, \mathbf{f}_{T''}) + d_\phi(\mathbf{f}_{T''}, \widetilde{\mathbf{f}}_{T'}) \\
\leq \; & \left\| \sum_n f_T[n] \phi\left(\frac{x}{T} - n\right) - \sum_n f_{T''}[s] \phi\left(\frac{x}{T''} - k\right) \right. \\
& \left. + \sum_n f_{T''}[k] \phi\left(\frac{x}{T''} - k\right) - \sum_m f_{T'}[m] \phi\left(\frac{x}{T'} - m\right) \right\|_{L^2} \\
= \; & \left\| \sum_n f_T[n] \phi\left(\frac{x}{T} - n\right) - \sum_m f_{T'}[m] \phi\left(\frac{x}{T'} - m\right) \right\|_{L^2} \\
= \; & d_\phi(\mathbf{f}_T, \widetilde{\mathbf{f}}_{T'})
\end{aligned}
\tag{4.22}
$$

□

Equality holds when $\mathbf{f}_T$, $\widetilde{\mathbf{f}}_{T'}$ and $\widetilde{\mathbf{f}}_{T'}$, $\mathbf{f}_{T''}$ are consistently resampled pairs. Under these circumstances, the pair of sequences $\mathbf{f}_T$ and $\mathbf{f}_{T''}$ are also consistent.

4.1.4 Completeness

Proposition 4.1.4. *If the input sequence $\boldsymbol{f}_T$ is chosen from a complete subspace $V_T \subset \ell^2$, then the solution space $V_{T'}$ of its consistently resampled sequence $\widetilde{\boldsymbol{f}}_{T'}$ is also complete.*

Proof. Assume $\mathbf{f}_T$, $\mathbf{f}'_T \in V_T$ and $\|\mathbf{f}_T - \mathbf{f}'_T\|_{\ell^2} < \alpha$. Let their consistently resampled sequences be $\mathbf{f}_{T'}$ and $\mathbf{f}'_{T'}$ respectively. From Proposition 3.2.2,

$$\mathbf{f}_{T'} = \sum_m \left\langle \sum_n f_T[n]\phi\left(\frac{x}{T} - n\right), \phi_d(\frac{x}{T'} - m) \right\rangle \tag{4.23}$$

Thus, the distance between $\widetilde{\mathbf{f}}_{T'}$ and $\mathbf{f}'_{T'}$ in ℓ^2 can be computed by

$$\begin{aligned} \|\mathbf{f}_{T'} - \mathbf{f}'_{T'}\|_{\ell^2} &\leq \left\| \sum_n f_T[n]\phi\left(\frac{x}{T} - n\right) \right\|_{L^2} \left\|\phi_d\left(\frac{x}{T'}\right)\right\|_{L^2} \\ &\leq \|\mathbf{f}_T - \mathbf{f}'_T\|_{\ell^2} \left\|\phi\left(\frac{x}{T}\right)\right\|_{L^2} \left\|\phi_d\left(\frac{x}{T'}\right)\right\|_{L^2} && (4.24) \\ &\leq C\alpha && (4.25) \end{aligned}$$

where C is a constant which relates to $\|\phi\|_{L^2}$ and is independent of α. When $\mathbf{f}_T$ approaches $\mathbf{f}'_T$, α approaches zero and so does $\|\mathbf{f}_{T'} - \mathbf{f}'_{T'}\|_{\ell^2}$. Therefore the space of consistently resampled sequences form a complete subspace $V_{T'}$. $\square$

4.1.5 Bandlimited Resampling

We shall show that our metric is consistent with the Shannon uniform sampling theorem for bandlimited signals. Assume that the discrete input signal $\mathbf{f}_a$ of the resampling system be obtained by sampling a continuous signal $f(x)$ which has a bandwidth of B, i.e. $F(\Omega) = 0$ for $|\Omega| \geq B$. Let the sampling rate be $\frac{1}{a} \geq 2B$. Using the interpolation function $\phi(x) = sinc(x/a)$ in the resampling system in Figure 3.1, the reconstructed continuous signal is given by

$$\widetilde{f} = \sum_n f_a[n] sinc\left(\frac{x}{a} - n\right) \tag{4.26}$$

Since the sampling rate higher larger than the Nyquist rate, we have $\widetilde{f}(x) = f(x)$.

The discrete output $\mathbf{f}_b$ of the resampling system is obtained by ideally sampling $\widetilde{f}$ at interval b, i.e. $f_b[m] = \widetilde{f}(x)|_{x=mb}$. If the resampling rate is higher than the Nyquist rate, i.e. $\frac{1}{b} \geq 2B$, then from Definition 4.1.1, the distance between $\mathbf{f}_a$ and $\mathbf{f}_b$ is calculated by

$$d_\phi(\mathbf{f}_a, \mathbf{f}_b) = \left\| \sum_n f_a[n] sinc\left(\frac{x}{a} - n\right) - \sum_m f_b[m] sinc\left(\frac{x}{b} - m\right) \right\|_{L^2} \tag{4.27}$$

Since the resampling rate is high enough, interpolating $\mathbf{f}_b$ using $sinc(x/b)$ results in the perfect reconstruction of $\widetilde{f}(x)$. Therefore,

$$\sum_m f_b[m] sinc\left(\frac{x}{b} - m\right) = \widetilde{f} \tag{4.28}$$

and so $d_\phi(\mathbf{f}_a, \mathbf{f}_b) = 0$.

However, if $\frac{1}{b} < 2B$, then

$$d_\phi(\mathbf{f}_T, \widetilde{\mathbf{f}}_{T'}) = \left\| \widetilde{f}(x) - \sum_m \widetilde{f}(mb) sinc(\frac{x}{b} - m) \right\|_{L^2} \tag{4.29}$$

Since $\widetilde{f}$ is sampled at a rate lower than the Nyquist rate, the signal can never be perfectly reconstructed from the under-sampled sequence $\mathbf{f}_b$. Therefore, $d_\phi(\mathbf{f}_T, \widetilde{\mathbf{f}}_{T'}) \neq 0$.

A particular example is shown in Figure 4.1. Here, $f(x) = sinc(x)$, and $B = \frac{1}{2}$Hz. The input signal is obtained by sampling $f(x)$ at $a = 1$. Since $\frac{1}{a} = 1 = 2B$, $\mathbf{f}_a$ can be used to reconstruct $f(x)$ perfectly. We shall denote this reconstructed signal by $f_1(x)$. Then f_1 is resampled at the rate $\frac{1}{b}$. Let the continuous signal reconstructed using $\mathbf{f}_b$ be denoted by f_2. If $b = 0.8$, then the resampling rate is higher than the Nyquist rate and $f_2 = f_1$ exactly. However, if $b = 1.1$, then f_2 will be different from f_1 as shown in the figure. The distance $d_\phi(\mathbf{f}_T, \widetilde{\mathbf{f}}_{T'})$ is measured by the square root of the area under the curve of $(f_1 - f_2)^2$. We shall examine $d_\phi(\mathbf{f}_T, \widetilde{\mathbf{f}}_{T'})$ using more general cases in Section 4.4.1.

Thus our metric is applicable to conventional resampling of bandlimited signals.

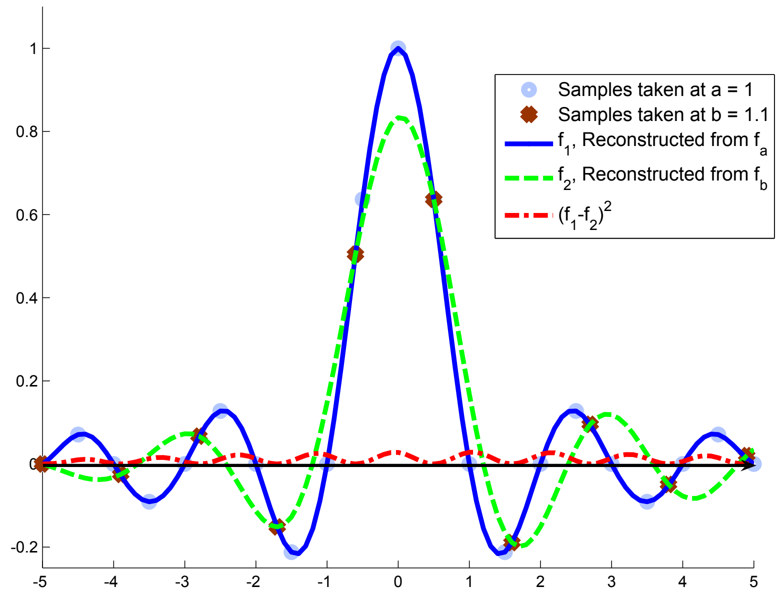

Figure 4.1: Resampling performance when the signal is bandlimited.

4.2 Fourier Analysis of Resampling Performance

Definition 4.1.1 mapped the performance of resampling to the distance between $\widetilde{f}$ and $\widehat{f}$. It in turn can be viewed as a measure of how closely $\widehat{f}$ approximates $\widetilde{f}$. Using $\widetilde{f}$ as the input and $\widehat{f}$ as the output, the resampling system of Figure 3.1 can be re-arranged as an approximation system as shown in Figure 4.2 to facilitate performance analysis.

The structure in Figure 4.2 is essentially the same as the generalized sampling and reconstruction system in Figure 2.10. As we discussed in Section 2.4, the performance of such a system can be evaluated easily in the Fourier domain [47]. Applying (2.27) to the present system, the resampling performance can be expressed as

$$\eta_{\widetilde{f}}(T') = \left[\frac{1}{2\pi}\int |\widetilde{F}(\Omega)|^2 E_r(T'\Omega)d\Omega\right]^{\frac{1}{2}} \tag{4.30}$$

where the resampling error kernel $E_r(\Omega)$ is given by

$$E_r(\Omega) = \underbrace{1 - \frac{|\Phi(\Omega)|^2}{A_\phi(\omega)}}_{E_{\min}(\Omega)} + \underbrace{A_\phi(\omega)\|\Psi^2(\Omega) - \Phi_d(\Omega)\|^2}_{E_{\mathrm{res}}(\Omega)} \tag{4.31}$$

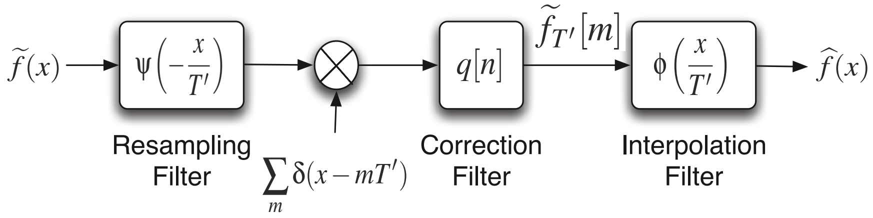

Figure 4.2: The reformed resampling system for performance analysis.

where $\Psi(\Omega)$ is the frequency response of the resampling function ψ. Here, $A_\phi(\Omega)$ and $\Phi_d(\Omega)$ are the Fourier transforms of the sampled autocorrelation and dual functions of ϕ respectively, as defined in (2.19) and (2.20). $E_{\min}$ measures the approximation power of the interpolation function while E_{res} depends on the idealness of the resampling function.

Suppose $\widetilde{f}(x)$ is an approximation of some continuous signal $f(x)$, obtained by sampling $f(x)$ using φ and reconstructing using ϕ at rate T. Then the error of this approximation can be expressed by

$$\eta_f(T) = \left[\frac{1}{2\pi}\int |F(\Omega)|^2 E_a(T\Omega)d\Omega\right]^{\frac{1}{2}} \tag{4.32}$$

where the approximation error kernel $E_a(\Omega)$ is

$$E_a(\Omega) = \underbrace{1 - \frac{|\Phi(\Omega)|^2}{A_\phi(\Omega)}}_{E_{\min}(\Omega)} + \underbrace{A_\phi(\Omega)\|\Upsilon^2(\Omega) - \Phi_d(\Omega)\|^2}_{E_{\text{res}}(\Omega)} \tag{4.33}$$

where $\Upsilon(\Omega)$ is the frequency response of the sampling function φ used to obtain the input sequence. Since

$$\left\|\widetilde{f}(x) - f(x)\right\|^2 = \eta_f^2(T) \tag{4.34}$$

and $\widetilde{f}(x)\perp\eta_f(T)$ in the space V_ϕ^T, we have

$$\left\|\widetilde{f}(x)\right\|^2 = \|f(x)\|^2 - |\eta|_f^2(T) \tag{4.35}$$

Using Parseval's theorem, this becomes

$$\left|\widetilde{F}(\Omega)\right|^2 = |F(\Omega)|^2 - 2\pi\left|\eta_f^2\right|(T) \tag{4.36}$$

Substitute (4.36) into (4.30), we obtain

$$\begin{aligned} \eta_{\widetilde{f}}(T') &= \left[\frac{1}{2\pi}\int \left[|F(\Omega)|^2 - 2\pi\eta_f^2(T)\right] E_r(T'\Omega)d\Omega\right]^{\frac{1}{2}} \\ &= \left[\frac{1}{2\pi}\left\{\int |F(\Omega)|^2 E_r(T'\Omega)d\Omega - \int |\eta_T(\Omega)|^2 E_r(T'\Omega)d\Omega\right\}\right]^{\frac{1}{2}} \end{aligned} \quad (4.37)$$

Comparing the second term with the resampling error in (4.30), it can be observed that it is equal to evaluate the resampling error of η_T while the resampling error kernel is defined by $E_r(T'\Omega)$. Therefore, (4.37) can be reduced to

$$\eta_{\widetilde{f}}(T') = \eta_f(T') - \eta_{\eta_f}(T') \quad (4.38)$$

The overall resampling performance is composed of two terms. The first one, $\eta_f(T')$, measures how well $f(x)$ can be reconstructed in $V_{T'}^{\phi}$. The second one, $\eta_{\eta_f}(T')$, measures how much the interpolation error $\eta_f = (\widetilde{f} - f)$ would be preserved in the resampling system. It is noteworthy that this amount is deducted from the first term.

Although here we based the performance of resampling on that of sampling, there are two main differences. First, sampling is concerned about preserving the characteristics of the original continuous signal $f(x)$ by its samples. But basic concern in resampling is the preservation of the information carried by the input discrete signal $\mathbf{f}_T$ by the resampled discrete signal. If $\mathbf{f}_T$ is obtained by sampling a certain continuous signal $f(x)$, the interpolated signal $\widetilde{f}$ within the resampling system may not be the same as $f(x)$. Thus how well $\widetilde{f}$ is preserved by the resampled signal is a more suitable choice for resampling performance, especially when $\mathbf{f}_T$ is fundamentally discrete and is not obtained by sampling. Second, in sampling the reconstruction space is defined by $\phi\left(\frac{x}{T}\right)$ whereas in resampling it is defined by $\phi\left(\frac{x}{T'}\right)$. This is because the resampled signal has, in general, a different sampling interval.

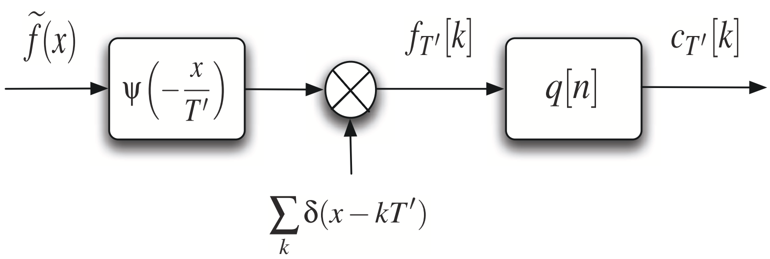

Figure 4.3: The resampling and post filtering part of resampling process.

4.3 Correction Filter in Consistent Resampling

4.3.1 Effect of Correction Filtering

A resampling system can be designed such that the error measured by the metric defined by (4.31) is minimized. The resampling performance depends on the approximation power of the interpolation function ($E_{\min}$) and the idealness of the resampling function (E_{res}). When ϕ and T' are fixed, performance can be improved by eliminating E_{res}. This in turn requires that the resampling function satisfy $\psi(x) = \phi_d$, where ϕ_d is the dual function of ϕ.

This requirement is in general very restrictive. Sometimes the resampling function is given *a priori* for the specific application. In Chapter 3, we used a correction filter given by (3.36) to achieve consistent resampling in such circumstances. We shall now show that with the insertion of the correction filter, the effective resampling function and the interpolation function are duals of each other.

The resampling portion of Figure 3.2 is shown again in Figure 4.3. Let the resampling function be ψ and the resampling interval be T', the output $f_{T'}$ is given by

$$\begin{aligned} f_{T'}[k] &= \left\langle \widetilde{f}(x), \psi\left(\frac{x}{T'} - k\right)\right\rangle \\ &= \sum_n f_T[n] \left\langle \phi\left(\frac{x}{T} - n\right), \psi\left(\frac{x}{T'} - k\right)\right\rangle \end{aligned} \tag{4.39}$$

From (3.34), the cross-correlation of ϕ and ψ is defined to be:

$$c_{\phi\psi}[n,k] = \int_x \phi\left(\frac{x}{T} - n\right)\psi\left(\frac{x}{T'} - k\right)dx \tag{4.40}$$

Therefore, (4.39) can be expressed as

$$f_{T'}[k] = (\mathbf{f}_T * \mathbf{c}_{\phi\psi})[k] \tag{4.41}$$

The output of the correction filter in Figure 4.3 is given by

$$\begin{aligned} c_{T'}[k] &= (\mathbf{f}_{T'} * \mathbf{q})[k] \\ &= (\mathbf{f}_T * \mathbf{c}_{\phi\psi} * \mathbf{q})[k] \end{aligned} \tag{4.42}$$

Taking the Fourier transform,

$$C_{T'}(\omega) = F_T(\omega) C_{\phi\psi}(\omega) Q(\omega) \tag{4.43}$$

The frequency response $Q(\omega)$ of the correction filter is given by (3.36). Substituting this into (4.43), we have

$$\begin{aligned} C_{T'}(\omega) &= F_T(\omega) C_{\phi\psi}(\omega) \frac{C_{\phi\phi_d}(\omega)}{C_{\phi\psi}(\omega)} \\ &= F_T(\omega) C_{\phi\phi_d}(\omega) \end{aligned} \tag{4.44}$$

The inverse Fourier transform of this equation gives us

$$\begin{aligned} c_{T'}[k] &= (\mathbf{f}_T * \mathbf{c}_{\phi\phi_d})[k] \\ &= \sum_m f_T[m] c_{\phi\phi_d}[m,k] \end{aligned} \tag{4.45}$$

Substitute the definition of $\mathbf{c}_{\phi\phi_d}$ in (3.35) into (4.45), we obtain

$$c_{T'}[k] = \sum_m f_T[m] \int_x \phi\left(\frac{x}{T} - m\right) \phi_d\left(\frac{x}{T'} - k\right) dx \tag{4.46}$$

Exchanging the order of summation and integration,

$$\begin{aligned} c_{T'}[k] &= \int_x \sum_m f_T[m] \phi\left(\frac{x}{T} - m\right) \phi_d\left(\frac{x}{T'} - k\right) dx \\ &= \left\langle \widetilde{f}(x), \phi_d\left(\frac{x}{T'} - k\right) \right\rangle \end{aligned} \tag{4.47}$$

Therefore, with the correction filter, the effective resampling function is ϕ_d, the dual function of ϕ. In this case, E_{res} in (4.31) becomes zero and thus we have optimal resampling performance.

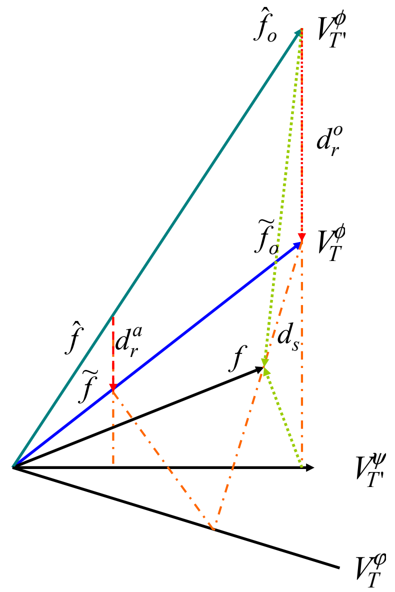

Figure 4.4: The geometric interpretation of the resampling metric.

4.3.2 Geometric Interpretation

The effect of the correction filter can be better understood by taking the geometric view.

Suppose $\mathbf{f}_T$ is obtained by sampling $f(x)$ using φ at rate T. Geometrically, this is equivalent to projecting $f(x)$ onto V_T^{φ}. Similarly, the interpolation of $\mathbf{f}_T$ to $\widetilde{f}(x)$ using ϕ can be viewed as a projection onto V_T^{ϕ}, the space spanned by $\left\{\phi\left(\frac{x}{T}-n\right)\right\}_{n\in\mathbb{Z}}$. With consistent resampling, the effective resampling function, which is the resampling function followed by correction filtering, has to be a dual of the interpolation function. Therefore $\widehat{f}(x)$ is obtained by projecting $\widetilde{f}(x)$ onto $V_{T'}^{\phi} \perp V_{T'}^{\psi}$, where $V_{T'}^{\psi} = \operatorname{span}\left\{\psi\left(\frac{x}{T'}-n\right)\right\}_{n\in\mathbb{Z}}$. These geometric relationships are shown in Figure 4.4. Since $\widetilde{f}(x)$ is obtained by directly interpolating $\mathbf{f}_T$ using ϕ, we assume no *a priori* knowledge of the sampling function φ.

The metric defined by (4.8) measures the distance between $\widetilde{f}(x)$ and $\widehat{f}(x)$, represented by d_r^a. Assume that the knowledge of the sampling function φ is available. For given interpolation function ϕ, the optimal approximation $\widetilde{f}_o(x)$ of $f(x)$ in the MSE sense can be obtained through the generalized sampling theory as described in Section 2.4. $\widetilde{f}_o(x)$ is the projection of $f(x)$ onto $V_T^{\phi} \perp V_T^{\varphi}$, as shown in Figure 4.4. For an input $\widetilde{f}_o(x)$, the output $\widehat{f}_o(x)$ of the consistent sampling system in Figure 4.2 is obtained by projecting $\widetilde{f}_o(x)$ onto $V^{\phi}_{T'} \perp V^{\psi}_{T'}$. The difference between $\widetilde{f}_o(x)$ and $\widehat{f}_o(x)$ is measured by the distance d^o_r. It can be observed that $d^o_r = (f - \widetilde{f}_o) - (f - \widehat{f}_o)$. Since $\widetilde{f}_o$ is the optimal approximation of $f(x)$ from the sequence $\mathbf{f}_T$, $(f - \widetilde{f}_o)$ measures how well the information of $f(x)$ is preserved in $\mathbf{f}_T$. Similarly, $(f - \widehat{f}_o)$ measures that of $\widetilde{\mathbf{f}}_{T'}$. Since $\mathbf{f}_T$ and $\widetilde{\mathbf{f}}_{T'}$ are the input and output of the resampling system, the distance d^o_r indicates the loss of information of $f(x)$ during the resampling process.

Similar to d^o_r, d^a_r measures the difference between the capabilities of $\mathbf{f}_T$ and $\mathbf{f}_{T'}$ to approximate $f(x)$. This is consistent with the interpretation of (4.38) that the resampling performance is the interpolation error which is inherited from the sampling process, η_{η_f}, deducted from the total interpolation error η_f.

Comparing d^o_r and d^a_r, it can be observed they are in the same direction but with different magnitudes. While d^a_r is scaled by $\|\widetilde{f}\|$, d^o_r is scaled by $\|\widetilde{f}_o\|$.

Further, the difference between resampling and sampling performance is illustrated in Figure 4.4. The sampling error is given by d_s, which depends on the difference between f and V^{ϕ}_T. On the other hand, d^a_r depends on the difference between V^{ϕ}_T and $V^{\phi}_{T'}$, the space spanned by a different dilation factor of the interpolation function ϕ.

4.4 Performance Analysis

4.4.1 Resampling of Bandlimited Signal

The resampling of bandlimited signal is a special case of generalized resampling for non-bandlimited signals. In this case, the resampling function is $\psi = \delta$ and the interpolation function is $\phi = sinc(\frac{x}{T})$. In Section 4.1.5, a specific example has been used to show the performance of resampling when the resampling rate does not meet the Nyquist rate. In this section, we shall use (4.31) to analyze the relationship between the resampling error kernel and the resampling rate for bandlimited signals.

Let the sample period of the discrete input $\mathbf{f}_T$ to the resampling system be T and the resampling period be T'. Assume that the bandwidth of this signal is $\Omega_0/2$ and

$\frac{1}{T} \geq \pi\Omega_0$. Let $a_\phi(x) = \phi(x) * \phi(-x)$. Then its Fourier transform is given by $\Phi(\Omega)\overline{\Phi}(\Omega)$. Since $\phi = sinc(x)$, $\Phi(\Omega) = 1$ for $\Omega \leq \pi$ and zero otherwise. Thus $A_\phi(\Omega) = \Phi(\Omega)$. Also, in this case, $\Phi_d(\Omega) = \Phi(\Omega)$.

Now the sampled autocorrelation of the interpolation function is given by

$$\begin{aligned} a_\phi[k] &= \langle \phi(x), \phi(x-k) \rangle && (4.48) \\ &= \phi(x) * \phi(-x)|_{x=k} && (4.49) \end{aligned}$$

Therefore,

$$\begin{aligned} A_\phi(\omega) &= \sum_m A_\phi(\Omega + 2\pi m) && (4.50) \\ &= 1 && (4.51) \end{aligned}$$

Further, since $\psi = \delta(x)$, $\Psi(\Omega) = 1$.

Substituting the above into (4.31), the error kernel is given by

$$\begin{aligned} E_r(\Omega) &= 1 - |\Phi(\Omega)|^2 + \|1 - \Phi(\Omega)\|^2 \\ &= \begin{cases} 2, & \Omega > \pi \\ 0, & \Omega \leq \pi \end{cases} && (4.52) \end{aligned}$$

For a resampling interval T', the dilated error kernel $E_r(T'\Omega)$ is

$$E_r(T'\Omega) = \begin{cases} 2, & \Omega > \pi T' \\ 0, & \Omega \leq \pi T' \end{cases} \quad (4.53)$$

Resampling performance $\eta_{\widetilde{f}}(T')$ is given by (4.30). When the resampling rate is at least as high as the Nyquist rate, i.e. $\frac{1}{T'} \geq \pi\Omega_0$, we have $E_r(T'\Omega) = 0$ and therefore $\eta_{\widetilde{f}}(T') = 0$. When the resampling rate is below the Nyquist rate, i.e. $\frac{1}{T'} < \pi\Omega_0$, then

$$\eta_{\widetilde{f}}(T') = \left[\frac{2}{2\pi} \int_{\Omega_1}^{\Omega_0} |\widetilde{F}(\Omega)|^2 d\Omega \right]^{\frac{1}{2}} \quad (4.54)$$

where $\Omega_1 = \frac{1}{T'\pi} < \Omega_0$. This is a measure of the aliased part of the signal.

4.4.2 Image Resizing

We continue with the image resizing example in Section 3.4.2. The four resampling techniques used in Section 3.4.2 are compared using (4.30) in the frequency domain. The interpolation function is $\phi = \beta^1$ and the resampling function is $\psi = \delta(x)$. Since the interpolating function is the same for all methods, for the same image the interpolated signal $\widetilde{f}(x)$ and its frequency response $\widetilde{F}(\Omega)$ are the same. Consequently, we only need to compare their corresponding error kernels $E_r(T'\Omega)$. Since the error kernel depends on the resampling interval, we shall treat image enlargement and reduction separately.

For image enlargement, $T = 1$ and $T' = 0.8$. From Table 2.1,

$$\begin{aligned} A_\phi(\omega) &= A_{\beta^1}(\omega)|_{\omega=\Omega T} && (4.55) \\ &= 1 - \frac{2}{3}\sin\left(\frac{\Omega}{2}\right)^2 && (4.56) \end{aligned}$$

From (2.34), the frequency response of β^1 is given by

$$B^1(\Omega) = \left[B^0(\Omega)\right]^2 = \left[sinc\left(\frac{\Omega}{2\pi}\right)\right]^2 \tag{4.57}$$

The response of the dual function $\phi_d = \beta^1_d$ is obtained by substituting (4.56) and (4.57) into (2.20). Thus,

$$\Phi_d = B^1_d(\Omega) = \frac{\left[sinc\left(\frac{\Omega}{2\pi}\right)\right]^2}{1 - \frac{2}{3}\sin\left(\frac{\Omega}{2}\right)^2} \tag{4.58}$$

On the other hand, according to Figure 4.3, the output is given by

$$\begin{aligned} c_{T'}[k] &= \sum_n \left\langle \widetilde{f}(x), \psi\left(\frac{x}{T'} - n\right)\right\rangle q[k-n] \\ &= \left\langle \widetilde{f}(x), \sum_n q[k-n]\psi\left(\frac{x}{T'} - n\right)\right\rangle && (4.59) \end{aligned}$$

giving us the effective resampling filter

$$\psi_e(x) = \sum_n q[n]\psi\left(\frac{x}{T'} - n\right) \tag{4.60}$$

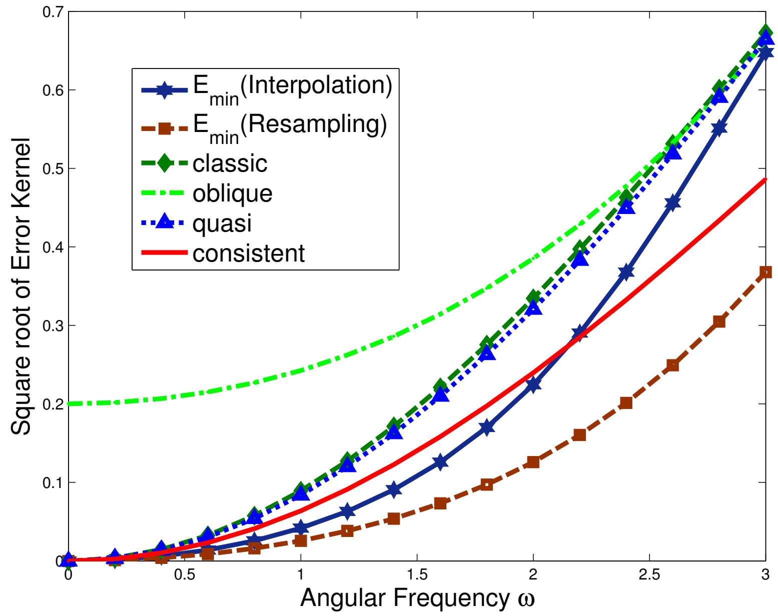

Figure 4.5: Square root of the error kernels for four resampling schemes when an image is enlarged by 25%.

Since $\psi = \delta(x)$, we have

$$\Psi_e(\Omega) = Q(\omega) \tag{4.61}$$

with $\omega = \Omega T'$. The frequency responses $Q(\omega)$ of the correction filter for each interpolation method have been derived in Section 3.4.2 and can be found in Table 3.4. Substituting (4.56), (4.58) and (4.61) into (4.31), the error kernel $E_r(T'\Omega)$ can be evaluated correspondingly. In Figure 4.5, the squared root of $E_r(T'\Omega)$ for each of the four methods for the image enlargement are plotted against each other.

For image reduction, $T = 1$ and $T' = 1.25$. The squared root of $E_r(T'\Omega)$ for each method is plotted against each other in Figure 4.6.

There are a few points we wish to highlight. From the discussion in Section 3.4.2 we noted that for classic, oblique and quasi interpolation, the design of the correction filter does not depend on the resampling interval. Therefore, the same correction filter can be used for both enlargement and reduction. As a result, $E_r(\Omega)$ defined in (4.33) is the same in these two cases. Therefore, the curves for these three methods in Figures 4.5 and 4.6 are the same except for a scaling factor.

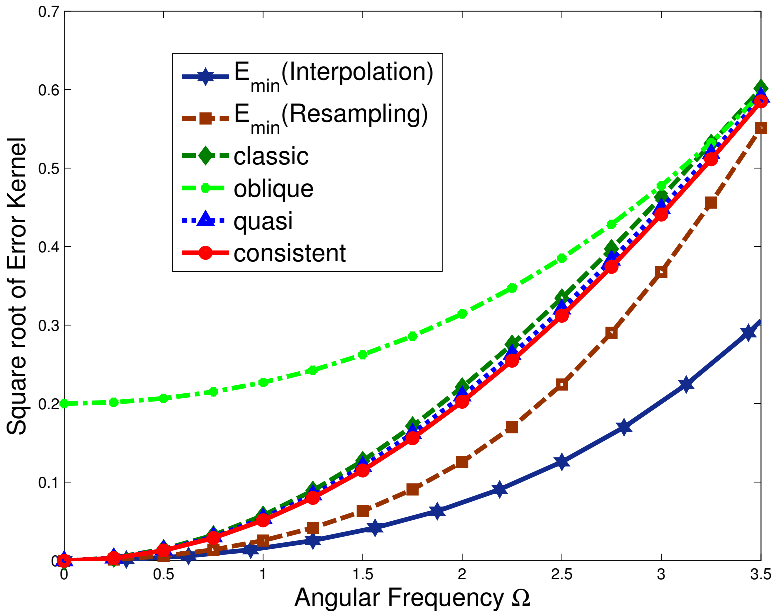

Figure 4.6: Square root of the error kernels for four resampling schemes when the image is reduced to 80% of its original size.

Since the classic, oblique and quasi interpolation methods are designed to minimize the sampling error $\|f(x) - \widetilde{f}(x)\|$, their performances are lower bounded by $E_{\min}$, the minimum sampling error. For $\phi = \beta^1$ and $T = 1$, $E_{\min}$ is obtained by substituting (4.57) and (4.56) into (4.33). $E_{\min}$ (interpolation) for image enlargement and reduction are shown in Figures 4.5 and 4.6 respectively. It can be observed that at higher Ω, the rate of increase of $E_{\min}$ (interpolation) becomes higher. Among the classic, oblique and quasi interpolation techniques, the performance of oblique resampling is worst because of the overshooting problem in the low frequency range as we discussed in Section 3.4.2. Since $E_{\min}$ (interpolation) depends only on T and ϕ, it is the same for both enlargement and reduction. This contradicts with the intuition that for image reduction, details of the image are lost and the resampling performance should not be identical to that for enlargement.

The minimum resampling errors denoted by $E_{\min}$ (resampling) in Figures 4.5 and 4.6 are obtained by rescaling $E_{\min}$ (interpolation) by $T' = 0.8$ for enlargement and $T' = 1.25$ for reduction respectively. For both enlargement and reduction, consistent resampling achieves the best performance among the four techniques. The advantage of consistent

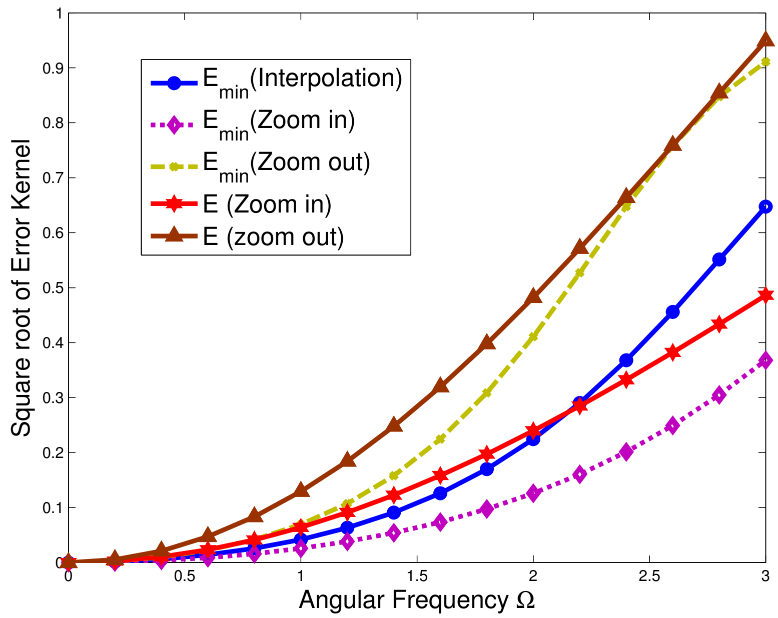

Figure 4.7: Comparison of the resampling performance when the image is enlarged by 25% and reduced by 20%.

resampling can be clearly observed in case of image enlargement. For image reduction, the performance of quasi resampling approaches that of consistent resampling. Both these methods outperform oblique resampling.

Figure 4.7 shows the relationship between the minimum interpolation error $E_{\min}$ (interpolation), the minimum resampling error for enlargement $E_{\min}$ (zoom in) and reduction $E_{\min}$ (zoom out). It can be observed that $E_{\min}$ (zoom out) is always larger than $E_{\min}$ (zoom in), which is consistent with the intuition. The interpolation performance resides between $E_{\min}$ (zoom out) and $E_{\min}$ (zoom in). The performance of consistent resampling for both enlargement E (zoom in) and reduction E (zoom out) are also included in Figure 4.7. It can be observed that the actual resampling performance may be better than the ideal interpolation performance at high frequencies. For example, in this case, when $\Omega \geq 2.2$ or 0.701 radians, E (zoom in) is smaller than $E_{\min}$ (interpolation). This is because from (4.38), the resampling performance is obtained by deducting the interpolation error of η_f from the interpolation error of f at rate T'. In Figure 4.7, η_f is represented by $E_{\min}$ (interpolation). Since the rate of increase of η_f becomes higher for larger Ω, there exist an Ω_0 above which the rate of increase of η_{η_f} is higher than that of η_f. In our case, $\Omega_0 = 2.2$.

4.4.3 De-interlacing

Let $f(x)$ denote the underlying scene which is sampled with a period $T_1 = 2$ at the odd (even) line positions to obtain the interlaced samples. The motion compensated samples are obtained from the corresponding interlaced samples in the preceding field. Therefore they have the same sampling period T_1. The continuous signal obtained by interpolation of the input using $\beta_1(x)$ is given by

$$\widetilde{f}(x) = \sum_n f(2n)\beta_1(x-2n) + \sum_m f(2m+a)\beta_1(x-2m-a) \tag{4.62}$$

This signal is resampled at both the odd and even line positions. Thus the resampling period T_2 is 1. Denote the de-interlaced output sequence by $\mathbf{f}_o$. Interpolating this output by $\beta_1(x)$, we have

$$\widehat{f}(x) = \sum_k f_o[k]\beta_1(x-k) \tag{4.63}$$

where $f_o[k] = \widetilde{f}(x)\delta(x-k)$. The distance between the input $\mathbf{f}_i$ and the output $\mathbf{f}_o$ of the de-interlacing system is

$$\begin{aligned} d_\beta(f_i[n], f_o[s]) = \Bigg\| &\sum_n f(2n)\left[\beta_1(x-2n) - \sum_s \beta_1(s-2n)\beta_1(x-k)\right] \\ &+ \sum_m f(2m+a)\left[\beta_1(x-2m-a) - \sum_k \beta_1(k-2m-a)\beta_1(x-k)\right]\Bigg\| \end{aligned} \tag{4.64}$$

obtained by substituting (4.62) and (4.63) into (4.8).

Consider the optimal consistent resampling case where $d_\beta(\mathbf{f}_i, \mathbf{f}_o) = 0$. The interpolating function $\beta_1(x)$ satisfies the Nyquist property, i.e. $\beta_1[k] = \delta[k] \quad \forall k \in \mathbb{Z}$. Since $\beta_1[k-2n] = \delta[k-2n]$,

$$\sum_k \beta_1(k-2n)\beta_1(x-k) = \beta_1(x-2n) \tag{4.65}$$

for $k, n \in \mathbb{Z}$. Thus the first term on the right-hand-side of (4.64) is zero. For the second term of this equation to be zero, we require

$$\beta(x - 2m - a) = \sum_k \beta[k - 2m - a]\beta(x - k) \tag{4.66}$$

$$\Rightarrow \quad \beta[k - 2m - a] = \delta[k - 2m - a] \tag{4.67}$$

for all m. The equation only holds when a is an integer. Since $0 < a \leq 1$, we conclude that the resampling error is minimal when $a = 1$. This is consistent with intuition. In general, when the interpolating function satisfies the Nyquist property, optimal resampling performance can be achieved when $a = 1$.

4.5 Summary

In this chapter we proposed a metric to calculate the distance between discrete sequences within the framework of consistent resampling. We showed that it satisfies the basic requirements of a distance metric. A formula is then derived for evaluating the performance of a resampling system in the frequency domain using the proposed metric. We showed that the correction filter used to achieve consistent resampling is indeed optimal under the derived performance measure. It produces results that are consistent with conventional theory when applied to the resampling of bandlimited signals and to the example of de-interlacing. It has also been used to compare the four resampling methods used in the image resizing experiments discussed previously in Section 3.4.2.

Chapter 5

Consistent Resampling in the Presence of Noise

In Chapter 3, the idea of consistent resampling is developed for signals that are not necessarily bandlimited. However, consistent resampling is only attainable when the system and the input sequence are both free from noise. In practice, the input sequence may be contaminated by discrete noise such as quantization error. For some applications, it may be more convenient to model it as noise that is added to the interpolated signal.

In this chapter we shall study the effect of noise on consistent resampling. We shall consider noise that is added to the discrete input signal as well as noise which is introduced to the reconstructed continuous signal after the interpolation filter. In Section 5.2, the performance of resampling with noise is analyzed using the distance metric proposed in Chapter 4. It is shown that the correction filter for consistent resampling developed in Chapter 3 is unbiased, but it is not necessarily optimal when noise is present. The task is then to solve the correction filter which minimizes the resampling error. In Section 5.3, the optimal filtering problem is formulated as a convex optimization problem and solved using existing numerical methods. The results are applied to image de-noising and mobile channel detection using Pilot Symbol Assisted Modulation (PSAM) in Section 5.4.1 and Section 5.4.2 respectively.

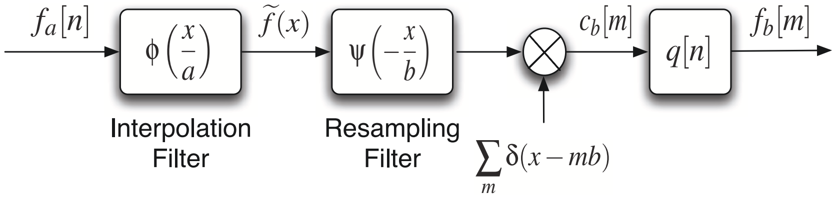

Figure 5.1: A consistent resampling system with correction filter.

5.1 Notations

With a little abuse of notation, the capital letters in this chapter stand for set transformations instead of Fourier transforms. The synthesis process is described by $\Phi : \mathbb{R}^u \to \mathcal{H}$. The superscript u is the length of the input sequence. When the input is infinitely long, u is ∞. For a uniformly sampled sequence $\mathbf{f}_a \in \mathbb{R}^u$, this implies

$$\Phi_a \mathbf{f}_a = \sum_{j=1}^{u} f_a[j]\phi\left(\frac{x}{a} - j\right) \tag{5.1}$$

where the subscript a is used to denote the dilation factor of the interpolation function.

The synthesis space is denoted by $\Re(\Phi)$, which is the range of the transformation. It is equivalent to the space V_a^ϕ spanned by $\{\phi\left(\frac{x}{a} - j\right)\}_{j\in[1,u]}$. Similarly, the null space is denoted by $\aleph(\Phi)$. Let $\Phi^\dagger$ and Φ^* denote the Moore-Penrose pseudoinverse and its adjoint respectively. Then $\Phi^\dagger$ and Φ^* are related by

$$\Phi^\dagger = (\Phi^*\Phi)^{-1}\Phi^* \tag{5.2}$$

The adjoint Φ^* describes a set transformation $\Phi^* : \mathcal{H} \to \mathbb{R}^u$. It can be used to represent the acquisition process. It follows that if $\mathbf{f}_a = \Phi^* f$ then the sequence $\mathbf{f}_a \in \mathbb{R}^u$ can be obtained by $f_a[i] = \left\langle \phi\left(\frac{x}{a} - i\right), f \right\rangle$ for $i \in [1, u]$.

For the sake of convenience, the resampling system with correction filter is shown again in Figure 5.1. This resampling process can be expressed compactly using the above notation. The output of the system is given by

$$\mathbf{f}_b = \mathbf{Q}\Psi_b^*\Phi_a\mathbf{f}_a \tag{5.3}$$

where Ψ_b^* describes the acquisition process $\Psi_b^* : \mathcal{H} \rightarrow \mathbb{R}^v$ and v is the length of the output sequence. For consistent resampling, we require

$$\begin{aligned}\Phi_a \mathbf{f}_a &= \Phi_b \mathbf{f}_b & (5.4)\\ &= \Phi_b \mathbf{Q} \Psi_b^* \Phi_a \mathbf{f}_a & (5.5)\end{aligned}$$

Multipling both side by $\Phi_b^\dagger$, we have

$$\begin{aligned}\Phi_b^\dagger \Phi_a \mathbf{f}_a &= \Phi_b^\dagger \Phi_b \mathbf{Q} \Psi_b^* \Phi_a \mathbf{f}_a \\ &= \mathbf{Q} \left(\Psi_b^* \Phi_a\right) \mathbf{f}_a & (5.6)\end{aligned}$$

Therefore, the consistent resampling correction filter is given by

$$\mathbf{Q} = \left(\Psi_b^* \Phi_a\right)^{-1} \Phi_b^\dagger \Phi_a \tag{5.7}$$

$\mathbf{Q}$ defines a process which is $\mathbb{R}^v \rightarrow \mathbb{R}^v$.

Expressed in the matrix form, the input and output sequences are given by

$$\begin{aligned}\mathbf{f}_a &= [f_a[1]\ f_a[2]\ \cdots f_a[u]]^T & (5.8)\\ \mathbf{f}_b &= [f_b[1]\ f_b[2]\ \cdots f_b[v]]^T & (5.9)\end{aligned}$$

$\Psi_b^* \Phi_a$ is a $v \times u$ matrix whose elements are defined by: for $i \in [1, v]$, $j \in [1, u]$,

$$\Psi_b^* \Phi_a[i, j] = \left\langle \psi\left(\frac{x}{b} - i\right), \phi\left(\frac{x}{a} - j\right)\right\rangle \tag{5.10}$$

It describes how the i-th element in $\mathbf{f}_a$ is related to the j-th element of $\mathbf{c}_b$. Similarly, the elements of the matrix $\Phi_b^\dagger \Phi_a$ are given by

$$\Phi_b^\dagger \Phi_a[i, j] = \left\langle \phi_d\left(\frac{x}{b} - i\right), \phi\left(\frac{x}{a} - j\right)\right\rangle \qquad i \in [1, v],\ j \in [1, u] \tag{5.11}$$

The Moore-Penrose Pseudoinverse $\Phi^\dagger$ describes a set transformation $\Phi^\dagger : \mathcal{H} \rightarrow \mathbb{R}^u$. If

$$\mathbf{f}'_a = \Phi_a^\dagger f \tag{5.12}$$

then

$$f'_a[i] = \left\langle f, \phi_d\left(\frac{x}{a} - i\right)\right\rangle \tag{5.13}$$

Using (5.10) and (5.11) in (5.7), $\mathbf{Q}$ can thus be represented by a $v \times v$ matrix which maps $\mathbf{c}_b$ to $\mathbf{f}_b$. According to Figure 5.1, $\mathbf{c}_b$ and $\mathbf{f}_b$ are related by

$$f_b[k] = \sum_n q[n]c_b[k-n] \tag{5.14}$$

where $\{q[n]\}_{n\in\mathbb{Z}}$ is the impulse response of the digital correction filter $\mathbf{q}$. Therefore, the matrix $\mathbf{Q}$ is given by

$$\mathbf{Q} = \begin{bmatrix} Q_{1,1} & Q_{1,2} & \cdots & Q_{1,v} \\ Q_{2,1} & \ddots & & Q_{2,v} \\ \vdots & & \ddots & \\ Q_{v,1} & \cdots & Q_{v,v-1} & Q_{v,v} \end{bmatrix} \tag{5.15}$$

$$= \begin{bmatrix} q[0] & q[-1] & \cdots & q[-v+1] \\ q[1] & \ddots & & q[-v+2] \\ \vdots & & \ddots & \\ q[v-1] & \cdots & q[1] & q[0] \end{bmatrix} \tag{5.16}$$

Note that it is a Toeplitz matrix. Furthermore, if $\mathbf{q}$ is symmetric, then $\mathbf{Q}$ is Hermitian circulant.

5.2 Performance of Resampling System with Noise

5.2.1 Discrete Noise

We shall first consider the case where the discrete input is contaminated by additive noise. The task is to design the correction filter such that the resampling performs optimally when measured using the metric proposed in Chapter 4.

Figure 5.2 illustrates the resampling system with noisy discrete input. The noisy input to the system is $\mathbf{f}_a + \mathbf{n}_a$. Therefore the reconstructed continuous signal $\widetilde{f}$ is given

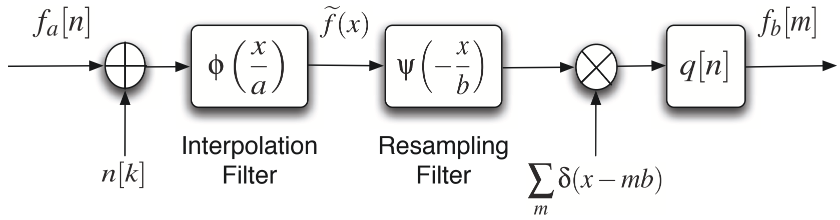

Figure 5.2: A consistent resampling system with discrete noisy input.

by

$$\widetilde{f}(x) = \Phi_a \mathbf{f}_a + \Phi_a \mathbf{n}_a \tag{5.17}$$

The output of the system is

$$\begin{aligned} \mathbf{f}_b &= \mathbf{Q}\Psi^* \widetilde{f} && (5.18) \\ &= \mathbf{Q}\Psi^* \left(\Phi_a \mathbf{f}_a + \Phi_a \mathbf{n}_a\right) && (5.19) \end{aligned}$$

where $\Psi^* : \mathcal{H} \to \mathbb{R}^v$ represents the resampling process. Based on the performance metric defined by (4.8), the distance between $\mathbf{f}_a$ and $\mathbf{f}_b$ is given by

$$\begin{aligned} d_\phi(\mathbf{f}_a, \mathbf{f}_b) &= \|\Phi_a \mathbf{f}_a - \Phi_b \mathbf{f}_b\| \\ &= \|\Phi_a \mathbf{f}_a - \Phi_b \mathbf{Q}\Psi_b^* \Phi_a \mathbf{f}_a - \Phi_b \mathbf{Q}\Psi_b^* \Phi_a \mathbf{n}_a\| \\ &= \|\left(I - \mathbf{Q}\Phi_b \Psi_b^*\right) \Phi_a \mathbf{f}_a - \mathbf{Q}\Phi_b \Psi_b^* \Phi_a \mathbf{n}_a\| && (5.20) \end{aligned}$$

Assume that the noise is zero-mean with a positive-definite covariance matrix W_n. The average performance of the resampling system can be measured by the expected value of squared distance.

$$\begin{aligned} E\left[d_\phi^2\left(\mathbf{f}_a, \mathbf{f}_b\right)\right] &= E\left[\|\left(I - \Phi_b \mathbf{Q}\Psi_b^*\right) \Phi_a \mathbf{f}_a - \Phi_b \mathbf{Q}\Psi_b^* \Phi_a \mathbf{n}_a\|^2\right] \\ &= E\left[\|\left(I - \Phi_b \mathbf{Q}\Psi_b^*\right) \Phi_a \mathbf{f}_a\|^2\right] + E\left[\|\Phi_b \mathbf{Q}\Psi_b^* \Phi_a \mathbf{n}_a\|^2\right] \\ &= \underbrace{\|\left(I - \Phi_b \mathbf{Q}\Psi_b^*\right) \Phi_a \mathbf{f}_a\|^2}_{E_{\mathbf{f}_a,\mathbf{Q}}} + \underbrace{E\left[\left(\Phi_b \mathbf{Q}\Psi_b^* \Phi_a \mathbf{n}_a\right)^* \left(\Phi_b \mathbf{Q}\Psi_b^* \Phi_a \mathbf{n}_a\right)\right]}_{E_{\mathbf{n}_a,\mathbf{Q}}} && (5.21) \end{aligned}$$

The expression for the average performance in (5.21) can be decomposed into two parts. The first part, $E_{\mathbf{f}_a,\mathbf{Q}}$, is dependent on the input signal and the second part, $E_{\mathbf{n}_a,\mathbf{Q}}$, is dependent on the discrete noise. Therefore (5.21) cannot be minimized if $\mathbf{f}_a$ is unbounded. However, an unbiased resampling system can be obtained if $\mathbf{Q}$ is chosen such that $E_{\mathbf{f}_a,\mathbf{Q}} = 0$, i.e.

$$\Phi_a \mathbf{f}_a = \Phi_b \mathbf{Q} \Psi_b^* \Phi_a \mathbf{f}_a \tag{5.22}$$

In this case, the average performance is independent of the input. Note that this requirement is the same as the consistent resampling condition given by (5.5). Therefore, the consistent correction filter given by (5.7) is an unbiased filter when discrete noise is present. The residue error is given by

$$E_{\text{res}} = E\left[\left(\Phi_b \mathbf{Q} \Psi_b^* \Phi_a \mathbf{n}_a\right)^* \left(\Phi_b \mathbf{Q} \Psi_b^* \Phi_a \mathbf{n}_a\right)\right] \tag{5.23}$$

5.2.2 Continuous Noise

Now we consider the cases where the interpolated signal is corrupted by noise. The system is shown in Figure 5.3. Under these circumstances, the output of the resampling system is given by

$$\mathbf{f}_b = \mathbf{Q} \Psi_b^* \left(\Phi_a \mathbf{f}_a + n\right) \tag{5.24}$$

We shall assume that the noise $n(x)$ is a stationary zero-mean process with variance σ.

Following the approach in Section 5.2.1, the distance between the input $\mathbf{f}_a$ and the output $\mathbf{f}_b$ is

$$\begin{aligned} d_\phi(\mathbf{f}_a, \mathbf{f}_b) &= \|\Phi_a \mathbf{f}_a - \Phi_b \mathbf{f}_b\| \\ &= \|\Phi_a \mathbf{f}_a - \Phi_b \mathbf{Q} \Psi_b^* \left(\Phi_a \mathbf{f}_a + n\right)\| \\ &= \|\left(I - \Phi_b \mathbf{Q} \Psi_b^*\right) \Phi_a \mathbf{f}_a - \mathbf{Q} \Phi_b \Psi_b^* n\| \end{aligned} \tag{5.25}$$

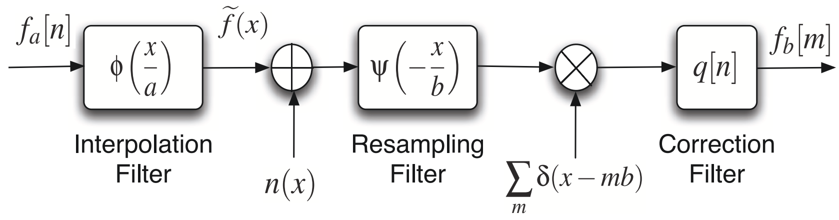

Figure 5.3: Resampling system with noise added to the interpolated signal.

The average performance is therefore given by

$$\begin{aligned} E\left[d_\phi^2\left(\mathbf{f}_a, \mathbf{f}_b\right)\right] &= E\left[\left\|\left(I - \Phi_b \mathbf{Q} \Psi_b^*\right) \Phi_a \mathbf{f}_a - \Phi_b \mathbf{Q} \Psi_b^* n\right\|^2\right] \\ &= \underbrace{\left\|\left(I - \Phi_b \mathbf{Q} \Psi_b^*\right) \Phi_a \mathbf{f}_a\right\|^2}_{E_{\mathbf{f}_a, \mathbf{Q}}} + \underbrace{\sigma \mathrm{Tr}\left[\left(\Phi_b \mathbf{Q} \Psi_b^*\right)^* \left(\Phi_b \mathbf{Q} \Psi_b^*\right)\right]}_{E_{n, \mathbf{Q}}} \end{aligned} \tag{5.26}$$

Comparing (5.26) with (5.21), the parts that are dependent on the input signal are identical. Thus the same conclusion can be drawn for the system with continuous noise. That is, (5.26) cannot be minimized when $\mathbf{f}_a$ is unbounded. But the consistent resampling correction filter in (5.7) guarantees that the average performance of the system is independent of the input. In this case, the residue error is given by

$$E_{\text{res}} = \sigma \mathrm{Tr}\left[\left(\Phi_b \mathbf{Q} \Psi_b^*\right)^* \left(\Phi_b \mathbf{Q} \Psi_b^*\right)\right] \tag{5.27}$$

5.3 Design of Correction Filter for Minimax Mean Square Error

Unfortunately, the unbiased correction filter derived in Sections 5.2.1 and 5.2.2 do not necessarily produce a small error. This is because the residue errors in (5.23) and (5.27) are functions of the filter $\mathbf{Q}$ as well. The same problem has been encountered in generalized sampling systems as discussed in Section 2.4. When a generalized sampling process is corrupted by noise, the residue error of unbiased consistent sampling may not be small at all.

In [128–131], the effects of noise in generalized sampling systems are explored. The author introduced the concept of admissible and dominating estimations $\widetilde{f}$ of a signal

f from its noisy samples. For a signal $f(x) \in \mathcal{S}$, an estimator $\widetilde{f}_1$ dominates another estimator $\widetilde{f}_2$ if

$$E\left\{\left\|f - \widetilde{f}_1\right\|^2\right\} \leq E\left\{\left\|f - \widetilde{f}_2\right\|^2\right\}, \qquad \text{for all } f \in \mathcal{S} \tag{5.28}$$

$$E\left\{\left\|f - \widetilde{f}_1\right\|^2\right\} < E\left\{\left\|f - \widetilde{f}_2\right\|^2\right\}, \qquad \text{for some } f \in \mathcal{S} \tag{5.29}$$

An estimator $\widetilde{f}$ is admissible if it is not dominated by any other linear estimator. It was shown that an admissible estimation can be obtained from the solution of the minimax optimization problem

$$\widetilde{f}' = \arg\min \left\{ \sup_{f \in \mathcal{S}} \left[E\left(\left\|f - \widetilde{f}\right\|^2\right) - E\left(\left\|f - \widetilde{f}_0\right\|^2\right)\right]\right\} \tag{5.30}$$

where $\widetilde{f}_0$ is any other linear estimation.

The same concept can be used to obtain the optimal output sequence when noise is present in the resampling process. From (5.3), the output is obtained from input by a linear transformation. Further, the performance of resampling is defined by the MSE error $d(\mathbf{f}_a, \mathbf{f}_b) = \|\Phi_a \mathbf{f}_a - \Phi_b \mathbf{f}_b\|$. When noise is present, an admissible $\mathbf{f}_b$ can be obtained by the solution of the optimization problem

$$\mathbf{f}_b' = \arg\min \left\{ \sup_{\mathbf{f}_a \in \mathcal{S}} \left[E\left[d_\phi^2\left(\mathbf{f}_a, \mathbf{f}_b\right)\right] - E\left[d_\phi^2\left(\mathbf{f}_a, \mathbf{f}_{0b}\right)\right]\right]\right\} \tag{5.31}$$

where $\mathbf{f}_{0b}$ is any other sequence of sampling interval b.

5.3.1 Minimax MSE Solution for Discrete Noise

Denote the space of all discrete signal sequences with bounded ℓ^2 norm, i.e. finite energy signals, by U. Mathematically, $U = \{\mathrm{u} : \|\mathbf{u}\|_{\ell^2} \leq A,\ 0 < A < \infty\}$. The specific problem here is to find a solution for $\mathbf{Q}$ among all possible $v \times v$ Toeplitz matrices S_v such that the maximum average distance between the input and output of the resampling system for all possible input $\mathbf{u} \in U$ is minimized.

From (5.21), the average distance depends on the input sequence $\mathbf{f}_a$ and the correction filter $\mathbf{Q}$. Hence we shall use the notation $\overline{D}(\mathbf{f}_a, \mathbf{Q}) = E\left[d_\phi^2\left(\mathbf{f}_a, \mathbf{f}_b\right)\right]$. From (5.21),

$$\overline{D}(\mathbf{f}_a, \mathbf{Q}) = E_{\mathbf{f}_a,\mathbf{Q}} + E_{\mathbf{n}_a,\mathbf{Q}} \tag{5.32}$$

Our aim is to obtain a unique solution to the following minimax problem:

$$\min_{\mathbf{Q}\in S_v} \max_{\mathbf{u}\in U} \left\{\overline{D}(\mathbf{u}, \mathbf{Q}) - \overline{D}(\mathbf{u}, \mathbf{Q}_0)\right\} \tag{5.33}$$

where $\mathbf{Q}_0$ is any other filter in S_v. Substituting (5.32) into (5.33), the problem becomes

$$\min_{\mathbf{Q}\in S_v} \max_{\mathbf{u}\in U} \left\{E_{\mathbf{u},\mathbf{Q}} + E_{\mathbf{n}_a,\mathbf{Q}} - E_{\mathbf{u},\mathbf{Q_0}} - E_{\mathbf{n}_a,\mathbf{Q_0}}\right\} \tag{5.34}$$

Since the last term $E_{\mathbf{n}_a,\mathbf{Q_0}}$ does not depend on $\mathbf{u}$ or $\mathbf{Q}$, it can be removed from (5.34). Grouping the terms that depend on $\mathbf{u}$, we have

$$\begin{aligned} \Xi(\mathbf{u}) &= E_{\mathbf{u},\mathbf{Q}} - E_{\mathbf{u},\mathbf{Q_0}} \\ &= \left[\left(I - \Phi_b\mathbf{Q}\Psi_b^*\Phi_a\right)^*\left(I - \Phi_b\mathbf{Q}\Psi_b^*\Phi_a\right) - \left(I - \Phi_b\mathbf{Q}_0\Psi_b^*\Phi_a\right)^*\left(I - \Phi_b\mathbf{Q}_0\Psi_b^*\Phi_a\right)\right]\|\mathbf{u}\|^2 \end{aligned} \tag{5.35}$$

Thus (5.34) becomes

$$\min_{\mathbf{Q}\in S_v} \max_{\mathbf{u}\in U} \left\{\Xi(\mathbf{u}) + E_{\mathbf{n}_a,\mathbf{Q}}\right\} \tag{5.36}$$

and we are looking for $\mathbf{Q}_{opt}$ such that

$$\mathbf{Q}_{opt} = \arg\min_{\mathbf{Q}\in S_v} \left\{E_{\mathbf{n}_a,\mathbf{Q}} + \max_{\mathbf{u}\in U} \Xi(\mathbf{u})\right\} \tag{5.37}$$

In general, the optimal solution can be found numerically using the Semi-Definite Programming (SDP). A brief review of SDP is provided in Appendix A.3.

To formulate (5.37) as an SDP problem, let

$$\mathcal{M} = \Phi_b\mathbf{Q} \tag{5.38}$$

and

$$\mathcal{P} = \Psi_b^* \Phi_a \tag{5.39}$$

Then (5.35) becomes

$$\Xi(\mathbf{u}) = \max_{\|\mathbf{u}\| \leq A} \mathbf{u}^* \left[(I - \mathcal{M}\mathcal{P})^* (I - \mathcal{M}\mathcal{P}) - Y \right] \mathbf{u} \tag{5.40}$$

where

$$Y = (I - \Phi_b \mathbf{Q}_0 \mathcal{P})^* (I - \Phi_b \mathbf{Q}_0 \mathcal{P}) \tag{5.41}$$

Let $Z = (I - \mathcal{M}\mathcal{P})^* (I - \mathcal{M}\mathcal{P}) - Y$. Then (5.40) is of the form $\max_{\|\mathbf{u}\| \leq A} \mathbf{u}^* Z \mathbf{u}$. Since Z is a symmetric matrix, from (A.14) the order of production can be rearranged as

$$\begin{aligned} \max_{\|\mathbf{u}\| \leq A} \mathbf{u}^* Z \mathbf{u} &= \max_{\|\mathbf{u}\| \leq A} Z \mathbf{u}\mathbf{u}^* \\ &= \max_{\|\mathbf{u}\| \leq A} Z \|\mathbf{u}\|^2 \end{aligned} \tag{5.42}$$

Solving the term $\max_{\mathbf{u} \in U} \Xi(\mathbf{u})$ in (5.37) is equivalent to finding the largest eigenvalue of the matrix Z, or the minimum $\lambda \geq 0$ such that

$$\begin{aligned} Z &\preceq \lambda I \\ Z &\succeq 0 \end{aligned} \tag{5.43}$$

We have $\max_{\mathbf{u} \in U} \Xi(\mathbf{u}) = \max_{\mathbf{u} \in U} \lambda \|\mathbf{u}\|^2 = A^2 \lambda$.

At the same time, the term $E_{\mathbf{n}_a, \mathbf{Q}}$ in (5.34) can be simplified as well. Substituting (5.38) and (5.39) into (5.21), we have

$$\begin{aligned} E_{\mathbf{n}_a, \mathbf{Q}} &= E\left[(\mathcal{M}\mathcal{P}\mathbf{n}_a)^* (\mathcal{M}\mathcal{P}\mathbf{n}_a) \right] \\ &= E\left[\mathbf{n}_a^* (\mathcal{M}\mathcal{P})^* (\mathcal{M}\mathcal{P}) \mathbf{n}_a \right] \\ &= \mathrm{Tr}\left[W_n (\mathcal{M}\mathcal{P})^* (\mathcal{M}\mathcal{P}) \right] \end{aligned} \tag{5.44}$$

where $\mathrm{Tr}(X) = \sum_i^{i=v} X[i,i]$ denotes the trace of a square matrix X. Since the noise $\mathbf{n}_a$ is assumed to be Gaussian with zero mean, its covariance matrix W_n is diagonal. Using (5.43) and (5.44), the optimization problem (5.37) becomes

$$\min_{\mathcal{M},\lambda\geq 0} \left\{ \mathrm{Tr}\left[W_n \left(\mathcal{M}\mathcal{P}\right)^* \left(\mathcal{M}\mathcal{P}\right)\right] + A^2\lambda \right\} \tag{5.45}$$

subject to

$$\left[\left(I-\mathcal{M}\mathcal{P}\right)^* \left(I-\mathcal{M}\mathcal{P}\right) - Y\right] \preceq \lambda I \tag{5.46}$$

By introducing a slack variable τ, as in (A.7) and (A.8), (5.45) is equivalent to

$$\begin{array}{ll} \text{minimize} & \tau \\ \text{subject to} & \tau - A^2\lambda - \mathrm{Tr}\left[W_n \left(\mathcal{M}\mathcal{P}\right)^* \left(\mathcal{M}\mathcal{P}\right)\right] \succeq 0 \end{array} \tag{5.47}$$

Consider the Schur complement defined in (A.16). Let $A = I$, $B = \mathbf{m} = \mathrm{vec}(W_n^{1/2}\mathcal{M}\mathcal{P})$, the vector obtained by stacking the columns of the matrix $W_n^{1/2}\mathcal{M}\mathcal{P}$, and $C = \tau - A^2\lambda$, (5.47) can be represented in the matrix form as in (A.15). Thus,

$$\begin{bmatrix} I & \mathbf{m}^* \\ \mathbf{m} & \tau - A^2\lambda \end{bmatrix} \succeq 0 \tag{5.48}$$

At the same time, (5.46) can be rewritten as

$$\lambda I + Y - \left(I-\mathcal{M}\mathcal{P}\right)^* \left(I-\mathcal{M}\mathcal{P}\right) \succeq 0 \tag{5.49}$$

It can also be represented in matrix form by

$$\begin{bmatrix} I & \left(I-\mathcal{M}\mathcal{P}\right)^* \\ \left(I-\mathcal{M}\mathcal{P}\right) & \lambda I + Y \end{bmatrix} \succeq 0 \tag{5.50}$$

Substituting (5.48) and (5.50) into (5.45) and (5.46), we have the SDP problem:

$$\begin{array}{ll} \text{minimise} & \tau \\ \text{subject to} & \begin{bmatrix} I & \mathbf{m}^* \\ \mathbf{m} & \tau - A^2\lambda \end{bmatrix} \succeq 0 \\ & \begin{bmatrix} I & (I - \mathcal{M}\mathcal{P})^* \\ (I - \mathcal{M}\mathcal{P}) & \lambda I + Y \end{bmatrix} \succeq 0 \\ & \tau \geq 0 \\ & \mathcal{M} \geq 0 \\ & \lambda \geq 0 \end{array} \tag{5.51}$$

From (5.38), given the solution $\mathcal{M}_{opt}$ of this SDP, the optimal correction filter is

$$\mathbf{Q}_{opt} = \Phi_b^{\dagger}\mathcal{M}_{opt} \tag{5.52}$$

5.3.2 Minimax MSE Solution for Continuous Noise

The correction filter for resampling system with continuous noise can be derived in a similar manner. The only difference between the system with discrete noise and the system with continuous noise resides in the terms relating to the noise, $E_{\mathbf{n}_a,\mathbf{Q}}$ and $E_{n,\mathbf{Q}}$ respectively. The other terms remain unchanged. Therefore, the correction filter can be obtained by solving the following minimax problem.

$$\mathbf{Q}_{opt} = \arg\min_{\mathbf{Q}\in S_v} \left\{ E_{n,\mathbf{Q}} + \max_{\mathbf{u}\in U} \Xi(\mathbf{u}) \right\} \tag{5.53}$$

with $E_{n,\mathbf{Q}}$ and $\Xi(\mathbf{u})$ given by (5.26) and (5.35) respectively. Use the expression for $\mathcal{M}$ defined in (5.38) and let

$$\mathcal{R} = \Psi_b^* \tag{5.54}$$

$E_{n,\mathbf{Q}}$ can be simplified as

$$E_{n,\mathbf{Q}} = \sigma \mathrm{Tr}\left[(\Phi_b \mathbf{Q} \Psi_b^*)^* (\Phi_b \mathbf{Q} \Psi_b^*) \right] \tag{5.55}$$

$$= \sigma \mathrm{Tr}\left[(\mathcal{M}\mathcal{R})^* (\mathcal{M}\mathcal{R}) \right] \tag{5.56}$$

The SDP formulation of this problem easily follows.

$$\min_{\mathcal{M},\lambda\geq 0} \left\{\sigma \mathrm{Tr}\left[(\mathcal{M}\mathcal{R})^* (\mathcal{M}\mathcal{R})\right] + A^2\lambda\right\} \tag{5.57}$$

subject to

$$\left[(I-\mathcal{M}\mathcal{P})^* (I-\mathcal{M}\mathcal{P}) - A\right] \leq \lambda I \tag{5.58}$$

Using the Schur complements, we have

$$\min_{\tau,\mathcal{M},\lambda\geq 0} \tau$$

subject to

$$\begin{bmatrix} I & \mathbf{m}^* \\ \mathbf{m} & \tau - A^2\lambda \end{bmatrix} \succeq 0 \tag{5.59}$$

$$\begin{bmatrix} I & (I-\mathcal{M}\mathcal{P})^* \\ (I-\mathcal{M}\mathcal{P}) & \lambda I + Y \end{bmatrix} \succeq 0 \tag{5.60}$$

where $\mathbf{m} = \sigma^{1/2}\mathrm{vec}(\mathcal{M}\mathcal{R})$ is the vector obtained by stacking the columns of the matrix $\mathcal{M}\mathcal{R}$. The optimal correction filter is given by

$$\mathbf{Q}_{opt} = \Phi_b^{\dagger}\mathcal{M}_{opt} \tag{5.61}$$

where $\mathcal{M}_{opt}$ is the solution to the SDP.

The mean square distances in (5.21) and (5.26) are convex functions. (5.33) and (5.53) are convex minimizations. This ensures the unique existence of the optimal correction filter $\mathbf{Q}_{opt}$. For any other filter $\mathbf{Q}_0$, it is always true that

$$\overline{D}(\mathbf{u}, \mathbf{Q}_{opt}) - \overline{D}(\mathbf{u}, \mathbf{Q}_0) < 0 \tag{5.62}$$

That is, the resampling error using the optimal correction filter $\mathbf{Q}_{opt}$ is always smaller than that of any other correction filter $\mathbf{Q}_0$.

5.4 Applications

5.4.1 Image De-noising

Image de-noising is an application where the input to the resampling system is corrupted by discrete noise. In this case, the sampling interval of the input and output are the same. The role of the correction filter is to remove as much noise as possible from the input.

As an example we use the image of Lena. The pixel values are in the range $[0, 1]$. Noise is assumed to be Gaussian with zero mean and variance 0.005. The covariance matrix W_n is therefore given by $W_n = 0.005I$. The original and noise-added images are shown in Figure 5.4. The performance of the correction filter and the Wiener filter are compared.

The optimal way to remove noise from a signal is to use a Wiener filter. It is based on a statistical approach and assumes we have full knowledge of the signal and the noise. The Wiener filter is designed such that the MSE between the estimated signal and the original signal is minimized [184]. The filter is implemented in MATLAB through the function “wiener2”. It filters the image using pixel-wise adaptive Wiener filtering. The user may specify the neighborhood size of $m \times n$ pixels for the estimation of local mean and standard deviation. We set $m = n = 2$ in our example. The restored image is shown in Figure 5.5.

To design the correction filter to remove the discrete noise from the image, we follow the steps in Section 5.3.1. Correction filtering is applied to each row of the image and then followed by the columns separately. The problem can be modeled as a system shown in Figure 5.2 where the sampling and resampling intervals are $a = b = 1$. Furthermore, since the input and output are of the same size, $u = v$. For a fair comparison, we use $\phi(x) = \beta^1(x)$ as the interpolation function since the support of β^1 is 2 which is identical to the neighborhood size used for Wiener filtering. The sampling and resampling functions are $\varphi = \psi = \delta$.

5.4.a: Noiseless image

5.4.b: Noisy image

Figure 5.4: The image of Lena.

Figure 5.5: The restored image by Wiener Filter

The SDP formulation is given in (5.50). Since the pixel values are in the range $[0,1]$ and the size of the image is 256×256, a suitable ℓ^2 norm bound is $A = 256$. We first look for the expression of $\mathcal{P}$. For $a = b = 1$, from (5.39) and (5.10) we have

$$\begin{aligned}
\mathcal{P}[i,j] = \Psi_b^* \Phi_a[i,j] &= \left\langle \psi\left(\frac{x}{b} - i\right), \phi\left(\frac{x}{a} - j\right)\right\rangle \\
&= \left\langle \delta\left(x-i\right), \beta^1\left(x-j\right)\right\rangle \\
&= \delta(i-j)
\end{aligned} \tag{5.63}$$

The matrix $\Psi_b^* \Phi_a$ is a diagonal matrix. Since $u = v$, $\Psi_b^* \Phi_a$ and hence $\mathcal{P}$ are identity matrices. Consequently, $\mathcal{M}\mathcal{P} = \mathcal{M}$, $Y = (I - \Phi_b \mathbf{Q_0})^*(I - \Phi_b \mathbf{Q_0})$ and $\mathbf{m} = vec(W_n^{1/2}\mathcal{M})$. Using these in (5.50), we have the problem to be solved which is

$$\min_{\tau, \mathcal{M}, \lambda \geq 0} \tau \tag{5.64}$$

Figure 5.6: The restored image by the correction filter

subject to

$$\begin{bmatrix} \tau - 256^2 & \mathbf{m}^* \\ \mathbf{m} & I \end{bmatrix} \succeq 0 \tag{5.65}$$

$$\begin{bmatrix} \lambda I + Y & (I - \mathcal{M})^* \\ (I - \mathcal{M}) & I \end{bmatrix} \succeq 0 \tag{5.66}$$

This SDP problem can be solved efficiently using computational methods, such as those provided by the MATLAB toolbox 'YALMIP' [185].

Figure 5.6 shows the result of our approach. This can be compared with the Wiener filtering result in Figure 5.5. It is obvious that the correction filter performs better than the Wiener filter. This is because the Wiener filter is only locally optimal since the means and standard deviations are estimated using a local neighborhood of pixels. On the other hand, although the interpolation function in our resampling system is chosen to be the locally supported β^1, from (5.37) the entire input sequence is taken into account nevertheless. Thus the correction filter is able to minimize the error globally.

Besides, the correction filter is more flexible than the Wiener filter. The Wiener filter requires that the input and output are of the same size. On the contrary, a correction filter can be designed for a different resampling interval so that the output can be of a different size. Furthermore, the Wiener filter is image-specific because it depends on the spectral properties of the input. The correction filter, on the other hand, is designed for all possible input sequences that belong to the bounded subspace and therefore is independent of the input. In our case, the correction filter can be applied to all images of size 256×256.

5.4.2 Mobile Channel Detection Using PSAM

Multipath fading distortion is a major problem in wireless communication systems. Pilot Symbol Assisted Modulation (PSAM) has been used effectively to combat multipath fading. A major advantage is that it does not effect the transmitted pulse shape or the peak to average power ratio. The loss of bandwidth to transmit the pilot symbols is well justifiable comparing to other techniques [186, 187]. The idea is simple. Pilot symbols are serially multiplexed onto the information symbols at the transmitter. The receiver has prior knowledge of the pilot symbol sequences and so it can extract the pilot symbols from the received data stream and subsequently estimate the required compensation for the fading effects on the data symbols.

In order for the PSAM technique to be effective, the pilot symbol rate must be at least two times higher than the fading rate. If not, estimation would be less accurate and a high error floor would be incurred. Assume perfect synchronization so that inter-symbol interference can be neglected. Based on Shannon's sampling theorem, a fading process with a maximum Doppler spread of f_D could be sampled without distortion using the Nyquist rate of $2f_D$. The channel response can be estimated by resampling the channel response obtained at the positions of the pilot symbols to those of the data symbols. Therefore the choice of interpolation method will have an affect on the performance of channel estimation and consequently on the error performance. High-order synthesis functions generally provide superior performances. However, it requires more pilot symbols to be buffered and the delay is certainly undesirable in some applications such as speech communications. It also greatly increases the complexity of the receiver.

For data frame k, let $d_{k,l}$ denote the $(L-1)$ data symbols so that $l = 1, \cdots, L-1$. Let p_k denote the pilot signals which are multiplexed onto the data symbols at a rate higher than $2f_D$. At the receiver end, the received pilot signal is detected and the noise contaminated mobile channel response h_k at the pilot symbol is computed. To detect the transmitted data symbols, we need to know the channel response at the time instants of data symbols $h_{k,l}$ [187, 188]. Then h_k is interpolated to approximate the continuous channel response which is resampled at the time instants of the data symbols. Thus it is essentially a resampling problem in presence of noise.

Theoretically, the ideal synthesis function is *sinc* since the ideal sampler is used at the receiver. However, other non-ideal interpolating functions are used in practice because of the slow decay of the *sinc* function. This leads to interpolation errors which affects channel estimation accuracy. Previous studies suggest that interpolation error results in an irreducible bit error rate (BER) floor [36, 188].

The minimax filter we derived in this chapter is clearly applicable to this situation. First, the non-ideal synthesis filter is taken care of by ensuring consistency resampling. Second, by deriving a minimax solution for MSE performance, the effects of the noise is reduced as well.

Without loss of generality, assume that the pilot symbol is inserted at zeroth $(l = 0)$ position in each frame. The received symbol at l-th position in the k-th frame is given by

$$r_{k,l} = \begin{cases} h_{k,l}d_{k,l} + n_{k,l}, & l = 1, \cdots, L-1 \\ h_{k,l}p_k + n_{k,l}, & l = 0 \end{cases} \tag{5.67}$$

where $n_{k,l}$ is white Gaussian noise with variance $2N_0$. The pilot symbol p_k has a constant amplitude $|p|$. The channel response $h_{k,l}$ and $h_{k,0}$ are complex variables that model the multi-path fading with variance $2E_s$. When the modulation is binary phase-shift keying (BPSK), the data is $[-1, 1]$. If the channel response is estimated correctly, the SNR of the pilot symbol is given by

$$SNR_p = E_s|p|^2/N_0 \tag{5.68}$$

The SNR for the data symboles is

$$SNR_d = E_s/N_0 \tag{5.69}$$

The average BER is related to the SNR by

$$BER = Q(\sqrt{SNR}) \tag{5.70}$$

where

$$Q(x) = \frac{1}{\sqrt{2\pi}} \int_x^\infty \exp^{-t^2/2} dt \tag{5.71}$$

is the error function.

The channel estimate at the pilot symbol position is given by

$$\widetilde{h}_{k,0} = \frac{r_{k,0}}{p_k} \tag{5.72}$$

$$= h_{k,0} + \frac{n_{k,0}}{p_k} \tag{5.73}$$

These estimates are interpolated and resampled to obtain $h_{k,l}$. Due to the slow decaying property of the *sinc* function, only its truncated version is used in practice. Thus interpolation is performed using the nearest K data frames. Assume that the bit duration is $T = 1$ and therefore $f_D = 1/2L$. Take the 0-th frame for example, the channel response at the l-th bit is given by

$$\widetilde{h}_l = \sum_{k=-K_1}^{K_2} \widetilde{h}_{k,0}\ sinc\left(\frac{l}{L} - k\right) \tag{5.74}$$

where $K_1 = \lfloor (K-1)/2 \rfloor$ and $K_2 = \lfloor K/2 \rfloor$.

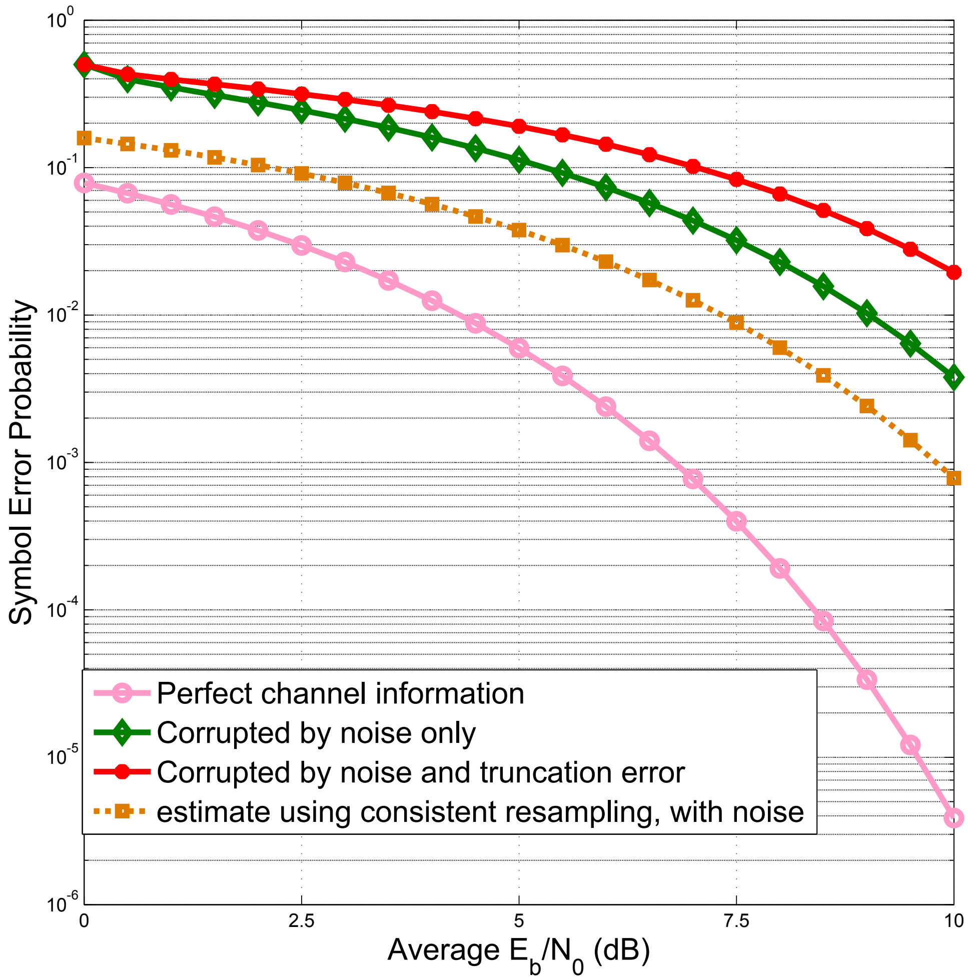

Figure 5.7: Performances of PSAM where channel interpolation is by consistent correction filtering and by a Hamming windowed *sinc* function.

Putting it into the context of our resampling system, the sampling and resampling intervals are $a = L$ and $b = 1$ respectively. Here $\Phi_a : \mathbb{C}^K \to \mathcal{H}$ and $\Psi_b : \mathcal{H} \to \mathbb{C}^L$ where

$$\Phi_a = \begin{bmatrix} sinc\,(x/L + K_1) \\ \vdots \\ sinc\,(x/L - K_2) \end{bmatrix} \tag{5.75}$$

$$\Psi_b = \begin{bmatrix} \delta(x-0) \\ \vdots \\ \delta(x - L + 1) \end{bmatrix} \tag{5.76}$$

The input signal is

$$\mathbf{h}_0 = \left[\widetilde{h}_{-K_1,0}, \cdots, \widetilde{h}_{K_2,0}\right] \tag{5.77}$$

and the noise is

$$\mathbf{n} = [n_{-K_1,0}/p_{-K_1}, \cdots, n_{K_2,0}/p_{K_2}] \tag{5.78}$$

The resampled output is for the 0-th frame is

$$\mathbf{h}_l = [h_{0,0}, \cdots, h_{0,L-1}] \tag{5.79}$$

Note that the output samples reside in a single frame while the input samples are spread over K frames. Therefore the distance $\|\Phi_L \mathbf{h}_0 - \Phi_1 \mathbf{h}_l\|$ is evaluated for one frame only.

For $L = 15$, $K = 20$ and $|p|^2 = 1$, we have $MB = 20$ since $\|sinc(x)\|^2_{L^2} = 1$ and the functions $\{sinc(x-k)\}_{k \in Z}$ are orthogonal to each other. Therefore, $\mathcal{M} = \mathbf{q}$ and $\mathcal{H} = I$.

Figure 5.7 plots the Symbol Error Probability (SEP) versus SNR for consistent resampling and one that uses truncated *sinc* function for interpolation. We also plot the SEP versus SNR for situations where the perfect information of the channel is known while noise is present. Our consistent correction filter approach results in lower SER for the other two cases. It implies that the consistent resampling approach does not only compensate for the non-idealness of the interpolation function, but also the effect of the noise.

5.4.3 Comment on the Complexity

It can be observed that to derive the minimax filter is generally quite complex. Assuming that the length of the filter is N, the filter defined by (5.52) is of complexity $O(N^2)$, excluding the complexity of the SDP problem (5.51) to derive $\mathcal{M}$. On the other hand, for a Wiener filter of length N, it is obtained by solving the equation

$$\begin{bmatrix} R_f[0] & R_f[1] & \cdots & R_f[N] \\ R_f[1] & R_f[0] & \cdots & R_f[N-1] \\ \vdots & \vdots & \ddots & \vdots \\ R_f[N] & R_f[N-1] & \cdots & R_f[0] \end{bmatrix} \begin{bmatrix} a[0] \\ a[1] \\ \vdots \\ a[N] \end{bmatrix} = \begin{bmatrix} R_{fn}[0] \\ R_{fn}[1] \\ \vdots \\ R_{fn}[N] \end{bmatrix} \tag{5.80}$$

where $R_f[m]$ is the autocorrelation of the input sequence and R_{fn} is the cross correlation sequence of input and noise. The matrix appearing in the equation is a symmetric Toeplitz matrix. To solve the euqation, an efficient algorithm called Levinson-Durbin can be used and the complexity is $O(N^2)$.

It is arguable whether the improvement in performance is justifiable by the additional complexity required to obtain the minimax filter. We want to highlight that despite the performance improvement, the minimax filter also offers flexibility that Wiener filter does not. Wiener filter is only applicable to noise filtering. From the point of view of a resampling system, the input and output sequence are required to be obtained by the sampling function and the same sampling period. On the other hand, the minimax filter is designed to minimize the distance between the input and output. As we mentioned in Chapter 4, there is no restriction on the sampling function or the period of the input and output to use our proposed metric to evaluate the distance between them. Therefore, the minimax filter is more flexible than the Wiener filter.

This drawback of Wiener filter can be noticed from Section 5.4.2. When the sampling period and resampling rate are different, Wiener filter is no longer applicable. To justify the addition complexity incurred to derive the minimax filter, we suggest it shall be used under conditions when (1) high quality performance is preferred; and (2) great flexibility is demanded.

5.5 Summary

In this chapter, we use the distance metric proposed in Chapter 4 to derive the performance of resampling in the MSE sense when noise is present. Two different types of noise are considered. One is the discrete noise that is added to the input signal and the other is continuous noise which is added to the interpolated signal. A correction filter is designed to minimize the maximum possible error, assuming that the input sequences are ℓ^2-norm bounded. The optimal filter can be obtained by numerically solving an SDP problem. The proposed design is applied to images de-noising which shows that it performs better than the Wiener filter. The advantage of our approach is derived from the fact that besides considering the effects of noise, the correction filter takes care of the non-idealness of the interpolating function as well. For PSAM, it has been shown that the correction filter produces lower BER using BPSK for the same SNR compared with using a Hamming-windowed *sinc* function for interpolation.

Chapter 6

Innovation Sampling and Resampling Rate

In this chapter, we consider the minimum resampling rate required for consistent resampling. We approach it through the rate of innovation introduced by innovation sampling discussed in Section 2.5. First, computation of the RI for signals in shift invariant spaces is studied in Section 6.1. Then acquisition filters that are more general that those are considered in Section 6.2. The results obtained herein are used to obtain the minimum resampling rate for consistent resampling. Thus the main result is presented in Section 6.2.2.

6.1 RI of Signals in Shift Invariant Spaces

The rate of innovation ρ of a signal measures the degree of freedom of a signal per unit time. The degree of freedom is the number of parameters required to uniquely specify the signal. For example, an N-th order polynomial defined by

$$f(x) = \sum_{i=0}^{N} c[i]x^i \tag{6.1}$$

is uniquely determined by the $N+1$ coefficients $c[i]$ and therefore the degree of freedom is $N+1$. If this signal crosses the axis at $x = a$, then $(x-a)$ is a factor of $f(x)$ and so it can be expressed as

$$f(x) = (x-a)\sum_{i=0}^{N-1} c'[i]x^i \tag{6.2}$$

In this case, the degree of freedom of $f(x)$ is N.

The RI may be intuitive for some signals, e.g. the periodic pulse train (2.76) we discussed in Section 2.5. However, it is not so easy for other non-trivial signals.

Proposition 6.1.1. *Consider a signal $f(x)$ of the form*

$$f(x) = \sum_k c[k]\phi\left(\frac{x}{T}-k\right) \tag{6.3}$$

where $\phi \in \mathcal{H}$ and T is a constant. The rate of innovation ρ_f of $f(x)$ satisfies

$$\rho_f \leq \frac{1}{T} \tag{6.4}$$

Equality holds only when ϕ is a generating function and $\{\phi\left(\frac{x}{T}-k\right)\}_{k\in\mathbb{Z}}$ forms a Riesz basis.

Proof. For a signals given by (6.3), in every time interval $[kT,(k+1)T)$, there is one coefficient $c[k]$ to specify. This means that there is at most one degree of freedom every T seconds. If the coefficients are independent of each other, then $\rho_f = 1/T$. If the coefficients are not independent, then $\rho_f < \frac{1}{T}$.

To prove the condition for equality, we shall show that the coefficients $c[k]$ are independent if $\{\phi\left(\frac{x}{T}-k\right)\}_{k\in\mathbb{Z}}$ is a Riesz basis. Assume that the value of the coefficient $c[k_1]$ for a certain constant k_1 has been changed to $\Delta c[k_1]$. Using the set of sample values $\{\cdots, c[k_1-1], \Delta c[k_1], c[k_1+1], \cdots\}$ in V_T^{ϕ} we can reconstruct a signal $\widetilde{f}(x)$ by

$$\widetilde{f}(x) = \sum_{k\neq k_1} c[k]\phi\left(\frac{x}{T}-k\right) + \Delta c[k_1]\phi\left(\frac{x}{T}-k_1\right) \tag{6.5}$$

Sampling $\widetilde{f}(x)$ by the dual function ϕ_d of ϕ with a sampling period of T is equivalent to projecting $\widetilde{f}(x)$ onto V_T^{ϕ} again. This results in

$$\begin{aligned} \widetilde{f}[m]_T &= \left\langle \widetilde{f}(x), \phi_d\left(\frac{x}{T} - m\right)\right\rangle \\ &= \sum_{k \neq k_1} c[k]\left\langle \phi\left(\frac{x}{a} - k\right), \phi_d\left(\frac{x}{a} - m\right)\right\rangle + \Delta c[k_1]\left\langle \phi\left(\frac{x}{a} - k_1\right), \phi\left(\frac{x}{a} - m\right)\right\rangle \end{aligned} \tag{6.6}$$

Since ϕ and ϕ_d are dual functions,

$$\left\langle \phi\left(\frac{x}{T} - k\right), \phi_d\left(\frac{x}{T} - m\right)\right\rangle = \delta[m-k] \tag{6.7}$$

Therefore, (6.6) is reduced to

$$\widetilde{f}_T[m] = \begin{cases} c[k], & m = k \neq k_1 \\ \Delta c[k_1], & m = k_1 \end{cases} \tag{6.8}$$

Thus a change in the value of $c[k_1]$ has no effect on the other samples. Hence we can conclude that the coefficients $c[k]$ are independent of each other. Since the dual function in (6.6) only exists when $\{\phi\left(\frac{x}{T} - k\right)\}_{k\in\mathbb{Z}}$ is a Riesz basis, the equality part of the Proposition 6.1.1 is proved. □

Let $\phi\left(\frac{x}{T} - k\right)$ be denoted by $\phi_{Tk}(x)$ for any $k \in \mathbb{Z}$. It can be expressed in the form of (6.3) as

$$\phi_{Tk}(x) = \phi\left(\frac{x}{T} - k\right) \tag{6.9}$$

$$= \sum_m \delta[m-k]\phi\left(\frac{x}{T} - m\right) \tag{6.10}$$

The unit impulse sequences $\{\delta[m-k]\}_{m\in\mathbb{Z}}$ are independent of each other regardless of whether $\{\phi\left(\frac{x}{T} - k\right)\}_{k\in\mathbb{Z}}$ forms a Riesz basis. The RI of ϕ_{T_k} is $\frac{1}{T}$. If a signal $f(x)$ can be expressed as (6.3), then it is made up of functions ϕ_{Tk}. Based on Proposition 6.1.1, we can say that the RI of such a signal cannot be greater than the RI of its component functions. Thus,

$$\rho_f \leq \rho_{\phi_T} = \frac{1}{T} \tag{6.11}$$

6.2 Acquisition Functions for Innovation Sampling

The principle behind having ρ_f as the minimum sampling rate is that N independent equations are required to solve for N unknowns uniquely. Hence, if $f(x)$ has an RI of ρ_f, then we need to solve for ρ_f unknowns per unit time in order to reconstruct $f(x)$. Each sample obtained in the interval $1/\rho_f$ is able to provide us with one equation. So we need a total of ρ_f equations per unit time.

The RI of a signal is the minimum sampling rate at which the signal should be sampled. However, sampling at this minimum rate is possible only if a proper acquisition function is used. For example, consider a bandlimited signal $f(x)$ with a bandwidth of Ω_0. It can be expressed in the form of (6.3) with $\phi(x) = Bsinc(Bx)$ where $B = 1/T$. Thus

$$f(x) = \sum_k f_T[k] Bsinc\left(B\left(x - kT\right)\right) \tag{6.12}$$

for all $B \geq \rho_f = \Omega_0/2\pi$. Although the bandwidth, or equivalently ρ_f and hence the minimum sampling rate, is a constant, the actual sampling rate $f_s = 1/T$ used to obtain the samples $f_T[k] = f(x)|_{x=kT}$ can be any value higher than the minimum. Thus the same $f(x)$ can be expressed as (6.12) using ϕ with different dilations. A possible interpretation is that when ϕ is dilated by $1/T$ and $f(x)$ for a sampling rate $f_s = 1/T$, each sample $c[k]$ obtained within an interval of T second gives us a unique ϕ_{T_k}. From the various ϕ_{T_k} obtained, ϕ can be derived and thus $f(x)$ can be reconstructed.

In general, if a signal $f(x)$ can be expressed as (6.3), then a suitable acquisition function is the dual function of ϕ. If the dual ϕ_d exists, then the samples can be obtained by

$$c[k] = \left\langle f(x), \phi_d\left(\frac{x}{T} - k\right)\right\rangle \tag{6.13}$$

at sampling rate of $f_s = 1/T$. Proposition 6.1.1 tells us that $\rho_f \leq 1/T$ and the equality holds only when $\{\phi_{Tk}\}_{k\in\mathbb{Z}}$ is a Riesz basis. Therefore, the minimum sampling rate is attainable only when $\phi(x)$ is a generating function.

More generally, the acquisition function φ is not a dual function of ϕ, similar to the scenario for consistent sampling. It is therefore desirable to derive the conditions on the acquisition function such that a signal with finite rate of innovation of the form (6.3) can be sampled at the minimum rate.

6.2.1 Sampling with General Acquisition Functions

Here we restrict $\varphi \in \mathcal{H}$ to generating functions only such that $\{\varphi(\frac{x}{T} - k)\}_{k\in\mathbb{Z}}$ is a Riesz basis and its dual function φ_d exists. When $f(x)$ is sampled using φ at ρ_f, the samples are given by

$$f[k] = \left\langle f(x), \varphi\left[\frac{1}{\rho_f}\left(x - \frac{k}{\rho_f}\right)\right]\right\rangle \tag{6.14}$$

When φ is known and φ_d exists, $f(x)$ can be reconstructed from the samples $f[k]$ by

$$\widetilde{f}(x) = \sum_k f[k]\varphi_d\left[\rho_f\left(x - \frac{k}{\rho_f}\right)\right] \tag{6.15}$$

Therefore, to derive the conditions on φ is equivalent to examining the conditions on φ_d such that a signal given by (6.3) can be represented by (6.15).

Our approach is to express both ϕ and φ_d as polynomials. The Weierstrass's Approximation Theorem [39] states that every finite signal $\phi \in [a, b]$ where $a, b \in \mathbb{R}$ can be approximated arbitrarily well by a polynomial

$$P(x) = \sum_{k=0}^{n} c_1[k]x^k \tag{6.16}$$

such that

$$\|\phi - P\|_\infty \leq \epsilon \tag{6.17}$$

The order of P depends on ϵ, ϕ and the interval $[a, b]$. Assume that ϕ is approximated by a polynomial of order $n = L_\phi - 1$. Then the parameters associated with ϕ are the weights $\{c_1[k]\}_{k\in\mathbb{Z}}$ and hence the total degree of freedom is $\mathcal{N}_\phi = L_\phi$.

More specifically, as discussed in Section 2.3.1, if ϕ is a Maximum approximation Order with Minimum Support (MOMS) function of order L_ϕ, it can be expressed by weighted sum of derivatives of B-splines [48, 96]. Thus,

$$\phi(x) = \sum_{k=0}^{L_\phi - 1} p_k \frac{d^k}{dx^k} \beta^{L_\phi - 1}(x) \tag{6.18}$$

Since β^k is indeed a k-th order polynomial, (6.18) can be rewritten as

$$\phi(x) = \sum_{k=0}^{L_\phi - 1} c_1[k] x^k \tag{6.19}$$

We shall assume that $\phi(x)$ are MOMS functions such that the order of the polynomials that approximate the functions with negligible error is equal to the approximation order L_ϕ. Therefore, if φ_d is of approximation order L_{φ_d}, it can be expressed in polynomial form as

$$\varphi_d(x) = \sum_{k=0}^{L_{\varphi_d} - 1} c_2[k] x^k \tag{6.20}$$

The number of coefficients associated with φ_d is given by L_{φ_d}.

The function ϕ_{Tk} as defined in (6.10) can also be represented in the polynomial form by

$$\phi_{Tk} = \sum_{m=0}^{L_\phi - 1} c_1[m] \left(\frac{x - kT}{T} \right)^m \tag{6.21}$$

When ϕ is known, for every k, i.e. an interval of T seconds, there is one ϕ_{Tk} and the degree of freedom is L_ϕ. By substituting (6.21) into (6.3), we have

$$\begin{aligned} f(x) &= \sum_k c[k] \phi \left(\frac{x}{T} - k \right) \\ &= \sum_k \sum_{m=0}^{L_\phi - 1} (c[k] c_1[m]) \left(\frac{x - kT}{T} \right)^m \end{aligned} \tag{6.22}$$

Therefore, if $f(x)$ is represented in the polynomial form, the number of coefficients per unit time is at most L_ϕ/T. Similarly, substituting (6.20) into (6.15), we have

$$\begin{aligned}\widetilde{f}(x) &= \sum_k f[k]\varphi_d\left[\rho_f\left(x - \frac{k}{\rho_f}\right)\right] \\ &= \sum_k \sum_{m=0}^{L_{\varphi_d}-1} \left(f[k]c_2[m]\right)\left(\rho_f x - k\right)^m \qquad (6.23)\end{aligned}$$

For every sample $f[k]$ in an interval of $1/\rho_f$, there are at most L_{φ_d} coefficients. Comparing (6.22) and (6.23), the conditions on φ_d such that $f(x)$ can be represented by $\widetilde{f}(x)$ can be obtained.

Proposition 6.2.1. *Let $f(x)$ be a signal given by (6.3) with an RI of ρ_f. Assume that ϕ is a MOMS function with an approximation order of L_ϕ. $f(x)$ can be represented by a MOMS function $\varphi_d \neq \phi$ with approximation order L_{φ_d} at dilation level ρ_f as given by (6.15) if*

(i) $L_{\varphi_d} \geq L_\phi$; *and*

(ii) *the set* $\{\varphi_d(x - \frac{k}{\rho_f})\}_{k\in\mathbb{Z}}$ *is Riesz basis of its span.*

Proof. From (6.22), $f(x)$ is a polynomial of order $L_\phi - 1$. On the other hand, from (6.23), the order of polynomials that can be represented by φ_d is $L_{\varphi_d} - 1$. Therefore, if $f(x)$ can be represented by φ_d as in (6.15), then

$$L_{\varphi_d} \geq L_\phi \qquad (6.24)$$

When $f(x)$ is represented by φ_d at dilation level ρ_f as in (6.15), the RI of $f(x)$ is equal to the inverse of the dilation level. Following Proposition 6.1.1, equality holds only when $\{\varphi_d(x - \frac{k}{\rho_f})\}_{k\in\mathbb{Z}}$ is Riesz basis of its span. Hence this proposition is proved. □

Another possible interpretation of Proposition 6.2.1 is as follows. When $f(x)$ is expressed in the form of (6.22), within each interval $[kT,(k+1)T)$, the coefficients $\{c_1[m]\}_{m\in[0,L_\phi-1]}$ are known. For each sample $c[k]$ obtained, the total number of coefficients that can be solved is given by $N_1 = L_\phi$. Therefore, it has N_1 degrees of freedom per unit time. Similarly, for a signal given by (6.23), within each interval $[k/\rho_f,(k+1)/\rho_f)$, for each φ_{dT_k} the number of parameters is $N_2 = L_{\varphi_d}$. In order to represent $f(x)$ using φ_d, we require

$$\begin{aligned} \frac{N_2}{1/\rho_f} &\geq \frac{N_1}{T} \\ \Rightarrow L_{\varphi_d} &\geq \frac{L_\phi}{T\rho_f} \end{aligned} \tag{6.25}$$

From Proposition 6.1.1, $\rho_f \leq \frac{1}{T}$ and therefore $L_{\varphi_d} \geq L_\phi$.

This interpretation can lead to a more general condition on the dilation level D for a given φ_d such that $f(x)$ can be represented by

$$f(x) = \sum_k f_D[k]\varphi_d\left[\frac{1}{D}(x-kD)\right] \tag{6.26}$$

First, we shall show that the approximation order of φ is identical to the approximation order of its dual φ_d.

Proposition 6.2.2. *The approximation orders of a function φ and its dual φ_d are the same.*

Proof. As discussed in Section 2.2, if the approximation order of φ is L_φ, its frequency response $\Psi(\Omega)$ satisfies the Strang-Fix condition given by (2.15), i.e.

$$\begin{cases} \Psi[2\pi k] = \delta[k] \\ \Psi^{(m)}[2k\pi] = 0, \quad k \in \mathbb{Z},\ m = 0,\cdots,L_\varphi - 1 \end{cases} \tag{6.27}$$

We shall use mathematical induction to prove that the frequency response of φ_d satisfies the Strang-Fix condition also.

The frequency response of φ_d is given by (2.20) as

$$\Psi_d(\Omega) = \frac{\Psi(\Omega)}{A_\varphi(\omega)} \tag{6.28}$$

where

$$A_\varphi(\omega) = \sum_k |\Psi(\Omega + 2k\pi)|^2 \tag{6.29}$$

with $\omega = \Omega$. The first order derivative of $\Psi_d(\Omega)$ with respect to Ω is given by

$$\begin{aligned}
\Psi_d^{(1)}(\Omega) &= \frac{d}{d\Omega}\Psi_d(\Omega) \\
&= \frac{d}{d\Omega}\frac{\Psi(\Omega)}{A_\varphi(\Omega)} \\
&= \frac{\Psi^{(1)}(\Omega)A_\varphi(\Omega) - \Psi(\Omega)A_\varphi^{(1)}(\Omega)}{A_\varphi^2(\Omega)}
\end{aligned} \tag{6.30}$$

where

$$\begin{aligned}
A_\varphi^{(1)}(\Omega) &= \frac{d}{d\Omega}A_\varphi(\Omega) \\
&= 2\sum_k |\Psi(\Omega + 2k\pi)|\ |\Psi^{(1)}(\Omega + 2k\pi)|
\end{aligned} \tag{6.31}$$

For $\Omega = 2n\pi$, $n \in \mathbb{Z}$,

$$\begin{aligned}
A_\varphi^{(1)}(\Omega)|_{\Omega=2n\pi} &= 2\sum_k |\Psi\left[2(k+n)\pi\right]|\ |\Psi^{(1)}\left[2(k+n)\pi\right]| \\
&= 0
\end{aligned} \tag{6.32}$$

since $\Psi^{(1)}\left[2(k+n)\right]\pi = 0$ for all $k, n \in \mathbb{Z}$. Substituting (6.32) into (6.30), we have

$$\begin{aligned}
\Psi_d^{(1)}(\Omega)|_{\Omega=2n\pi} &= \frac{\Psi^{(1)}(\Omega)A_\varphi(\Omega) - \Psi(\Omega)A_\varphi^{(1)}(\Omega)}{A_\varphi^2(\Omega)} \\
&= \frac{0-0}{A_\varphi^2(\Omega)} \\
&= 0
\end{aligned} \tag{6.33}$$

Assume that $\Psi_d^{(m-1)}(\Omega)$ satisfies the Strang-Fix condition. Then for $n \in \mathbb{Z}$ and $m = 0, \cdots, L_\varphi - 1$, we have

$$\Psi_d^{(m-1)}(2n\pi) = 0 \tag{6.34}$$

From the chain rule of differentiation,

$$\begin{aligned}\Psi_d^{(m)}(\Omega) &= \frac{d^m}{d\Omega^m}\Psi_d(\Omega) \\ &= \frac{d}{d\Omega}\Psi_d^{(m-1)}(\Omega) \\ &= \Psi_d^{(m)}(\Omega)\Psi_d^{(1)}(\Omega) \qquad (6.35)\end{aligned}$$

Hence,

$$\Psi_d^{(m)}(\Omega)|_{\Omega=2n\pi} = \Psi_d^{(m)}(2n\pi)\Psi_d^{(1)}(2n\pi) \qquad (6.36)$$

Since $\Psi_d^{(1)}(2n\pi) = 0$, we have $\Psi_d^{(m)}(2n\pi) = 0$ for $n \in \mathbb{Z}$ and the Strang-Fix condition is satisfied for $\Psi_d^{(m)}(\Omega)$. By mathematical induction, we have $\Psi_d^{(m)}(2n\pi) = 0$ for $n \in \mathbb{Z}$, $m = 0, \cdots, L_\varphi - 1$. Therefore, $\Psi_d(\Omega)$ satisfies the Strang-Fix condition up to order $L_\varphi - 1$ and the approximation order of φ_d is L_φ as well. □

Now we shall return to the conditions on D for (6.26).

Proposition 6.2.3. *Let ϕ be a known function and $f(x)$ be a signal given by (6.3) with a finite RI of ρ_f. If $f(x)$ is to be expressed using a function φ_d as in (6.26), then the dilation level D should satisfy*

$$D \leq \begin{cases} T\frac{L_{\varphi_d}}{L_\phi}, & L_\phi \geq L_{\varphi_d} \\ T, & L_\phi \leq L_{\varphi_d} \end{cases} \qquad (6.37)$$

where both ϕ and φ_d are assumed to be MOMS functions with approximation orders L_ϕ and L_{φ_d} respectively.

Proof. Given $f(x)$ as in (6.26), it can be sampled by using the acquisition function φ which is the dual function of φ_d at the rate $1/D$. The sample values are

$$\begin{aligned} f[k] &= \left\langle f(x), \varphi\left[\frac{1}{D}(x-kD)\right]\right\rangle \qquad (6.38) \\ &= \left\langle f(x-kD), \varphi\left(\frac{x}{D}\right)\right\rangle \qquad (6.39)\end{aligned}$$

For every k, we have a $\varphi_{D_k} = \varphi(\frac{x}{D} - k)$ similar to (6.9). If the approximation order of φ is L_φ, then the degree of freedom is L_φ.

On the other hand, if $f(x)$ is expressed as a polynomial of order $L_\phi - 1$ as in (6.22), then the degree of freedom is L_ϕ. Thus for each k, the degree of freedom must be given by

$$N_1 = \min(L_\phi, L_\varphi) \tag{6.40}$$

From Proposition 6.2.2, $L_\varphi = L_{\varphi_d}$. Therefore

$$N_1 = \min(L_\phi, L_{\varphi_d}) \tag{6.41}$$

Following Proposition 6.2.1, the degree of freedom per unit time is L_ϕ/T. To express $f(x)$ using φ_d of dilation level $1/D$, it requires

$$\frac{N_1}{D} \geq T\frac{L_\phi}{T} \tag{6.42}$$

If $L_\phi \geq L_\varphi$, then $N_1 = L_{\varphi_d}$ and hence

$$D \leq T\frac{L_{\varphi_d}}{L_\phi} \tag{6.43}$$

If $L_\phi \leq L_{\varphi_d}$, then $N_1 = L_\phi$ and

$$D \leq T \tag{6.44}$$

$\square$

Given an acquisition function φ of approximation order L_φ, the dilation level and hence the corresponding sampling rate can be chosen directly by using (6.37).

6.2.2 Application to Consistent Resampling Theory

In a resampling system, the input sequence $\mathbf{f}_T$ is interpolated by the interpolation function ϕ to produce

$$\widetilde{f}(x) = \sum_k f_T[k]\phi\left(\frac{x}{T} - k\right) \tag{6.45}$$

The output $\mathbf{f}_{T'}$ is obtained by resampling $\widetilde{f}(x)$ at the rate $1/T'$.

$$f_{T'}[k] = \left\langle \widetilde{f}(x), \psi\left(\frac{x}{T'} - k\right)\right\rangle \tag{6.46}$$

Assume that ϕ and ψ are MOMS functions with approximation orders L_ϕ and L_ψ respectively. From Proposition 6.2.3, the resampling interval T' is required to satisfy

$$T' \leq \begin{cases} T\frac{L_{\varphi_d}}{L_\phi}, & L_\phi \geq L_{\varphi_d} \\ T, & L_\phi \leq L_{\varphi_d} \end{cases} \tag{6.47}$$

Consider the image resizing example discussed in Section 3.4.2. The input is sampled with sampling period $T = 1$. The interpolation function and the resampling function used are $\phi = \beta^1$ and $\psi = \delta$ respectively. B-spline functions are MOMS functions. The approximation order of a B-spline of order $n-1$ is $L = n$. Thus in this case, we have

$$L_\phi = 2 \tag{6.48}$$

For the resampling function, since the dual of $\psi = \delta$ is $\psi_d = sincx$, from Proposition 6.2.2, the approximation order of ψ is given by

$$L_\psi = L_{\psi_d} = 1 \tag{6.49}$$

Since $L_\psi < L_\phi$, according to (6.47), the resampling period should satisfy

$$\begin{aligned} T' &\leq T\frac{L_\psi}{L_\phi} \\ \Rightarrow T' &\leq \frac{1}{2} \end{aligned} \tag{6.50}$$

in order to to resample $\widetilde{f}$ perfectly.

However, as we have discussed in Section 3.4.2, when the image is enlarged (zoomed in) by a factor of 1.25, the actual resampling interval is $T' = 0.8$. Also, when the image is reduced (zoomed out) by a factor of 0.8, $T' = 1.25$. The T' in both these cases are greater than the desired resampling period given by (6.50). That is, the resampling rates $1/T'$ is lower than the desired rates. Therefore, $\widetilde{f}$ is not perfectly resampled and some information in $\widetilde{f}$ is lost through each resizing process. This explains why after a series of zooming in and out, although the size of the original image is retained, the post-processed image is not identical to the original one.

6.3 Summary

In this chapter we provided an upper bound on the RI for signals in shift invariant spaces. We also specified the criteria for choosing a proper acquisition function for innovation sampling. Based on these results, a lower bound on the resampling rate used in consistent resampling is developed.

Chapter 7

Conclusions and Future Works

7.1 Conclusions

In this thesis, we have presented a new resampling theory for discrete signals with non-bandlimited frequency responses. We call it *consistent resampling*. When the resampling process is free of noise, it is possible to consistently resample a discrete signal using arbitrary acquisition and synthesis functions by introducing a suitable correction filter into the system. A new distance metric has been proposed to measure the closeness of the input and output discrete signals in a resampling system in both the time and frequency domains. The design of resampling systems when noise is present is guided by this metric. Finally, the conditions on the resampling rate under which consistent resampling is attainable have been explored.

The following conclusions can be drawn from the work presented in this thesis.

(i) Consistent resampling is an optimal way to resample a non-bandlimited discrete signal in the absence of noise. It is optimal in the sense that the original signal can be perfectly recovered from its consistently resampled output. Therefore, the consistent resampling process is lossless. The application of consistent resampling to demodulation of UWB signals demonstrates this lossless property.

(ii) For arbitrary acquisition function ψ and interpolation function ϕ, a correction filter can be designed and incorporated into the resampling system such that consistent resampling is achieved. ψ and ϕ are not restricted to the *sinc*-Dirac pair but can be any function from the Hilbert space. Applications to image resizing and rotation have been used to demonstrate the effectiveness of the consistent resampling system. Results obtained using consistent resampling are generally better than other techniques because the signals are not assumed to be bandlimited.

(iii) If a signal is the consistently resampled version of another, then the projections of these signals onto the subspace generated by the interpolation function dilated by the corresponding sampling intervals are equal. Hence, the distance between two discrete signals can be measured by the distance between the respective projections onto a subspace generated by a common function. The distance metric defined in this manner is applicable to any resampling system. It produces results that are consistent with intuition for well established problems such as de-interlacing.

(iv) The performance of a resampling system depends on the resampling rate as well as the interpolation function used. Additional error is caused by the non-idealness of the resampling function. It has been shown that for arbitrary pairs of interpolation and resampling functions, the correction filter is able to compensate for the non-idealness and optimal performance can be achieved. A simple formula has been derived so that the resampling performance can be easily evaluated.

(v) When noise is present in the resampling process, consistent resampling is no longer achievable. If the input signal belongs to a bounded subspace, then the correction filter from the solution to a minimax problem such that the maximum possible error for all signals in that subspace is minimized. The resampled output obtained in this manner always has smallest distance to the input signal and therefore is optimal. Applications have been found in mobile channel estimation and image noise removal. These application examples show that our approach out-performs existing techniques with no additional computational cost.

(vi) There are conditions on the resampling rate such that consistent resampling is attainable. These conditions are derived through the innovation sampling theory.

It has been shown that the minimum resampling rate depends on the approximation order of the interpolation function as well as the resampling function.

It has been shown that consistent resampling theory outperforms current techniques in terms of accurate modeling of resampling process, great extent of admissible signals, flexible to be adapted to any resampling case, robust against non-ideal filters and noise corruption. Nevertheless, there is also some limitations on the use of consistent resampling theory. First, to implement a system that enforces consistent resampling theory can be complicated. It is noticed from the example of image applications that the correction filters used for upsampling and downsampling are different. Second, in case of resampling with noise, to derive the correction filter requires the knowledge of the signal as well as the noise, which may not be available at the time of processing.

7.2 Further Research

Consistent resampling that has been developed in this thesis can be applied to many other areas of application. We shall give an overview of some future possibilities here.

7.2.1 Multidimensional and Multirate Systems

The most obvious avenue of further research is the extension of the present methods to multiple dimensions. In image processing applications considered in this thesis, all 2D processing are performed as separable 1D processes. However, there are cases where the dimensions are not separable, such as resampling a hexagonally sampled 2D sequences [107]. A proper multi-dimensional system should be developed. Tensor product construction can be used, but care must be taken to analyze the dependencies between dimensions.

Another possible extension is to multi-channel multirate systems which could result in shorter processing times. The de-interlacing example we used in this thesis could provide a glimpse of how the system could be designed. It is observed that the perfect reconstruct filter bank in conventional bandlimited scenario is analyzed in the frequency domain. In cases where the sampling functions are not necessarily ideal, the response of the digital filters can be analyzed by the algorithms proposed in the thesis.

7.2.2 Communication Systems

Since we concentrate on the theoretical analysis of the resampling system and the properties of its error function, for illustrative purposes the communication system examples used in this thesis are somewhat limited in scope. Further research is needed to study its applications in a wider context. For example, in the PSAM system discussed in Chapter 5, we only considered BPSK as the modulation scheme. Future works should include other more complex modulation schemes such as Quadrature Amplitude Modulation (QAM) [144,189]. In applying the resampling system to multi-dimensional constellations and noisy signals, the SDP formulation may need to be modified.

7.2.3 Sensor Networks

In this thesis, uniform sampling and constant dilation factors are assumed. A very interesting research direction would be to lift these restrictions. We can also study the use of multiple acquisition and synthesis functions in parallel. If the dilation factor for each acquisition function is different, then different degrees of detail can be analyzed at different resolution level, similar to the wavelet approach. An application of such a system is in *sensor networks* where spatially distributed sensors cooperate to monitor physical or environmental conditions [13, 190]. Success of a sensor network depends crucially on the sampling and communication processes. Systems with minimum sampling rates can be applied. However, new methods will need to be developed for computing the RI of the sampling functions.

7.2.4 Compressive Sensing

The concept of information preservation that has been used to develop the consistent resampling scheme opens up even more research directions. The minimum sampling rate is associated with the sampling function. In the extreme, if the signal itself is used as the sampling function, one sample is enough to reconstruct the signal completely. Very recently, an alternative sampling or sensing theory called *Compressive Sampling* or *Compressed Sensing* has emerged [191]. It allows the faithful recovery of signals and images from what appears to be highly incomplete sets of data. Underlying this methodology is a concrete protocol for sensing and compressing data simultaneously. There seems to be a link between consistent resampling and compressive sampling in the sense that they are both concerned with preserving the information contained in the signals rather than their structural properties. Both aim to preserve the information using less samples, therefore the problem is reduced to choosing an appropriate set of sampling functions. Further work to explore the similarities and differences in these two areas may result in new insights.

Appendix A

Appendices

A.1 List of Notations

Notations	
$\mathbb{Z}$	Integer Space
$\mathbb{N}$	Space of Natural Numbers
$f(x)$	Time domain signal
$\mathcal{H}$	Hilbert Space
Ω	Continuous frequency variable
$f_T(x)$	Sampled signal (continuous)
$\mathbf{f}_T$	Sampled sequence
$F(z)$	z-transform of a sequence
ϕ	Synthesis / Reconstruction function
φ	Sampling / Acquisition function
ψ	Resampling function
V_T^{ϕ}	The space spanned by $\{\phi\left(\frac{x}{T}-k\right)\}_{k\in\mathbb{Z}}$
$O(f(x))$	Big O Notation.
	If $g(x)=O(f(x))$ as $x\to\infty$, $\limsup_{x\to\infty}\left\|\frac{g(x)}{f(x)}\right\|<\infty$
$\mathcal{B}_{\phi}$	the support of function ϕ

A.2 List of Abbreviations

Abbreviations	
FT	Fourier Transform
IFT	Inverse Fourier Transform
DTFT	Discrete Time Fourier Transform
IR	Impulse Response
FR	Frequency Response
SRC	Sample Rate Conversion
GST	Generalized Sampling Theory
RI	Rate of Innovation
GR	Generalized Resampling
CR	Consistent Resampling
CRS	Consistent Resampling System

A.3 Semidefinite Programming

The Semi-Definite Programming (SDP) is an efficient tool to solve convex optimization problem [192, 193]. In general, a convex optimization problem can be represented as

$$\begin{aligned} \text{minimize} \quad & f_0(x) \\ \text{subject to} \quad & f_1(x) \;\leq\; b_i, \qquad i = 1, \cdots, m \end{aligned} \tag{A.1}$$

where the objective function f_0 and the constraint functions f_i are convex:

$$f_i(\alpha x + \beta y) \leq \alpha f_i(x) + \beta f_i(y) \tag{A.2}$$

if $\alpha + \beta = 1$, $\alpha \geq 0$, $\beta > 0$. For example, the least square problem is a special case of convex problem. The variable can be extended to multi-dimensional as well. For two points x_1 and x_2 in $\mathbb{R}^n$, the *line segment* is defined by all the points

$$x = \theta x_1 + (1 - \theta) x_2 \tag{A.3}$$

with $0 \leq \theta \leq 1$. A *convex set* contains all the line segments between any two points in the set

$$x_1, x_2 \in \mathcal{C}, 0 \leq \theta \leq 1 \qquad \Longrightarrow \qquad \theta x_1 + (1 - \theta) x_2 \in \mathcal{C} \tag{A.4}$$

For a function $f : \mathbb{R}^n \to \mathbb{R}$, it is convex if it satisfies (A.2) and its domain is a convex set. The same argument holds for variables of matrix type, $\mathbb{R}^{n \times m}$. Examples of convex functions over matrices include the linear transformation function

$$f(X) = \mathrm{Tr}(A^T X) + b = \sum_{i=1}^{m} \sum_{j=1}^{n} A_{ij} X_{ij} + b \tag{A.5}$$

and the norm of a matrix

$$\|X\|_2 = (\lambda_{\max}(X^T X))^{1/2} \tag{A.6}$$

where $\lambda_{\max}(X^T X)$ is the maximum eigenvalue of the matrix $X^T X$. There are many operation that preserve convexity, such as point-wise maximum and supremum as well as minimization.

In general, there are many representations of a convex optimization problem. One way is to introduce slack variables. For example,

$$\begin{array}{ll} \text{maximize} & f_0(x) \\ \text{subject to} & f_i(x) \;\leq\; b_i, \qquad i = 1, \cdots, m \end{array} \tag{A.7}$$

is equivalent to

$$\begin{array}{ll} \text{minimize} & \tau \\ \text{subject to} & \tau - f_0(x) \geq 0 \\ & f_i(x) \leq b_i, \qquad i = 1, \cdots, m \end{array} \tag{A.8}$$

Many convex optimization problems, such as linear programming and (convex) quadratically constrained quadratic programming can be cast as SDP. The generalized SDP problem is given by

$$\begin{array}{ll} \text{minimize} & c^T x \\ \text{subject to} & \sum_i^n x_i F_i + G \preceq 0 \\ & Ax = b \end{array} \tag{A.9}$$

where the variable $x \in \mathbb{R}^n$, and F_i and G are symmetric $k \times k$ matrix, denoted by $\mathcal{S}_k$. $\preceq$ is the component wise inequality. The linear program

$$\begin{array}{lll} \text{(LP)} & \text{minimize} & c^T x \\ & \text{subject to} & Ax \preceq b \end{array} \tag{A.10}$$

is equivalent to

$$\begin{array}{lll} \text{(SDP)} & \text{minimize} & c^T x \\ & \text{subject to} & \text{diag}(Ax - b) \preceq 0 \end{array} \tag{A.11}$$

diag(k) creates a square matrix whose diagonal is the vector k. The quadratic problem

$$\text{(QP)} \qquad \text{minimize} \qquad \|x\|_2 \tag{A.12}$$

can also be represented as an SDP by

$$\begin{array}{lll} \text{(SDP)} & \text{minimize} & t \\ & \text{subject to} & \begin{bmatrix} tI & x \\ x^T & tI \end{bmatrix} \succeq 0 \end{array} \tag{A.13}$$

where $t \in \mathbb{R}$ and $x \in \mathbb{R}^n$.

There are a collection of appealing properties for the symmetric matrices as required by the SDP configuration. For a $U \in \mathcal{S}$, the order of matrix production can be rearranged as

$$x^T U x = U x x^T \tag{A.14}$$

From (A.13), the matrix is of the form

$$U = \begin{bmatrix} A & B \\ B^T & C \end{bmatrix} \tag{A.15}$$

with $A, C \in \mathcal{S}$ and $A \succ 0$, then $U \succeq 0$ if and only if

$$C - B^T A^{-1} B \succeq 0 \tag{A.16}$$

The matrix $C - B^T A^{-1} B$ is called the Schur Complement of A. Similarly, the inequality $C - B^T A^{-1} B \succeq 0$ is equivalent to (A.15).

A.4 List of Publications

(i) Beilei Huang and Edmund M-K Lai, "Non-bandlimited Resampling of Images", in *Proceedings of IEEE International Conference on Multimedia and Expo*, Toronto, Canada, July 9 -12, 2006, pp. 149-152.

(ii) Beilei Huang, Edmund M-K Lai and A.P Vinod, "Sampling with Minimum Sampling Rates for Signals in Shift Invariant", in *Proceedings of IEEE International Symposium on Circuits and Systems*, New Orleans, LA, USA, May 27-30, 2007, pp. 4004-4007.

(iii) Beilei Huang and Edmund M-K Lai and A.P Vinod, "Demodulation of UWB Impulse Radio Signals Using B-spline", in P*roceedings of IEEE International Conference on Communication Systems*, Singapore, Oct. 30 - Dec. 1, 2006, pp.WP-6-5.

(iv) Beilei Huang and Edmund M-K Lai and A.P Vinod, "Implementation and Applications of Consistent Resampling", in *Proceedings of IEEE International Conference on Information, Communications and Signal Processing*, Singapore, Dec. 10-13, 2007, pp.

(v) Beilei Huang and Edmund M-K Lai, "Optimal Resampling of Finite Enerty Signals", in *Proceedings of the Fourteenth Electronics New Zealand Conference*, Wellington, New Zealand, Nov. 12-13, 2007, pp. 291-296.

References

[1] Y. C. Eldar, "Sampling with arbitrary sampling and reconstruction spaces and oblique dual frame vectors," *Journal of Fourier Analysis and Its Application*, vol. 9, no. 1, pp. 77–91, Jan. 2003.

[2] A. J. Jerri, "The shannon sampling theorem – its various extensions and applications: A tutorial review," *Proceedings of the IEEE*, vol. 65, no. 11, pp. 1565–1596, Nov. 1977.

[3] R. E. Crochiere and L. R. Rabiner, *Multirate Digital Signal Processing.* Prentice Hall : Englewood Cliffs, New Jersey, 1983.

[4] M. Unser and A. Aldroubi, "A general sampling theory for non-ideal acquisition devices," *IEEE Transactions on Signal Processing*, vol. 42, no. 11, pp. 2915–2925, Nov. 1994.

[5] L. Yang and G. Giannakis, "Ultra wideband communications: An idea whose time has come," *IEEE Signal Processing Magazine*, vol. 21, no. 6, pp. 26–54, Nov. 2004.

[6] A. G.Yarovoy and L. P. Ligthart, "Ultra wideband technology today," in *Proceedings of 15th International Conference on Microwaves, Radar and Wireless Communications (MIKON)*, vol. 2, Warszawa, Poland, May 17-19, 2004, pp. 456–460.

[7] M. Vetterli, P. Marziliano, and T. Blu, "Sampling signals with finite rate of innovation," *IEEE Transactions on Signal Processing*, vol. 50, no. 6, pp. 1417–1427, June 2002.

[8] M. Unser and J. Zerubia, "Generalized sampling theory: Stability and performance analysis," *IEEE Transactions on Signal Processing*, vol. 45, no. 12, pp. 2941–2950, Dec. 1997.

[9] A. Janssen and T. Kalker, "A note on Unser-Zerubia generalized sampling theory applied to the linear interpolator," *IEEE Transactions on Signal Processing*, vol. 47, no. 8, pp. 2332–2335, Aug. 1999.

[10] A. Segall and A. Katsaggelos, "Resampling for spatial scalability," in *Proceedings of IEEE International Conference on Image Processing*, Atlanta, GA, US, Oct. 8-11, 2006, pp. 181–184.

[11] X. Wu and L. Zhang, "Improvement of color video demosaicking in temporal domain," *IEEE Transactions on Image Processing*, vol. 15, no. 10, pp. 3138–3151, Oct. 2006.

[12] P. D. Tafti, S. Shirani, and X. Wu, "On interpolation and resampling of discrete data," *IEEE Signal Processing Letters*, vol. 13, pp. 733–736, Dec. 2006.

[13] M. Gastpar, M. Vetterli, and P. L. Dragotti, "Sensing reality and communicating bits: A dangerous liason," *IEEE Signal Processing Magazine*, vol. 23, pp. 70–83, 2006.

[14] C. E. Shannon, "A mathematical theory of communication," *The Bell System Technical Journal*, vol. 27, pp. 379–423, 623–656, 1948.

[15] ——, "Communication in the presence of noise," in *Proceedings of Institute of Radio Engineers*, vol. 37, no. 1, Jan. 1949, pp. 10–21.

[16] M. Unser, "Sampling - 50 years after Shannon," *Proceedings of the IEEE*, vol. 88, no. 4, pp. 569–587, Apr. 2000.

[17] F. Marvasti, M. Analoui, and M. Gamshadzahi, "Recovery of signals from nonuniform samples using iterative methods," *IEEE Transactions on Signal Processing*, vol. 39, no. 4, pp. 872–878, Apr. 1991.

[18] N. N. Brueller, N. Peterfreund, and M. Porat, "On non-uniform sampling of signals," in *Proceedings of IEEE International Symposium on Industrial Electronics*, vol. 1, Pretoria, Sud Afrika, July 7-10, 1998, pp. 249–252.

[19] P. Marziliano and M. Vetterli, "Reconstruction of irregularly sampled discrete-time bandlimited singals with unknown sampling locations," *IEEE Transactions on Signal Processing*, vol. 48, no. 12, pp. 3462–3471, Dec. 2000.

[20] J. Clark, M. Palmer, and D. Lawrence, "A transformation method for the reconstruction of functions from nonuniformly spaced samples," *IEEE Transactions on Acoustics, Speech, and Signal Processing*, vol. ASSP-33, no. 4, pp. 1151–1165, Oct. 1985.

[21] J. Yen, "On nonuniform sampling of bandwidth-limited signals," *IRE Transactions on Circuit Theory*, vol. 3, no. 4, pp. 251–257, Dec. 1965.

[22] V.-E. Neagoe, "Chebyshev nonuniform sampling cascaded with the discrete cosine transform for optimum interpolation," *IEEE Transactions on Acoustics, Speech, and Signal Processing*, vol. ASSP-38, no. 10, pp. 1812–1815, Oct. 1990.

[23] F. Papanfuß, Y. Artyukh, and D. Timmermann, "Optimal sampling functions in nonuniform sampling driver designs to overcome the Nyquist limit," in *Proceedings of IEEE International Conference on Acoustics, Speech and Signal Processing*, vol. 6, Hong Kong, Apr. 6-10, 2003, pp. VI–257–60.

[24] F. Gunnarsson, F. Gustafsson, and F. Gunnarsson, "Frequency analysis using nonuniform sampling with appliation to active queue management," in *Proceedings of IEEE International Conference on Acoustics, Speech and Signal Processing*, Montreal, Quebec, Canada, May 17-21, 2004, pp. 581–584.

[25] R. Vaughan, N. Scott, and D. White, "The theory of bandpass sampling," *IEEE Transactions on Signal Processing*, vol. 39, no. 9, pp. 1973–1984, Sept. 1991.

[26] J. Liu, X. Zhou, and Y. Peng, "Spectral arrangement and other topics in first order bandpasss sampling theory," *IEEE Transactions on Signal Processing*, vol. 49, no. 6, pp. 1260–1263, June 2001.

[27] J. Selva, "Interpolation of bounded bandlimited signals and applications," *IEEE Transactions on Signal Processing*, vol. 54, no. 11, pp. 4244–4260, Nov. 2006.

[28] R. W. Schafer and L. R. Rabiner, "A digital signal processing approach to interpolation," *Proceedings of the IEEE*, vol. 61, no. 6, pp. 692–702, June 1973.

[29] R. E. Crochiere and L. R. Rabiner, "Interpolation and decimation of digital signals - A tutorial review," *Proceedings of the IEEE*, vol. 69, no. 3, pp. 300–331, Mar. 1981.

[30] J. Kovacevic and M. Vetterli, "Perfect reconstruction filter banks with rational sampling factors," *IEEE Transactions on Signal Processing*, vol. 41, no. 6, pp. 2047–2066, June 1993.

[31] M. Vetterli, "Invertibility of linear periodically time-varying filters," *IEEE Transactions on Circuits and Systems*, vol. 36, no. 1, pp. 148–150, Jan. 1989.

[32] J. L. H. Webb, "Transposed FIR filter structure with time varying coefficients for digital data resampling," *IEEE Transactions on Signal Processing*, vol. 48, no. 9, pp. 2594–2600, Sept. 2000.

[33] S.-T. Tzeng, "Design of 2-D FIR digital filters with symmetric properties by genetic algorithm approach," in *Proceedings of IEEE Asia-Pacific Conference on Circuits and Systems*, vol. 1, Tainan, Taiwan, Dec. 6-9, 2004, pp. 417–420.

[34] A. Tirakis, A. Delopoulos, and S. Kollias, "Two dimensional filter bank design for optimal reconstruction using limited subband information," *IEEE Transactions on Image Processing*, vol. 4, no. 8, pp. 1160–1165, Aug. 1995.

[35] R. Venkataramani and Y. Bresler, "Optimal sub-nyquist nonuniform sampling and reconstruction for multiband signals," *IEEE Transactions on Signal Processing*, vol. 49, no. 10, pp. 2301–2013, Oct. 2001.

[36] Y. V. Zakharov, T. C. Tozer, and J. F. Adlard, "Polynomial spline-approximation of clarke's model," *IEEE Transactions on Signal Processing*, vol. 52, no. 5, pp. 1198–1208, May 2004.

[37] R. A. Scholtz, R. Weaver, E. Homier, J. Lee, P. Hilmes, A. Taha, and R. Wilson, "UWB radio deployment challeges," in *Proceedings of IEEE International Symposium on Personal, Indoor and Mobile Radio Communications*, vol. 1, London, UK, Sept. 18-21, 2000, pp. 620–625.

[38] P. Vaidyanathan, "Generalizations of the sampling theorem: Seven decades after nyquist," *IEEE Transactions on Circuits and Systems—Part I: Fundamental Theory and Applications*, vol. 48, no. 9, pp. 1094–1109, Sept. 2001.

[39] O. Christensen, *An Introduction to Frames and Riesz Basis*. Boston: Birkhäuser, 2003.

[40] M. Unser and I. Daubechies, "On the approximation power of convolution-based least squares versus interpolation," *IEEE Transactions on Signal Processing*, vol. 45, no. 7, pp. 1697–1711, July 1997.

[41] A. Z. Averbuch, V. A. Zheludev, and T. Cohen, "Interpolatory frames in signal space," *IEEE Transactions on Signal Processing*, vol. 54, no. 6, pp. 2126–2139, June 2006.

[42] T. Blu, P. Thevenaz, and M. Unser, "Complete parameterization of piecewise-polynomial interpolation kernels," *IEEE Transactions on Image Processing*, vol. 12, no. 11, pp. 1297–1309, Nov. 2003.

[43] M. Dalai and R. Leonardi, "Approximations of one-dimensional digital signals under the l^∞ norm," *IEEE Transactions on Signal Processing*, vol. 54, no. 8, pp. 3111–3114, Aug. 2006.

[44] Y. Lyubarskii and W. R. Madych, "Interpolation of functions from generalized paley-wiener spaces," *Jounal of Approximation Theory*, vol. 133, no. 2, pp. 251–268, Apr. 2005.

[45] E. Berdysheva, K. Jetter, and J. Stockler, "New polynomial preserving operators on simplices: direct results," *Journal of Approximation Theory*, vol. 131, no. 1, pp. 59–73, Nov. 2004.

[46] G. Strang and G. Fix, "A fourier analysis of finite element variational method," in *Constructive aspect of functional analysis*, Rome, Italy: Cremonese, 1971, pp. 796–830.

[47] T. Blu and M. Unser, "Quantitative fourier analysis of approximation techniques: Part I - interpolators and projectors," *IEEE Transactions on Signal Processing*, vol. 47, no. 10, pp. 2783–2795, Oct. 1999.

[48] T. Blu, P. Thevenaz, and M. Unser, "MOMS: Maximal-order interpolation of minimal support," *IEEE Transactions on Image Processing*, vol. 10, no. 7, pp. 1069–1080, July 2001.

[49] T. Werther, Y. C. Eldar, and N. K. Subbanna, "Dual gabor frames: Theory and computational aspects," *IEEE Transactions on Signal Processing*, vol. 53, no. 11, pp. 4147–4158, Nov. 2005.

[50] K. Bittner, "Biorthogonal wilson bases," in *Wavelet Applications in Signal and Image Processing VII*, ser. SPIE Proceedings, M. A. Unser, A. Aldroubi, and A. F. Laine, Eds., vol. 3813, Denver, CO, 1999, pp. 410–421.

[51] A. Aldroubi and M. Unser, "Sampling procedures in function spaces and asymptotic equivalence with Shannon's sampling theory," *Numerical Functional Analysis and Optimization*, vol. 15, no. 1-2, pp. 1–21, 1994.

[52] P. Prinz, "Calculating the dual Gabor window for general sampling sets," *IEEE Transactions on Signal Processing*, vol. 44, no. 8, pp. 2078–2082, Aug. 1996.

[53] P. P. Vaidyanathan and B. Vrcelj, "Biorthogonal partners and applications," *IEEE Transactions on Signal Processing*, vol. 49, no. 5, pp. 1013–1027, May 2001.

[54] A. F. Beardon and K. A. Driver, "The zeros of linear combinations of orthogonal polynomials," *Journal of Approximation Theory*, vol. 137, no. 2, pp. 179–186, Dec. 2005.

[55] L. Pastur, "From random matrices to quasi-periodic jacobi matrices via orthogonal polynomials," *Journal of Approximation Theory*, vol. 139, no. 1-2, pp. 269–292, Mar.-Apr. 2006.

[56] W. Chen, B. Han, and R.-Q. Jia, "Estimate of aliasing error for non-smooth signals prefiltered by quasi-projections into shift-invariant spaces," *IEEE Transactions on Signal Processing*, vol. 53, no. 5, pp. 1927–1933, May 2005.

[57] O. Holtz and A. Ron, "Approximation orders of shift-invariant subspaces of $w_2^s(r^d)$," *Jounal of Approximation Theory*, vol. 132, no. 1, pp. 97–148, Jan. 2005.

[58] H. Ozkaramanli and R. Yu, "Characterization of approximation order of multiscaling functions via refinable super functions," in *Proceedings of IEEE International Conference on Acoustics, Speech and Signal Processing*, vol. 6, Hong Kong, Apr. 6-10, 2003, pp. VI–405–8.

[59] T. Blu and M. Unser, "Quantitative fourier analysis of approximation techniques: Part II - wavelet," *IEEE Transactions on Signal Processing*, vol. 47, no. 10, pp. 2796–2806, Oct. 1999.

[60] P. Thevenaz, T. Blu, and M. Unser, "Interpolation revisited," *IEEE Transactions on Medical Imaging*, vol. 19, no. 7, pp. 739–758, July 2000.

[61] H. K. S. Mallat, D. Donoho, and A. S. Willsky, "Best basis algorithm for signal enhancement," in *Proceedings of IEEE International Conference on Acoustics, Speech and Signal Processing*, vol. 3, Detroit, Michigan, USA, May 9-12, 1995, pp. 1561–1564.

[62] A. N. Tikhonov and V. Y. Arsenin, *Solution of ill-posed formulated problems.* Winston & Sons : Washington, 1977.

[63] A. Neubauer, "Approximation error of shifted signals in spline spaces," *IEEE Transactions on Signal Processing*, vol. 52, no. 4, pp. 921–928, Apr. 2004.

[64] C. Riddell, A. Savi, M. C. Cilardi, and F. Fazio, "Frequency weighted least square reconstruction of truncated transmission SPECT data," *IEEE Transactions on Nuclear Science*, vol. 43, no. 4, pp. 2292–2298, Aug. 1996.

[65] T. Evgeniou, M. Pontil, and T. Poggio, "Regularization networks and support vector machines," *Advance un Computational Machematics*, vol. 13, no. 1, pp. 1–50, 2000.

[66] F. Weisz, "The maximal Riesz operator of two-dimensional fourier transforms and fourier series on $h_p(r \times r)$ and $h_p(t \times t)$," *Journal of Approximation Theory*, vol. 102, no. 1, pp. 21–45, Jan. 2000.

[67] G. Wan and W. Han, "Minimum error bound of signal reconstruction," *IEEE Signal Processing Letters*, vol. 6, no. 12, pp. 309–311, Dec. 1999.

[68] M. Unser, A. Aldroubi, and M. Eden, "Polynomial spline signal approximation: Filter design and asymptotic equivalence with shannon's sampling theorem," *IEEE Transactions on Information Theory*, vol. 38, no. 1, pp. 95–103, Jan. 1992.

[69] V. A. Prokhorov, "On best rational approximation of analytic functions," *Jounal of Approximation Theory*, vol. 133, no. 2, pp. 284–296, Apr. 2005.

[70] Y. Guan, S. Lu, and Y. Tang, "Characterization of compactly supported refinable splines whose shifts form a riesz basis," *Jounal of Approximation Theory*, vol. 133, no. 2, pp. 245–250, Apr. 2005.

[71] C. H. Lampert and O. Wirjadi, "An optimal nonorthogonal separaion of the anistotropic gaussian convolution filter," *IEEE Transactions on Image Processing*, vol. 15, no. 11, pp. 3502–3514, Nov. 2006.

[72] B. Widrow, P. Baudrenghien, and M. V. nad Paul F. Titchener, "Fundamental relations between the lms algorithms and the dft," *IEEE Transactions on Circuits and Systems*, vol. CAS-34, no. 7, pp. 814–820, July 1987.

[73] M. Zivanovic and A. Carlosena, "Nonparametric spectrum interpolation methods: A comparative study," *IEEE Transactions on Instrumentation and Measurement*, vol. 50, no. 5, pp. 1127–1132, Oct. 2001.

[74] M. J. Bastiaans, "On optimum oversampling in the gabor scheme," in *Proceedings of IEEE International Conference on Acoustics, Speech and Signal Processing*, vol. 3, Munich, Germany, Apr. 21-24, 1997, pp. 2101–2104.

[75] P. Balazs, H. G. Feichtinger, M. Hampejs, and G. Kracher, "Double preconditioning for Gabor frames," *IEEE Transactions on Signal Processing*, vol. 54, no. 12, pp. 4597–4610, Dec. 2006.

[76] S. Farkash and S. Raz, "Linear systems in Gabor time-frequency space," *IEEE Transactions on Signal Processing*, vol. 42, no. 3, pp. 611–617, Mar. 1994.

[77] A. Teuner, P. A. Nielsen, and B. J. Hosticka, "An extension to the analytical gabor expansion with applications in image coding," in *Proceedings of IEEE International Conference on Acoustics, Speech and Signal Processing*, vol. V, Adelaide, Australia, Apr. 19-22, 1994, pp. 585–588.

[78] Y. Lin, H. Chen, Z. H. Jiang, and H. F. Hsai, "Image resizing with raised cosine pulses," in *Proceedings of IEEE International Symposium on Intelligent Signal Processing and Communication Systems*, Seoul, Korea, Nov. 18-19, 2004, pp. 581–585.

[79] H. Murakami, "Discrete wavelet transform based on cyclic convolutions," *IEEE Transactions on Signal Processing*, vol. 52, no. 1, pp. 165–174, Jan. 2004.

[80] F. Luisier, T. Blu, and M. Unser, "A new SURE approach to image denoising: Interscale orthonormal wavelet thresholding," *IEEE Transactions on Image Processing*, vol. 16, no. 3, pp. 593–606, Mar. 2007.

[81] I. Schoenberg, "Contribution to the problem of approximation of equi-distant data by analytic functions," *Quarterly of Applied Mathematics*, vol. 4, pp. 45–99, 112–114, 1946.

[82] E. Rakhmanov and B. Shekhtman, "On discrete norms of polynomials," *Journal of Approximation Theory*, vol. 139, no. 1-2, pp. 2–7, Mar.-Apr. 2006.

[83] L. L. Schumaker, *Spline Functions: Basic Theory.* New York, USA: John Wiley & Sons, 1981.

[84] M. Unser, A. Aldroubi, and M. Eden, "The l_2 polynomial spline pyramid," *IEEE Transactions on Pattern Analysis and Machine Intelligence*, vol. 15, no. 4, pp. 364–379, Apr. 1993.

[85] I. Pesenson, "Polynomials splines and eigenvalue approximations on quantum graphs," *Journal of Approximation Theory*, vol. 135, no. 2, pp. 203–220, Aug. 2005.

[86] I. Schoenberg, "On interpolation by spline function and its minimal properties," in *Proceedings of the Conference on Approximation Theory*, P. Butzer and J.Korevaar, Eds. Basel: Verlag, 1964.

[87] M. Unser, "Splines - A perfect kit for signal and image processing," *IEEE Signal Processing Magazine*, vol. 16, no. 6, pp. 22–36, Nov. 1999.

[88] M. Unser, A. Aldroubi, and M. Eden, "Fast b-spline transformation for continuous image representation and interpolation," *IEEE Transactions on Pattern Analysis and Machine Intelligence*, vol. 13, no. 3, pp. 277–285, Mar. 1991.

[89] A. Gotchev and K. Egiazarian, "Spline-based resampling of noisy images," in *Proceedings of* 2^{nd} *International Symposium on Image and Signal Processing and Analysis*, Palm Springs CA, US, June 19-21, 2001, pp. 580–585.

[90] C. Berthaud, E. Bourennane, M. Paindavoine, and C. Milan, "Implementation of a real time image rotation using b-spline interpolation on fpga's board," in *Proceedings of IEEE International Conference on Image Processing*, vol. 3, Chicago, Illinois, US, Oct. 4-7, 1998, pp. 995–999.

[91] P. P. Vaidyanathan and B. Vrceli, "On sampling theorems for non bandlimited signals," in *Proceedings of IEEE International Conference on Acoustics, Speech and Signal Processing*, vol. 6, Salt Lake City, Utah, US, May 7-11, 2001, pp. 3897–3900.

[92] M. Unser, A. Aldroubi, and M. Eden, “B-spline signal processing: Part II - efficient design and applications,” *IEEE Transactions on Signal Processing*, vol. 41, no. 2, pp. 834–848, Feb. 1993.

[93] ——, “B-spline signal processing: Part I -theory,” *IEEE Transactions on Signal Processing*, vol. 41, no. 2, pp. 821–833, Feb. 1993.

[94] H. Hou and H. Andrews, “Cubic spline for image interpolation and digital filtering,” *IEEE Transactions on Acoustics, Speech, and Signal Processing*, vol. ASSP-26, no. 6, pp. 508–517, Dec. 1978.

[95] R. G. Keys, “Cubic convolution interpolation for digital image processing,” *IEEE Transactions on Acoustics, Speech, and Signal Processing*, vol. ASSP-29, no. 6, pp. 1153–1160, Dec. 1981.

[96] T. Blu, P. Thevenaz, and M. Unser, “Minimum support interpolators with optimum approximation properties,” in *Proceedings of IEEE International Conference on Image Processing*, Chicago, Illinois, USA, Oct. 4-7, 1998, pp. 242–245.

[97] A. B. Pevnyi, “On the interpolation by discrete splines with equidistant nodes,” *Journal of Approximation Theory*, vol. 102, no. 2, pp. 286–301, Feb. 2000.

[98] R. R. Grigorieff and I. H. Sloan, “Discrete orthogonal projections on multiple knot periodic splines,” *Journal of Approximation Theory*, vol. 137, no. 2, pp. 201–225, Dec. 2005.

[99] O. Kounchev and H. Render, “Cardinal interpolation with polysplines on annuli,” *Jounal of Approximation Theory*, vol. 137, no. 1, pp. 89–107, Nov. 2005.

[100] E. Maeland, “On the comparison of interpolation methods,” *IEEE Transactions on Medical Imaging*, vol. 7, no. 3, pp. 213–217, Sept. 1988.

[101] E. Meijering and M. Unser, “A note on cubic convolution interpolation,” *IEEE Transactions on Image Processing*, vol. 12, no. 4, pp. 477–479, Apr. 2003.

[102] O. Davydov and M. Sommer, “Interpolation by weak chebyshev spaces,” *Journal of Approximation Theory*, vol. 102, no. 2, pp. 243–262, Feb. 2000.

[103] K. Ichige, T. Blu, and M. Unser, “Interpolation of signals by generalized piecewise-linear multiple generators,” in *Proceedings of IEEE International Conference on Acoustics, Speech and Signal Processing*, vol. 6, Hong Kong, Apr. 6-10, 2003, pp. VI–261–4.

[104] J. Kybic, T. Blu, and M. Unser, "Generalized sampling: A variational approach - Part I: Theory," *IEEE Transactions on Signal Processing*, vol. 50, no. 8, pp. 1965–1976, Aug. 2002.

[105] ——, "Generalized sampling: A variational approach - Part II: Applications," *IEEE Transactions on Signal Processing*, vol. 50, no. 8, pp. 1977–1985, Aug. 2002.

[106] M. Unser and T. Blu, "Generalized smoothing splines and the optimal discretization of the wiener filter," *IEEE Transactions on Signal Processing*, vol. 53, no. 6, pp. 2146–2159, June 2005.

[107] L. Condat and D. V. D. Ville, "Quasi-interpolating spline models for hexagonally-sampled data," *IEEE Transactions on Image Processing*, vol. 16, no. 5, pp. 1195–1206, May 2007.

[108] F. Cobos and J. Martin, "On interpolation of function spaces by methods defined by means of polygons," *Journal of Approximation Theory*, vol. 132, no. 2, pp. 182–203, Feb. 2005.

[109] C. K. Chui, *An Introduction to Wavelets.* Academic Press, 1992.

[110] R. Neelamani, H. Choi, and R. Baraniuk, "Forward: Fourier-wavelet regularized deconvolution for ill-conditioned systems," *IEEE Transactions on Signal Processing*, vol. 52, no. 2, pp. 418–433, Feb. 2004.

[111] M. Unser and T. Blu, "Wavelet theory demystified," *IEEE Transactions on Signal Processing*, vol. 51, no. 2, pp. 470–483, Feb. 2003.

[112] S. Yea and W. A. Pearlman, "A wavelet-based two-stage near-lossless coder," *IEEE Transactions on Image Processing*, vol. 15, no. 11, pp. 3488–3500, Nov. 2006.

[113] M. Unser, "Vanishing moments and the approximation power of wavelet expansions," in *Proceedings of IEEE International Conference on Image Processing*, vol. 1, Lausanne, Switzerland, Sept. 1996, pp. 16–19.

[114] A. H. Tewfik and H. Zou, "Completeness of arbitrarily sampled discrete time wavelet transforms," *IEEE Transactions on Signal Processing*, vol. 43, no. 11, pp. 2570–2581, Nov. 1995.

[115] P. L. Dragotti and M. Vetterli, "Wavelet footprints: Theory, algorithms, and application," *IEEE Transactions on Signal Processing*, vol. 51, no. 5, pp. 1306–1323, May 2003.

[116] G. G. Walter, "A sampling theorem for wavelet subspaces," *IEEE Transactions on Information Theory*, vol. 38, no. 2, pp. 881–884, Mar. 1992.

[117] S. G. Mallat, "A theory for multiresolution signal decomposition: The wavelet representation," *IEEE Transactions on Pattern Analysis and Machine Intelligence*, vol. 11, no. 7, pp. 674–693, July 1989.

[118] M. Unser, P. Thevenaz, and A. Aldroubi, "Shift-orthogonal wavelet bases using splines," *IEEE Signal Processing Letters*, vol. 3, no. 3, pp. 85–88, Mar. 1996.

[119] B. Dong and Z. Shen, "Construction of biorthogonal wavelets from pseudo-splines," *Journal of Approximation Theory*, vol. 138, no. 2, pp. 211–231, Feb. 2006.

[120] D. Wang, L. Zhang, A. Vincent, and F. Speranza, "Curved wavelet transform for image coding," *IEEE Transactions on Image Processing*, vol. 15, no. 8, pp. 2413–2422, Aug. 2006.

[121] M. Unser and A. Aldroubi, "A review of wavelets in biomedical applications," *Proceedings of the IEEE*, vol. 84, no. 4, pp. 626–638, Apr. 1996.

[122] R. L. Kirlin and R. M. Dizaji, "Optimal sampling frequency in wavelet based signal compression," in *Proceedings of IEEE 2000 Canadian Conference on Electrical and Computer Engineering*, vol. 1, Halifax, Nova Scotia, Canada, Mar. 7-10, 2000, pp. 426–429.

[123] J.-L. Starck, J. Fadili, and F. Murtagh, "The undecimated wavelet decomposition and its reconstruction," *IEEE Transactions on Image Processing*, vol. 16, no. 2, pp. 297–309, 2007.

[124] D. P. Hardin and D. W. Roach, "Multiwavelet prefilters- I: Orthogonal prefilters preserving approximation order $p \leq 2$," *IEEE Transactions on Signal Processing*, vol. 45, no. 8, pp. 1106–1112, Aug. 1998.

[125] M. Unser and J. Zerubia, "A generalized sampling theory without band limiting constrains," *IEEE Transactions on Circuits and Systems—Part II: Analog and Digital Signal Processing*, vol. 45, no. 8, pp. 959–969, Aug. 1998.

[126] A. Hirabayashi and M. Unser, “Consistent sampling and signal recovery,” *IEEE Transactions on Signal Processing*, vol. 55, no. 8, pp. 4104–4115, Aug. 2007.

[127] S. Ramani, D. V. D. Ville, and M. Unser, “Sampling in practice: Is the best reconstruction space bandlimited?” in *Proceedings of IEEE International Conference on Image Processing*, vol. 2, Genoa, Italy, Sept. 11-14, 2005, pp. II–153–6.

[128] Y. C. Eldar and T. G. Dvorkind, “A minimum squared - error framework for generalized sampling,” *IEEE Transactions on Signal Processing*, vol. 54, no. 6, pp. 2155–2167, June 2006.

[129] Y. C. Eldar, “Comparing between estimation approaches: Admissible and dominating linear estimator,” *IEEE Transactions on Signal Processing*, vol. 54, no. 5, pp. 1689–1702, May 2006.

[130] ——, “Mean-squared error sampling and reconstruction in the presence of noise,” *IEEE Transactions on Signal Processing*, vol. 54, no. 12, pp. 4619–4633, Dec. 2006.

[131] Y. C. Eldar and M. Unser, “Nonideal sampling and interpolation from noisy observation in shift-invariant spaces,” *IEEE Transactions on Signal Processing*, vol. 54, no. 7, pp. 2636–2651, July 2006.

[132] M. Vetterli, P. Marziliano, and T. Blu, “A sampling theorem for periodic piecewise polynomial signals,” in *Proceedings of IEEE International Conference on Acoustics, Speech and Signal Processing*, vol. 6, Salt Lake City, Utah, US, May 7-11, 2001, pp. 3893–3896.

[133] I. Maravic and M. Vetterli, “Sampling and reconstruction of signals with finite rate of innovation in the presence of noise,” *IEEE Transactions on Signal Processing*, vol. 53, no. 8, pp. 2788–2805, Aug. 2005.

[134] P. L. Dragotti, M. Vetterli, and T. Blu, “Exact sampling results for signals with finite rate of innovation using strang-fix conditions and local kernels,” in *Proceedings of IEEE International Conference on Acoustics, Speech and Signal Processing*, vol. 4, Philadelphia, PA, US, Mar. 18-23, 2005, pp. IV/233–6.

[135] I. Jovanovic and B. Beferull-Lozano, “Oversampled A/D conversion and error-rate depenence of nonbandlimited signalswith finite rate of innovation,” *IEEE Transactions on Signal Processing*, vol. 54, no. 6, pp. 2140–2154, June 2006.

[136] Q. Sun, "Nonuniform average sampling and reconstruction of signals with finite rate of innovation," *SIAM Jounal of Mathematical Analysis*, vol. 38, no. 5, pp. 1389–1422, 2006.

[137] P. L. Dragotti and M. Vetterli, "Wavelet and footprint sampling of signals with a finite rate of innovation," in *Proceedings of IEEE International Conference on Acoustics, Speech and Signal Processing*, Montreal, Quebec, Canada, May 17-21, 2004.

[138] S. Lafon and J. L. Vehel, "An easily implementable sampling procedure for certain fractal and other non-band limited signals," in *Proceedings of* 6^{th} *Nordic Signal Processing Symposium*, Espoo, Finland, June 9-11, 2004, pp. 272–275.

[139] T. M. Lehmann, C. Gonner, and K. Spitzer, "Survey: Interpolation methods in medical image processing," *IEEE Transactions on Medical Imaging*, vol. 18, no. 11, pp. 1049–1075, Nov. 1999.

[140] D. Seidner, "Noise equalization in resampling of images," in *Proceedings of The* 22^{nd} *Convention of Electrical and Electronics Engineers in Israel*, Tel-Aviv, Israel, Dec. 1, 2002, pp. 75–77.

[141] ——, "Polyphase antialiasing in resampling of images," *IEEE Transactions on Image Processing*, vol. 14, no. 11, pp. 1876–1889, Nov. 2005.

[142] J. G. Proakis, *Digital Communications*, 3rd ed. McGraw-Hill, 1995.

[143] X. Dong and N. C. Beaulieu, "SER of two-dimensional signalings in rayleigh fading with channel estimation errors," in *Proceedings of IEEE International Conference on Communications*, Anchorage Alaska, USA, May 11-15, 2003, pp. 2763–2767.

[144] K. Yu, J. Evans, and I. Collings, "Performance analysis of pilot symbol aided QAM for Rayleigh fading channels," in *Proceedings of IEEE International Conference on Communications*, vol. 3, New York, USA, Apr. 28- May 2, 2002, pp. 1731–1735.

[145] J. W. Craig, "A new, simple and exact result for calculating the probability of error for two dimensional signal constellations," in *Conference Record on Military Communication Conference*. McLean, VA: IEEE, Nov. 4-7, 1991.

[146] S. K. Wilson and J. M. Cioffi, "Probability density functions for analyzing multi-amplitude constellations in Rayleigh and ricean channels," *IEEE Transactions on Communications*, vol. 47, no. 3, pp. 380–386, Mar. 1999.

[147] A. Aghamohammadi and H. Meyr, "On the error probability of linearly modulated signals on rayleigh frequency-flat fading channels," *IEEE Transactions on Communications*, vol. 38, no. 11, pp. 1966–1970, Nov. 1990.

[148] E. Meijering, "A chronology of interpolation: From ancient astronomy to modern signal and image processing," *Proceedings of the IEEE*, vol. 90, no. 3, pp. 319–342, Mar. 2002.

[149] W. Chen and Shuichi-Itoh, "A sampling theorem for shift-invariant subspaces," *IEEE Transactions on Signal Processing*, vol. 46, no. 10, pp. 2822–2824, Oct. 1998.

[150] D. D. Muresan and T. W. Parks, "Optimal recovery approach to image interpolation," in *Proceedings of IEEE International Conference on Image Processing*, vol. 3, Thessaloniki, Greece, Oct. 7-10, 2001, pp. 848–851.

[151] E. H. W. Meijering, W. J. Niessen, and M. A. Viergever, "Quantitative evaluation of convolution-based methods for medical image interpolation," *Medical Image Analysis*, vol. 5, no. 2, pp. 111–126, June 2001.

[152] T. Blu, P. Thevenaz, and M. Unser, "Linear interpolation revitalized," *IEEE Transactions on Image Processing*, vol. 13, no. 5, pp. 710–719, May 2004.

[153] N. A.Dodgson, "Quadratic interpolation for image resampling," *IEEE Transactions on Image Processing*, vol. 6, no. 9, pp. 1322–1326, Sept. 1997.

[154] S. E. Reichenbach and F. Geng, "Two-dimensional cubic convolution," *IEEE Transactions on Image Processing*, vol. 12, no. 8, pp. 857–895, Aug. 2003.

[155] J. R. Price and M. H. H. III, "Resampling and reconstruction with fractal interpolation functions," *IEEE Signal Processing Letters*, vol. 5, no. 9, pp. 228–230, Sept. 1998.

[156] S. Li, "A generalized non-separable 2-D discrete gabor expansion," in *Proceedings of IEEE International Conference on Image Processing*, vol. 1, Austin, Texas, USA, Nov. 13-16, 1994, pp. 810–814.

[157] S. Zhang and Y. Lapie, "Speech signal resampling by arbitrary rate," in *Proceedings of IEEE International Symposium on Signal Processing and Its Applications*, vol. 1, Paris, France, July 1-4, 2003, pp. 369–372.

[158] C. R. Appledorn, “A new approach to the interpolation of sampled data,” *IEEE Transactions on Medical Imaging*, vol. 15, no. 3, pp. 369–376, June 1996.

[159] G. Ramponi and S. Carrato, “Interpolation of the DC component of coded images using a rational filter,” in *Proceedings of IEEE International Conference on Image Processing*, vol. 1, Washington, DC, USA, Oct. 26-29, 1997, pp. 389–392.

[160] G. Chen and R. J. P. de Figueiredo, “A unified approach to optimal image interpolation problems based on linear partial differential equation models,” *IEEE Transactions on Image Processing*, vol. 2, no. 1, pp. 41–49, Jan. 1993.

[161] A. M. Darwish, M. S. Bedair, and S. I. Shaheen, “Adaptive resampling algorithm for image zooming,” *IEE Procedings Vision, Image & Signal Processing*, vol. 144, no. 4, pp. 207–212, Aug. 1997.

[162] K. Jensen and D. Anastassiou, “Subpixel edge localization and the interpolation of still images,” *IEEE Transactions on Image Processing*, vol. 4, no. 3, pp. 285–295, Mar. 1995.

[163] Y. Cha and S. Kim, “The Error Amended Sharp Edge (EASE) scheme for image zooming,” *IEEE Transactions on Image Processing*, vol. 16, no. 6, pp. 1496–1505, June 2007.

[164] L. Condat and A. Montanvert, “A framework for image magnification: Induction revisited,” in *Proceedings of IEEE International Conference on Acoustics, Speech and Signal Processing*, vol. 2, Philadelphia, PA, USA, Mar. 18-23, 2005, pp. 845–848.

[165] S. El-Khamy, M. Hadhoud, M. Dessouky, B. Salam, and F. Abd El-Samie, “A new edge preserving pixel-by-pixel cubic image interpolation approach,” in *Proceedings of* 21^{st} *National Radio Science Conference*, Nasr City, Cairo, Mar. 16-18, 2004, pp. C11–1–9.

[166] M. M. Hadhoud, F. E. A. El-Samie, and S. E. El-Khamy, “New trends high resolution image processing,” in *Proceedings of the Fourth Workshop on Photonics and Its Application*, May 4 2004, pp. 2–23.

[167] H. Takeda, S. Farsiu, and P. Milanfar, “Kernel regression for image processing and reconstruction,” *IEEE Transactions on Image Processing*, vol. 16, no. 2, pp. 349–366, Feb. 2007.

[168] M. Unser, A. Aldroubi, and M. Eden, "Enlargement or reduction of digital images with minimum loss of information," *IEEE Transactions on Image Processing*, vol. 4, no. 3, pp. 247–258, Mar. 1995.

[169] M. Unser, P. Thevenaz, and L. Yaroslavsky, "Convolution-based interpolation for fast, high-quality rotation of images," *IEEE Transactions on Image Processing*, vol. 4, no. 10, pp. 1371–1381, Oct. 1995.

[170] C. Lee, M. Eden, and M. Unser, "High-quality image resizing using oblique projection operators," *IEEE Transactions on Image Processing*, vol. 7, no. 5, pp. 679–692, May 1998.

[171] L. Condat, T. Blu, and M. Unser, "Beyond interpolation: Optimal reconstruction by quasi-interpolation," in *Proceedings of IEEE International Conference on Image Processing*, vol. 1, Genova, Italy, Sept. 11-14, 2005, pp. I–33–6.

[172] G. De Hann and E. Bellers, "Deinterlacing - an overview," *Proceedings of the IEEE*, vol. 86, no. 9, pp. 1839–1857, Sept. 1998.

[173] F. M. Wang, D. Anastassiou, and A. N. Netravali, "Time-recurive deinterlacing for idtv and pyramid coding," in *Proceedings of IEEE International Symposium on Circuits and Systems*, vol. 2, New Orleans, LA, USA, May 1-3, 1990, pp. 1306–1309.

[174] S. El-Khamy, M. Hadhoud, M. Dessouky, B. Salam, and F. abd El-Samie, "Optimization of image interpolation as an inverse problem using the LMMSE algorithm," in *Proc. Electrotechnical Conf.*, vol. 1, Dubrovnik, Croatia, May 12-15, 2004, pp. 247–250.

[175] D. Calle and A. Montanvert, "Super-resolution inducing of an image," in *Proceedings of IEEE International Conference on Image Processing*, vol. 3, Chicago, Illinois, USA, Oct. 4-7, 1998, pp. 232–236.

[176] M. Z. Win and R. A. Scholtz, "Ultra-wide bandwidth time-hopping spread-spectrum impulse radio for wireless multiple-access communications," *IEEE Transactions on Vehicular Communications*, vol. 48, no. 4, pp. 679–691, Apr. 2000.

[177] M.-G. Di Benedetto and G. Giancola, *Understanding Ultra Wide Band Radio Fundamentals*. Prentice-Hall, 2004.

[178] H. Khani and P. Azmi, "Novel modulation schemes for UWB-PPM systems," in *Proceedings of IEEE* 60^{th} *Conference on Vehicular Technology*, vol. 2, Dallas, Texas, USA, May 30-June1, 2005, pp. 1401–1405.

[179] S. Hoyos, B. M. Sadler, and G. R. Arce, "High-speed A/D conversion for ultra-wideband signals based on signal projection over basis functions," in *Proceedings of IEEE International Conference on Acoustics, Speech and Signal Processing*, vol. 4, Montreal, Canada, May 17-21, 2004, pp. IV–537–540.

[180] Z. Xu, B. M. Sadler, and J. Tang, "Data detection for UWB transmitted reference systems with inter-pulse interference," in *Proceedings of IEEE International Conference on Acoustics, Speech and Signal Processing*, Philadelphia, PA, USA, Mar. 18-23, 2005, pp. 156–160.

[181] X. Wu, Z. Tian, T. N. Davidson, and G. B. Giannakis, "Optimal waveform design for UWB radios," *IEEE Transactions on Signal Processing*, vol. 54, no. 6, pp. 2009–2021, June 2006.

[182] X. Luo, L. Yang, and G. B. Giannakis, "Designing optimal pulse-shapers for ultra-wideband radios," in *Proceedings of IEEE International Conference on Ultra Wide-band Systems and Technologies*, vol. 6, Reston, Virginia, USA, Nov. 16-19, 2003.

[183] J. E. Maisel and R. E. Morden, "Rotation of a two dimensional sampling set using one dimensional resampling," *IEEE Transactions on Acoustics, Speech, and Signal Processing*, vol. ASSP-29, no. 6, pp. 1218–1224, Nov. 1981.

[184] R. G. Brown and P. Y. C. Hwang, *Introduction to Random Signals and Applied Kalman Filtering.* John Wiley & Sons : New York, 1996.

[185] J. Löfberg, "YALMIP : A toolbox for modeling and optimization in MATLAB," in *Proceedings of the CACSD Conference*, Taipei, Taiwan, 2004. [Online]. Available: http://control.ee.ethz.ch/~joloef/yalmip.php

[186] J. K. Cavers, "An analysis of pilot symbol assisted modulation for Rayleigh fading channels," *IEEE Transactions on Vehicular Technology*, vol. 40, no. 4, pp. 686–693, Nov. 1991.

[187] J. M. Torrance and L. Hanzo, "Comparative study of pilot symbol assisted modem schemes," in *Proceedings of IEE International Conference on Radio Receivers and Associated Systems*, Bath, UK, Sept. 26-27, 1995, pp. 36–41.

[188] L. Xiao, X. Dong, and A. C.K.Song, "On the design of sinc interpolator for pilot symbol assisted modulation systems," *IEEE Transactions on Wireless Communications*, vol. 5, no. 9, pp. 2578–2585, Sept. 2006.

[189] K. E. Baddour and N. C. Beaulieu, "Improved pilot symbol- aided estimation of rayleigh fading channels with unknown autocorrelation statistics," in *Proceedingss of IEEE Vehicular Technology Conference – Fall*, Los Angeles, CA, Sept. 26-29, 2004.

[190] A. Kumar, P. Ishwar, and K. Ramchandran, "On distributed sampling of bandlimited and non-bandlimited sensor fields," in *Proceedings of IEEE International Conference on Acoustics, Speech and Signal Processing*, vol. 3, Montreal, Canada, May 17-21, 2004.

[191] E. J. Candes and T. Tao, "Near-optimal signal recovery from random projections: Universal encoding strategies," *IEEE Transactions on Information Theory*, vol. 52, no. 12, pp. 5406–5425, Dec. 2006.

[192] S. Boyd and L. Vandenberge, *Convex Optimization*. Cambridge University Press : Cambridge, 2004.

[193] L. Vandenberge and S. Boyd, "Semidefinite programming," *SIAM Review*, vol. 38, no. 1, pp. 49–95, Mar. 1996.